Dynamic Behaviour under Wind Loading of a 90 m Steel Chimney

Pär Tranvik Alstom Power Sweden AB, Växjö
Göran Alpsten Stålbyggnadskontroll AB, Solna

Alstom Power Sweden AB Report S-01041
Stålbyggnadskontroll AB Report 9647-3
March 2002

Contents

Appendices with recorded and calculated data (Not included in this printing but enclosed in the covered CD):

Preface

This report presents results from an investigation of the structural behaviour of a 90 m high steel chimney equipped with a mechanical damper at the top. Due to a mistake in installing the chimney the damper was not active in the first period of service life, causing large oscillations of the structure and fatigue cracks to occur within a few months of service. Because of this an extensive investigation was started to rectify the action of the damper, repair the steel structure and to monitor the behaviour of the structure adopting a fail-safe principle. Data from four years of continuous measurements are presented in the report.

VEAB of Växjö, Sweden is owner of the chimney, being part of a delivery of an electrostatic precipitator of the Sandvik II biomass power plant at Växjö. ABB Fläkt Industri AB of Växjö was contractor for the electrostatic precipitator including the chimney (activities of the company later subdivided between Alstom Power Sweden AB and ABB). The chimney was fabricated and erected by the subcontractor VL Staal A/S of Esbjerg, Denmark.

The authors are indebted to all parties involved for making it possible to present the results in this form. Special thanks are due to Mr Ulf Johnson of VEAB, Mr Lars Palmqvist of ABB Automation Systems AB, Mr Stig Magnell of Dryco AB, Messrs Rolf Snygg and Thomas Väärälä of Alstom Power Sweden AB, and Mr Stig Pedersen of VL Staal A/S.

The investigation presented in this report was initiated by VEAB, for which the second author acted as a consultant. The compilation of data and preparation of most parts of this report were made by the first author. The second author has acted mainly as advisor for the investigation.

Växjö and Solna in March 2002

Pär Tranvik Göran Alpsten

Abstract

The structural behaviour of the 90 m height VEAB steel chimney in southern Sweden has been investigated. After only nine months of service a great number of fatigue cracks were observed. The very slender chimney is equipped with a mechanical friction type damper to increase damping and reduce displacements from vortex shedding. Initially the friction damper did not operate properly and the chimney developed oscillations with large top deflections in the very first period of service.

An extensive program was initiated to study and repair the fatigue cracks, restore the mechanical damper, monitor the chimney behaviour and verify the chimney behaviour by theoretical models.

This report summarizes results collected from about four years of continuous measurements and regular observations of the chimney. The data obtained has some general relevance with respect to wind data, behaviour of a slender structure under wind loading, and the effect of a mechanical damper. Also included in the report are results from some theoretical studies related to the investigation of the chimney.

A full scale damping test was performed. An improvement of a simplified theoretical calculation model for the behaviour of tuned mass dampers was performed.

The report present a number of diagrams for wind pressure and top deflection range, accumulated wind pressure, accumulated top deflection range, elastic energy, wind turbulence, load spectra and frequency of wind velocity.

A comparison with some other chimneys reported in the literature shows that the VEAB chimney is unique in height and slenderness.

The economic incitements have to be great for using mechanical pendulum tuned dampers. This may not always be the case if inspection and maintenance costs are included in the cost estimate.

There is a need for revising the calculation model for vortex shedding of very slender chimneys, that is for chimneys with slenderness ratio (height through diameter) above approximately 30.

Key Words

Full scale measurements
Cross wind oscillations
Vortex shedding
Chimney
Mechanical damper
Dynamic wind loading

1. Introduction

1.1 Scope of investigation

This report presents results from an investigation of the structural behaviour of a 90 m high steel chimney erected at Växjö in southern Sweden in 1995. The chimney is equipped with a mechanical friction-type damper at the top.

Due to a mistake during erection and installation of the chimney the transport fixings of the damper were not released properly and the chimney developed extensive oscillations in the very first period of service. This caused a great number of fatigue cracks to occur within a few months of service.

After the functioning of the damper had been restored and the fatigue cracks repaired an extensive program was initiated in 1996 to monitor the structural behaviour of the chimney under wind loading. This included continuous measurement of stresses in the structure in order to record the stress history and thus monitor the risk for fatigue of the repaired structure. Visual inspection and magnetic particle evaluation have been performed at regular intervals, determined from a fail-safe principle.

This report summarises results collected from about four years of continuous measurements and regular observations of the chimney. The data obtained has some general relevance with respect to wind data, behaviour of a slender structure under wind loading, and the effect of a mechanical damper. Also included in the report are results from some theoretical studies related to the investigation of the chimney.

In addition to presenting results of general interest and discussions in the main part of the report, original data and further compilations of detailed results are given in Appendices to the report, in order to make possible further evaluation of the data for other investigators.

The observations and recordings from the VEAB chimney are unique because of the following items:

- It is a high and slender steel chimney equipped with a tuned pendulum damper.
- The natural frequencies are low and therefore also the critical resonance wind velocity for vortex-induced oscillations is low.
- Large top amplitude deflections have been observed with the damper mistakenly inactive.
- Vortex shedding oscillations were observed at both first and at rare occasions also at second mode of natural frequency.
- Field recordings have been made continuously during four years of service. Wind and temperature data and the response of the chimney to wind loading were recorded.

- A full-scale damping test was performed.

- A detailed examination of cracks was performed.

- Comparisons between theory and observations were made for natural frequencies, damping, dynamic behaviour, wind data, fatigue, cracks and finally there are a discussion about the use of tuned dampers.

1.2 Action of slender structures under wind loading

1.2.1 General

For slender structures subjected to wind loading there are three main actions to consider, gust wind, vortex shedding and ring oscillation ovalling.

Gust winds displace the chimney in the same direction as the wind load. For a rigid structure gust wind is independent of the dynamic properties of the structure but dependent for a flexible structure.

Vortex shedding occurs when the natural frequency of a structure corresponds with vortices shed from opposite sides of the structure resulting in cross gas flow oscillations. The vortex shedding will be discussed more in detail in Section 1.2.2, 2.4.2, 3.4, 3.5, 3.7 and 6.

Ring oscillations (ovalling) are a pulsating oval oscillation of for instance a cylindrical shell structure.

1.2.2 Vortex shedding

Vortex-induced oscillations occur when vortices are shed alternately from opposite sides of a structure. It gives rise to a fluctuating load perpendicular to the wind direction as shown schematically in Figure 1.2 a.

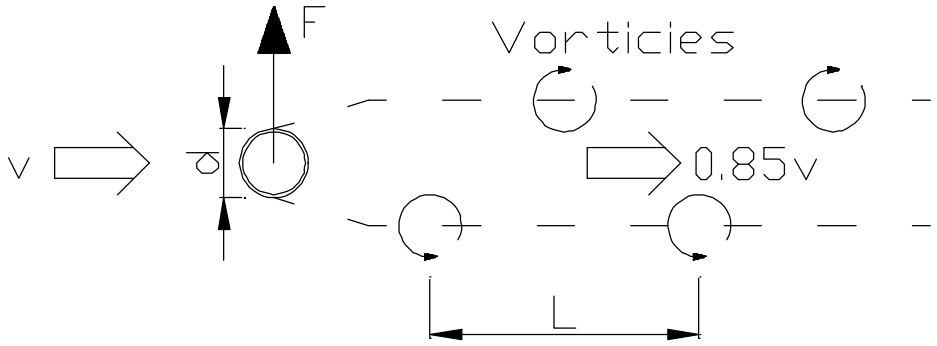

Figure 1.2 a Vortices formed behind a cylinder. *v* is the wind velocity in the undisturbed field. Distance between the vortices subject to wind loading *L* is approximately 4.3 times the diameter *d*.

When a vortex is formed on one side of the structure, the wind velocity increases on the other side [1]. This results in a pressure difference on the opposite sides and the structure is subjected to a lateral force away from the side where the vortex is formed. As the vortices are shed at the critical wind velocity alternately first from one side then the other, a harmonically varying lateral load with the same frequency as the frequency of the vortex shedding is formed.

Oscillations generated by vortex shedding may occur in slender structures such as cables, chimneys and towers. The risk of vortex-induced oscillations increases for slender structures and structures in line with a small distance between them.

Usually the first mode is critical for vortex shedding in actual steel structures subjected to wind loading, but in rare cases also the second mode is of interest.

The Reynold number is a non-dimensional parameter describing the influence of internal friction in fluid mechanics. The Reynold number is expressed as

$$Re = \frac{d \cdot v_{\infty}}{?} \quad \text{.....(1.1)}$$

where d = Diameter of chimney
v_{∞} = Undisturbed wind velocity
u = Kinematic viscosity of the air according to Section 3.8

In general large Reynold numbers means turbulent flow. For chimneys with circular cross section the flow is either in the supercritical or transcritical range for wind velocities of practical interest.

Subcritical	300	$\leqslant Re \leqslant$	10^5
Supercritical	10^5	$\leqslant Re \leqslant$	$3.5 \cdot 10^6$
Transcritical	$3.5 \cdot 10^6$	$\leqslant Re$	

Aero elasticity causes a regular vortex shedding also in the supercritical range.

For a non-vibrating chimney the distance L between vortices rotating in the same direction is proportional to the diameter of the chimney d. In slender structures, large oscillations may occur if the frequency of vortex shedding coincides with the natural frequency for the structure vibrating in a mode in the crosswind direction [1]. The proportionality factor for vortex shedding is named Strouhal number.

The Strouhal number is expressed as

$$St = \frac{d \cdot f_0}{v_\infty} \quad \text{.....(1.2)}$$

where f_0 = Natural frequency

The Strouhal number describes the dependence of the cross section, the surface roughness and the wind turbulence [1]. It depends on the Reynold number for a stationary smooth cylinder and for an aeroelastic chimney. The Strouhal number depends on the motion of the structure (aero elasticity).

Characteristic properties for crosswind are:

- Net gust load caused by lateral wind fluctuations.

- Loads caused by vortex shedding. The load occurs whether or not the structure is moving, but may be strongly dependent on the size of the motion [1], [6], [25]. The motion could start to rule the vortex shedding. This part of the load is called net vortex shedding load [1].

- Motion-induced forces. Most important is the negative aerodynamic damping generated by vortex shedding.

Vortex shedding structural oscillations are more probable if:

- Smooth laminar air flow which for instance occurs in the stable atmosphere during cold winter days.

- Increased small-scale turbulence, for instance that occurring in the wake of a slender, nearby structure of similar size.

Bearing in mind the risk of violent vortex-induced oscillations, aerodynamic damping is of primary concern.

The Scruton number is a non-dimensional parameter defined as

$$Sc = \frac{2 \cdot d_s \cdot m_e}{r \cdot d^2} \quad \text{.....(1.3)}$$

where d_s = The logarithmic decrement of the structural damping
m_e = Equivalent mass per unit of length according to the mode considered
r = Density of air

A comparison of the predicted amplitudes for steel chimneys with full-scale measurements is shown in [2]. Similar diagrams are found in [1].

1.3 Symbols and units

Symbols are explained in the text where they first occur. Unless otherwise noted basic SI units has been used through out this report.

2. Description of the VEAB chimney

2.1 VEAB Sandvik II plant

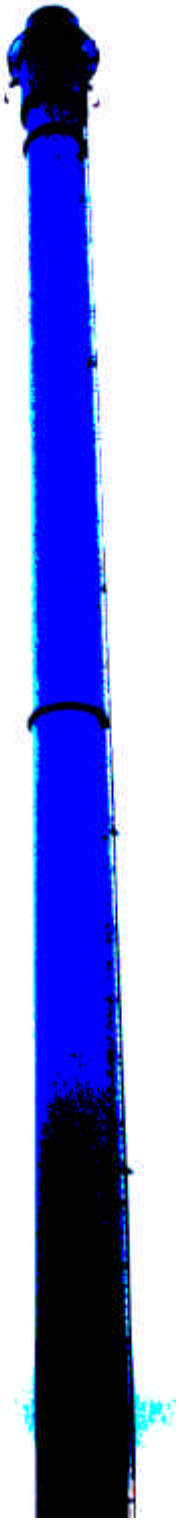

The VEAB Sandvik II cogeneration block is situated outside the town of Växjö in southern Sweden at a height of 164 m above sea level. Large forested areas and some lakes dominate the surroundings. The plant can be fired with most kinds of biomass, everything from wood chips to bark and peat. The boiler has an output of 104 MW, of which 66 MW is heat. The generator has an output of 38 MW of electricity.

The boiler is of circulating fluidised bed type, a so-called CFB-boiler. The particle collection equipment consists of an electrostatic precipitator for the separation of dust from the flue gases, an induced fan, a flue gas condenser to utilize the energy content in the flue gas, a dust transportation and storage system and a steel chimney, see Figure 2.1 a.

This chimney, being the subject of this report, is referred to as the VEAB chimney. A layout of the VEAB Sandvik II plant is shown in Figure 2.1 b. A photo of the VEAB chimney from the South showing neighbouring buildings is shown in Figure 2.1 c. More data about the VEAB Sandvik II plant may be found in Appendix A.

The distance between the VEAB chimney and the old concrete chimney is about 110 m or approximate 50 times the VEAB chimney diameter. The distance is much larger than 15 times the diameter were interaction between two equal chimneys may become insignificant [3], [9]. Furthermore, the properties of the old concrete chimney and the new steel chimney are drastically different. Thus interaction between the two chimneys should be insignificant.

Figure 2.1 a The VEAB chimney top half photographed from the boiler outer roof.

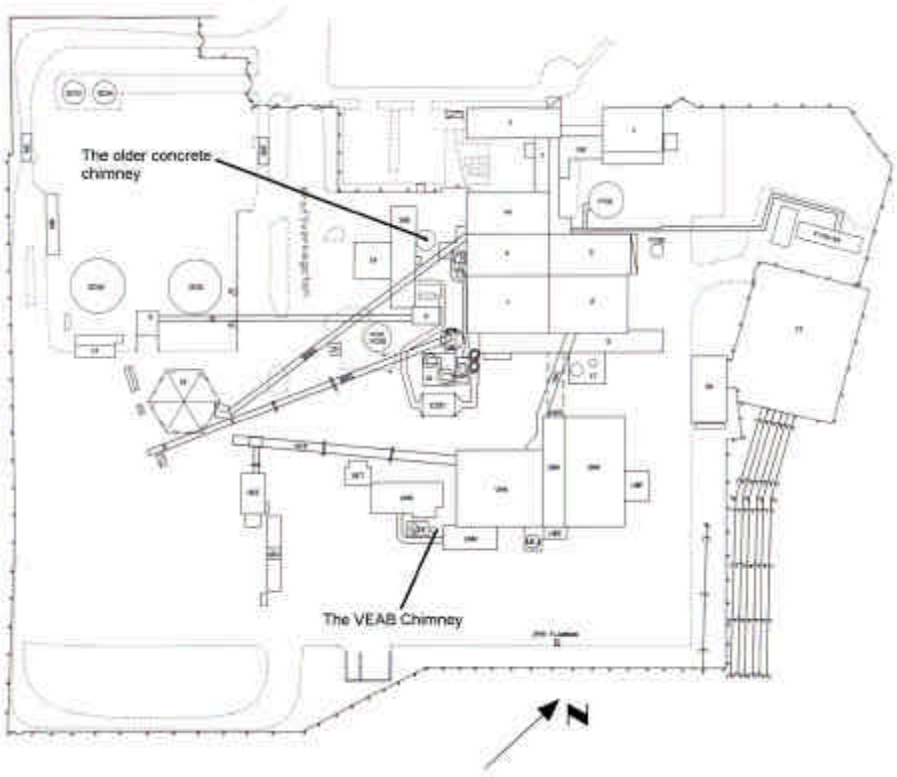

Figure 2.1 b Layout of the VEAB Sandvik plant.

Figure 2.1 c The VEAB chimney from south showing neighbouring buildings.

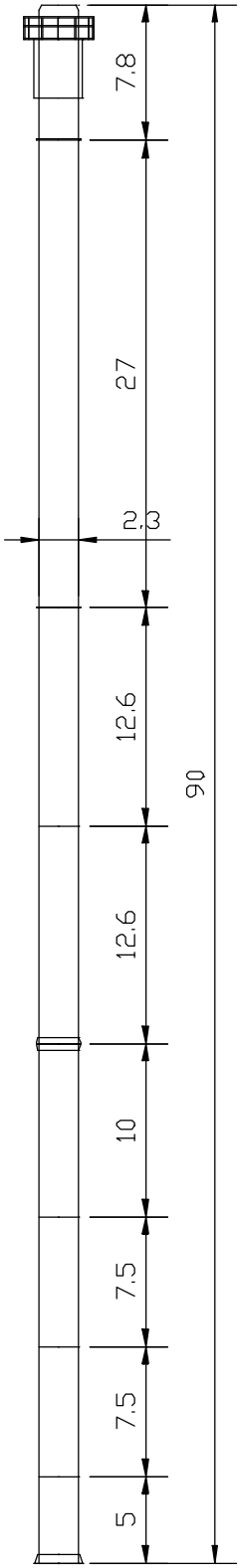

Figure 2.2 a Overall dimensions of the VEAB chimney.

2.2 Data for structure of the VEAB chimney

2.2.1 General data

The VEAB chimney has the following overall data:

Height	90	m
Diameter of structural shell	2.3	m
Diameter of inner pipe	2.0	m
Thickness of inner pipe	3	mm
Outer diameter of top portion with damper	2.8	m

The thickness of the structural shell varies from base to top as shown in Table 2.2 a.

Table 2.2 a Thickness of structural shell of the VEAB chimney.

Height (m)	Thickness (mm)
0	18
5	16
12.5	14
20	12
30	10
42.6	8
55.2	6
90	

Weights

Structural shell	50 080 kg
Inner pipe	13 592 kg
Insulation	4 954 kg
Damper pendulum	1 246 kg
Miscellaneous	9 628 kg
Total	79 500 kg

Material

Structural parts	Cor-ten, $R_e = 355$ MPa , $E = 210\ 000$ MPa
Inner pipe	Steel SS2350
Foundation bolts	Steel S355J2G3 according to EN10025, $R_e = 345$ MPa
Bolts at flanged splices	8.8, $R_m = 800$ MPa

Corrosion protection

Sand blasting to Sa 2.5
2 x 60 µm alkyd primer
2 x 60 µm top coat

For transport and erection purposes flanged splices are arranged at levels 30 m, 55.2 m and 82.2 m.

2 x 40 mm of thermal insulation of mineral wool are arranged between inner pipe and outer shell.

Just below the top of the chimney a mechanical pendulum damper is arranged to decrease top deflection caused by vortex shedding. The damper is described more in detail in Section 2.3.

Above the damper, at 88 m level, a platform is arranged.

From height 2.5 m level up to the platform at height 88 m level an outside ladder is arranged. The distance between ladder and chimney shell (equal to connection gusset plates width) is 200 mm (see also Figure 2.2 m).

Three warning lights for aircrafts are connected to the outside plate shell of the damper unit.

Some buildings as boiler house and electrostatic precipitator are located close to the chimney. Figure 2.1 b shows a layout of the VEAB plant and Figure 2.2 b a layout of the immediate surroundings of the VEAB chimney.

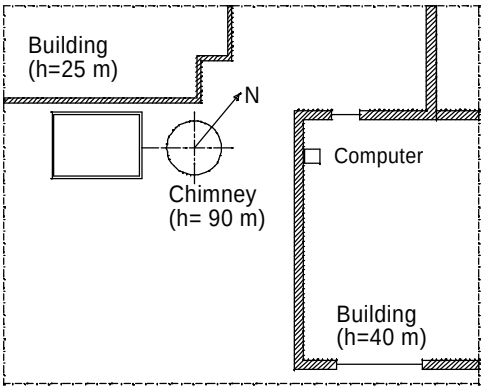

Figure 2.2 b The VEAB chimney, neighbouring buildings and the location of the recording computer.

The slenderness ratio for a chimney may be defined as

$$l = \frac{h}{d} \quad \text{.....(2.1)}$$

where h = height of the chimney
d = diameter of the chimney

For the VEAB chimney $l = \frac{90}{2.3} = 39$ which is greater than 30, the approximate limit value according to [3] for applicability of the code model for calculating vortex shedding forces.

2.2.2 Structural details

The base details consist of a bottom ring, 40 gusset plates at outside and 40 at inside. A total of 80 foundation bolts M56 connect the VEAB chimney to the concrete foundation structure. See Figures 2.2 c and 2.2 d. Initially the design had no ring placed at the top of the gusset plates.

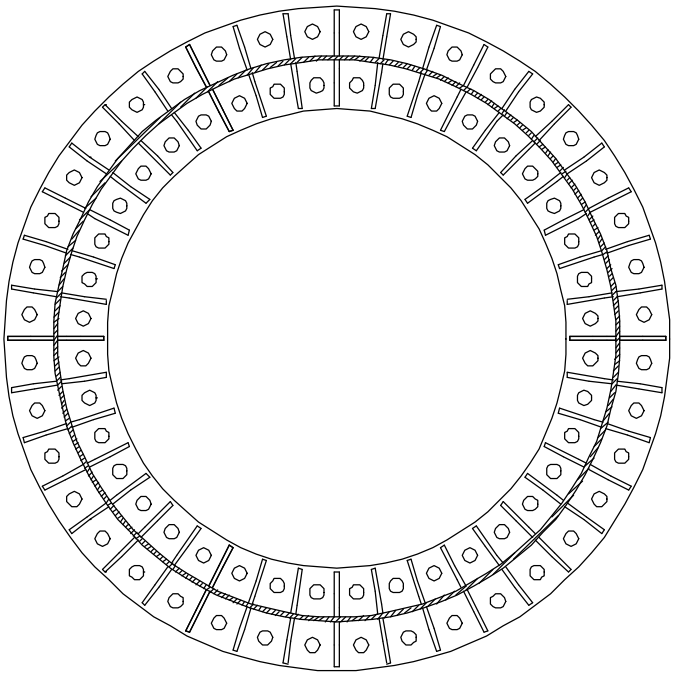

Figure 2.2 c Base plate with 2 x 40 foundation gusset plates and 2 x 40 bolt holes.

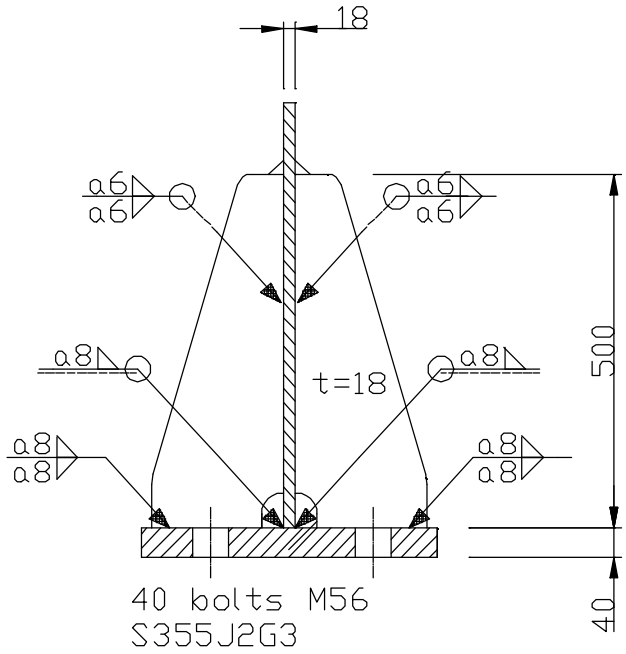

Figure 2.2 d Original base details with 40 gusset plates symmetrically at inside and outside of the shell plate. 2x40 bolts M56 S355J2G3 (Details of the later modified foundation ring are shown in Figure 2.1 g.

Flanged splices at 30 m and 55.2 m levels are shown in Figures 2.2 e and 2.2 f. Initially the flanged splice design at 30 m level had no ring placed at the top of the gusset plates.

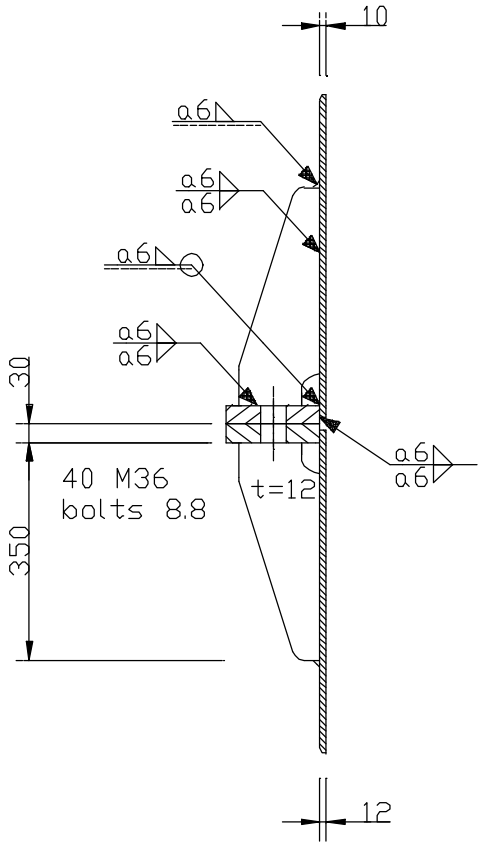

Figure 2.2 e Original flanged splice at h=30 m level. 40 gussets symmetrically on outside of the shell plate were applied (details of the later modified splice are shown in Figure 2.1 i).

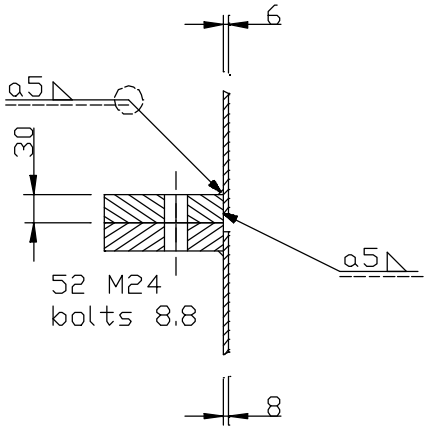

Figure 2.2 f Flanged splice at h=55.2 m level.

Figure 2.2 g shows the modified base details with the reinforcement ring on top of flanges.

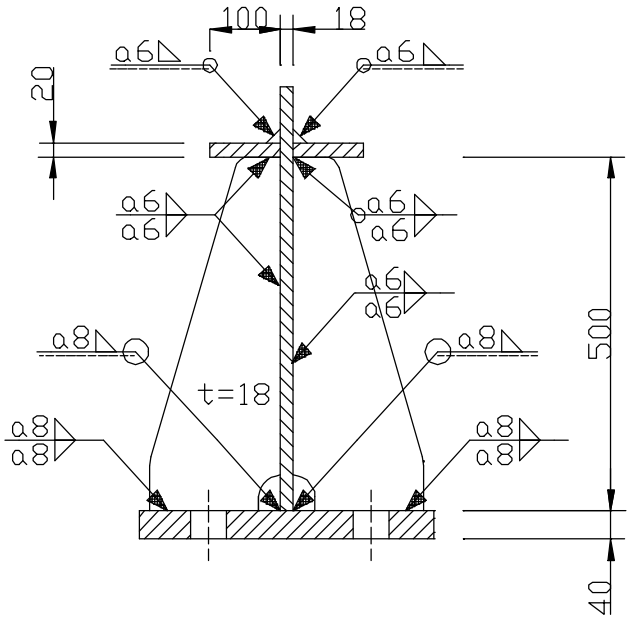

Figure 2.2 g Modified base details. Modification made in December 1998. The original base is shown in Figure 2.1 d.

The modified base details and details of the inspection door are shown in Figure 2.2 h.

Figure 2.2 h The modified base details and details of the inspection door. The cables above the inspection door are a part of the data collecting system.

Figures 2.2 i and 2.2 j show the modified flanged erection splice at 30 m level with the reinforcement ring on top respective bottom of flanges.

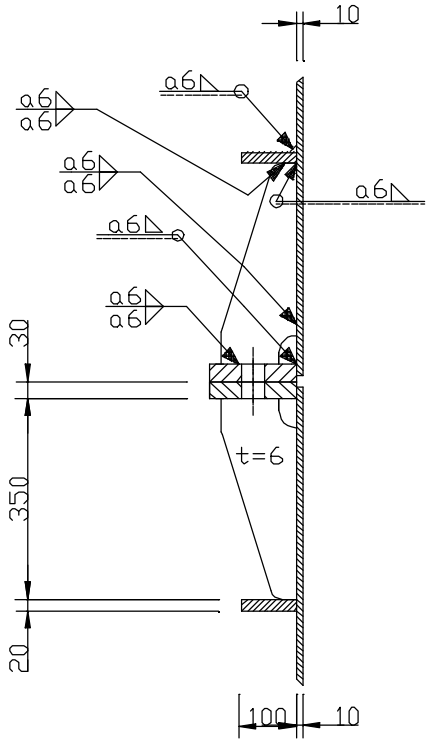

Figure 2.2 i The modified flanged erection splice at h=30 m level. Modification made in December 1998. The original flanged erection splice is shown in Figure 2.1 e.

Figure 2.2 j The modified flanged erection splice at h=30 m level. Modification made in December 1998.

Details of the reinforcements at the connection for inlet duct are shown in Figure 2.2 k.

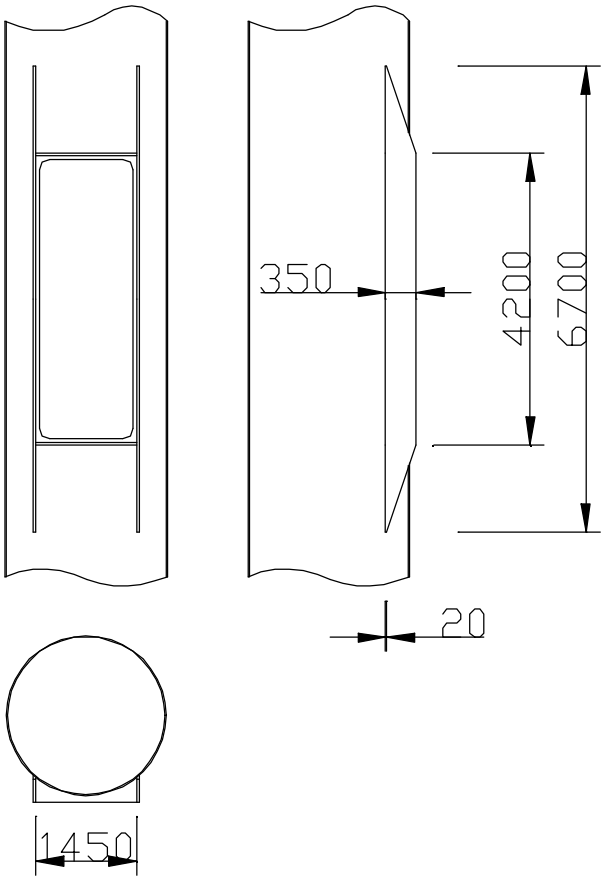

Figure 2.2 k Details of the reinforcements at the connection for inlet duct. Midpoint of hole at 13.3 m level. Thickness of the vertical reinforcement plates is 40 mm.

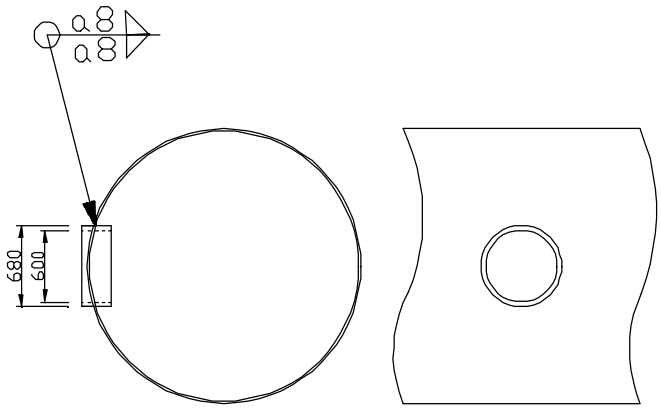

Figure 2.2 l Details of the inspection door at 1 m level (midpoint). See also Figure 2.1 h.

Details on ladder connections and inner pipe supports are shown in Figures 2.2 m and 2.2 n respectively.

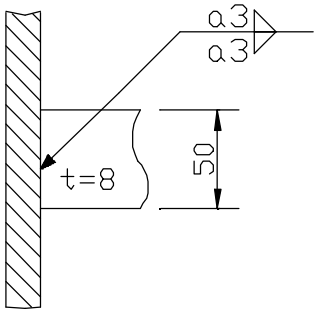

Figure 2.2 m Details of the ladder connection gusset plates.

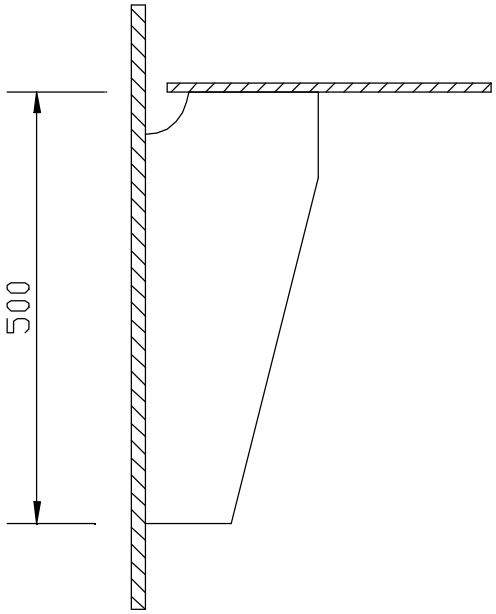

Figure 2.2 n Details of the support gusset plates for inner pipe at *h*=11 m level.

2.2.3 Manufacturing characteristics

The manufacturing was intended to follow Swedish regulations for load carrying steel structures [3], [4] and [17]. According to the manufacturers documentation:

Workmanship class	GB	
Cutting class	Sk2	
Weld class	WC	according to [4], that is, modified class C according to ISO 5817

From inspection of the delivered structure, a number of deviations from the intended quality were found. Most important, a large number of welds at base and at flanged erection splice at 30 m level not did satisfy weld class WC. Weld class WC is the lowest weld quality applicable for load carrying steel structures according to [4].

The manufacturing was made at the VL Staal a/s workshop in Esbjerg, Denmark. In the quality control of the chimney a third party was involved.

2.3 Mechanical damper

2.3.1 Common damping designs

Two principal solutions to reduce oscillations caused by vortex shedding are described in the literature, see for instance [1] and [6].

The first method is to apply helical strakes or any similar aerodynamic device for removing or reducing the magnitude of oscillations induced by regular vortex shedding. The periodic formation of vortices will be reduced or eliminated by the changed airflow. The design of the helical strakes is important for an effective reduction of vortex-induced oscillations. A disadvantage with the use of helical strakes is an increased projected area at chimney top and increased drag coefficient, thus causing increased gust wind loads.

Another method for reducing or eliminating the risk of oscillations induced by vortex shedding is to apply tuned mass dampers. There are two types of tuned mass dampers, passive and active. An active mass damper requires an automatic engineering system to trigger the mass damper to counteract any occurring oscillation.

The VEAB steel chimney uses a passive tuned mass damper and this type will be discussed here. Several designs for a tuned mass damper are suggested in [6], [7] and [8]. Figures 2.3 a through 2.3 g presents schematically some solutions for passive damping devices. The VEAB chimney uses the principle found in Figure 2.3 f.

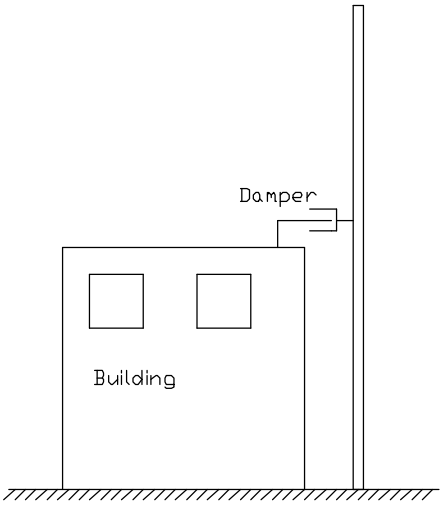

Figure 2.3 a The chimney is damped by connecting a damper to a neighbouring building.

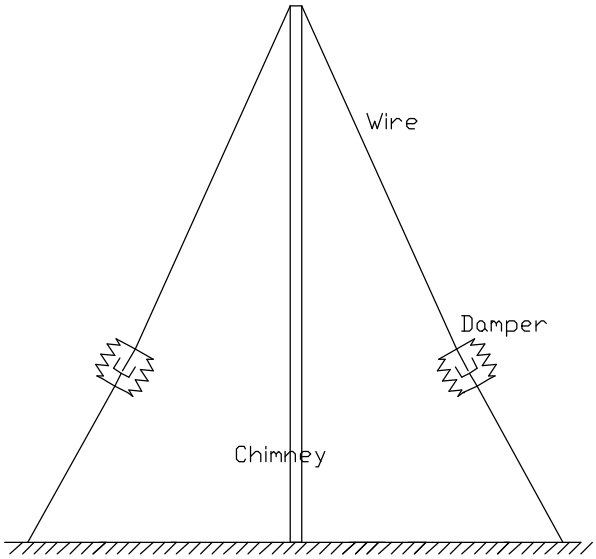

Figure 2.3 b The chimney is damped by using prestressed wires with spring-damper elements.

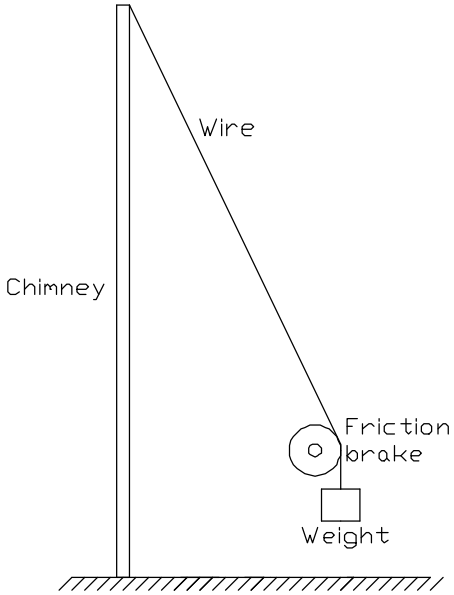

Figure 2.3 c The chimney is damped by using wires with an end mass and a friction device.

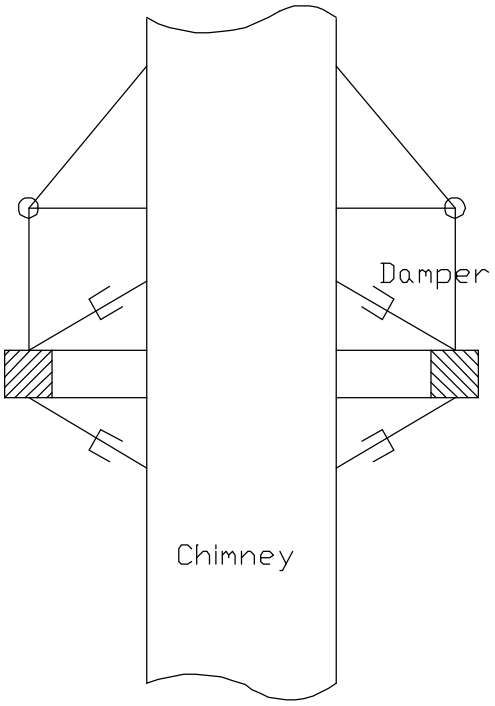

Figure 2.3 d The chimney is damped by using a pendulum ring connected to the chimney shell plate by hydraulic dampers.

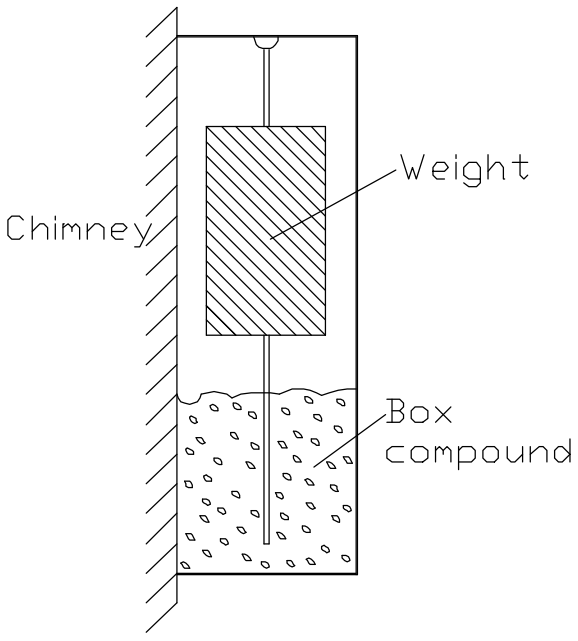

Figure 2.3 e The chimney is damped by using a pendulum mass with a bottom rod in a damping material.

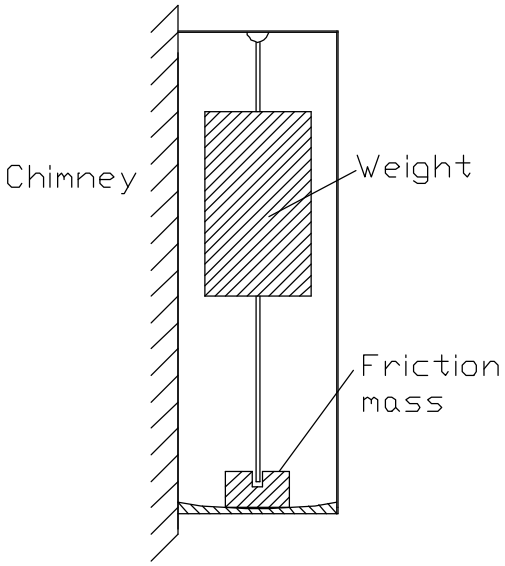

Figure 2.3 f The chimney is damped by using a pendulum mass with a bottom rod. A friction mass is guided by the rod. The damping is achieved by the friction mass that slips on a bottom plate.

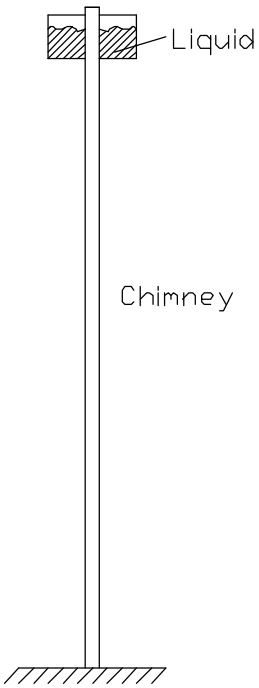

Figure 2.3 g The chimney is damped by using a dynamic liquid damper.

2.3.2 Tuned pendulum damper of the VEAB chimney

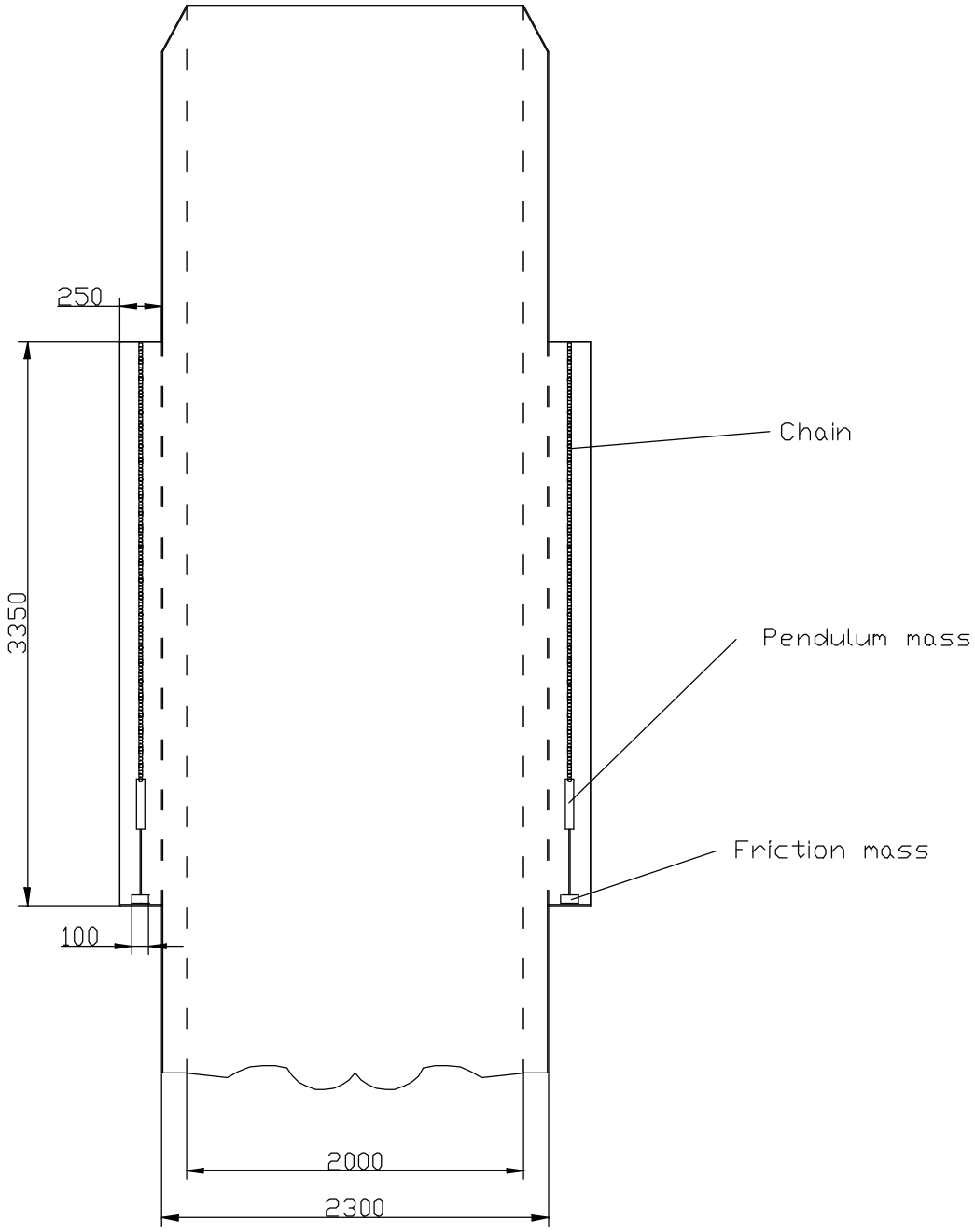

Figure 2.3 h The tuned pendulum damper of the VEAB chimney (schematic drawn but in scale). Compare with Figure 2.3 f.

The tuned pendulum damper of the VEAB chimney consists of a pendulum mass ring hinged in three chains, located in 120 degrees direction, connected to the damper house roof. Three symmetrically distributed guiding rods connect the pendulum mass movement to the movement of the three friction masses. The damping is achieved by friction between the friction mass and the damper house floor. The manufacturer calculated the generalised mass

to M_{gen}=12 460 kg. The pendulum mass was selected to 10 percent of the generalised mass to M=1 246 kg [6].

The generalised mass is defined as

$$M_{gen} = \int_0^H m(x) \cdot \left(\frac{y(x)}{y_{top}} \right)^2 \cdot dx \quad \text{.....(2.2)}$$

where

$m(x)$ = Mass per length at height x
$y(x)$ = Deflection at height x
y_{top} = Top deflection
dx = Integration segment
H = Chimney height

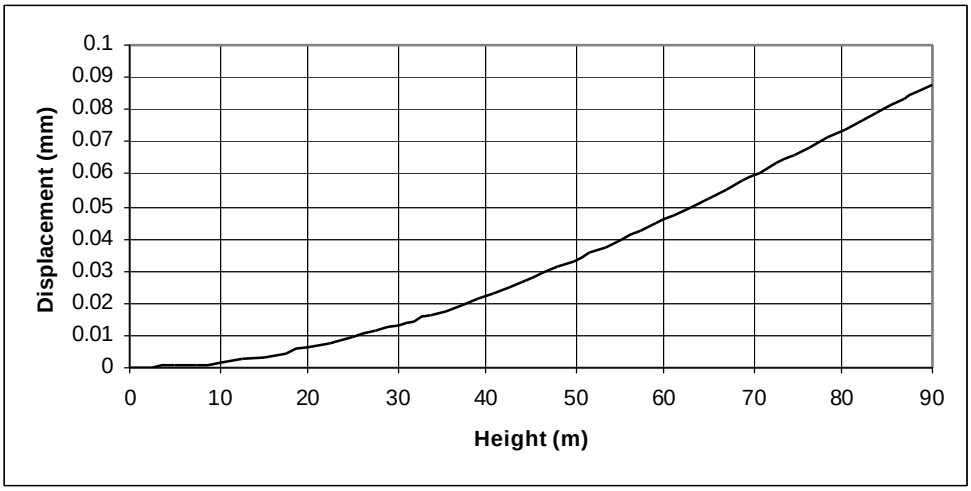

Figure 2.3 i Top deflection amplitude as a function of level according to the finite element calculation in Sections 2.4.1 and 3.3.2.2

By a stepwise integration of Equation 2.2 rewritten as finite differences and using the results from the finite element calculation in Section 2.4.1 and 3.3.2.2 it is found that

$$M_{gen} = \Delta m(x) \cdot \left(\frac{y(x)}{y_{top}} \right)^2 \cdot \Delta x \quad \text{.....(2.3)}$$

where

$\Delta m(x)$ = Mass per length at height x for a finite element
$y(x)$ = Deflection at height x for a finite element
Δx = Chimney height integration step

The generalised mass may be achieved as $M_{gen} = 16\,810$ kg which differs from 12 460 kg according to above.

The pendulum angle is limited by the damper house walls shown in Figure 2.3 j to an angle of

$$a \approx \arctan\left(\frac{250-100}{2 \cdot 3550}\right) \approx 1.2\ °$$

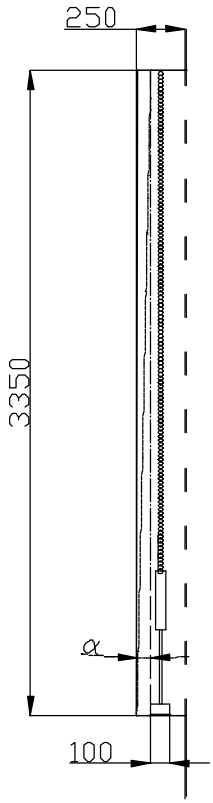

Figure 2.3 j Maximum possible pendulum angle a for the VEAB chimney damper (measured from the layout drawing).

The horizontal force necessary to accelerate the friction masses into motion by an inclination of the pendulum damper is

$$H = m \cdot N = m \cdot m_f \cdot g \quad \text{.....(2.4)}$$

where m = The friction coefficient which is 0.15 to 0.3 depending on the surface properties of the steel.
m_f = Friction mass

In Section 3.3.2.7 the influence of the magnitude of the acceleration is studied theoretically.

Both ventilation and drainage holes are arranged in the damper house.

2.4 Dynamic properties of the VEAB chimney

2.4.1 Natural frequencies

The three lowest modes of natural frequencies of the VEAB chimney were calculated with a finite element program.

The following assumptions were made:

- The chimney was modelled as a fixed end cantilever.
- The actual variation with height of the mass and the stiffness of the structure was considered
- An additional mass of 2 500 kg for the damper equipment was added in the node
  at the mass centre of the damper.
- Distributed masses of 310 kg/m were added to all nodes. It includes inner pipe, insulation, ladder, electrical cables and other non-structural elements.

The three lowest modes of natural frequencies are shown in Figure 2.4 a.

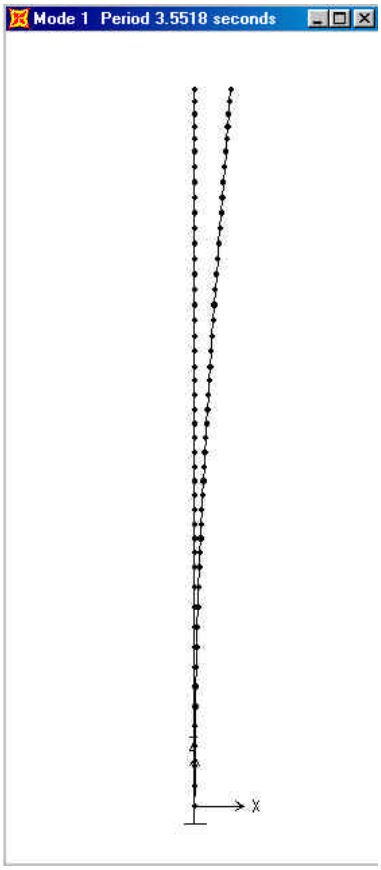

First mode of natural frequency

$$f = \frac{1}{T} = \frac{1}{3.5518} = 0.282 \text{ Hz}$$

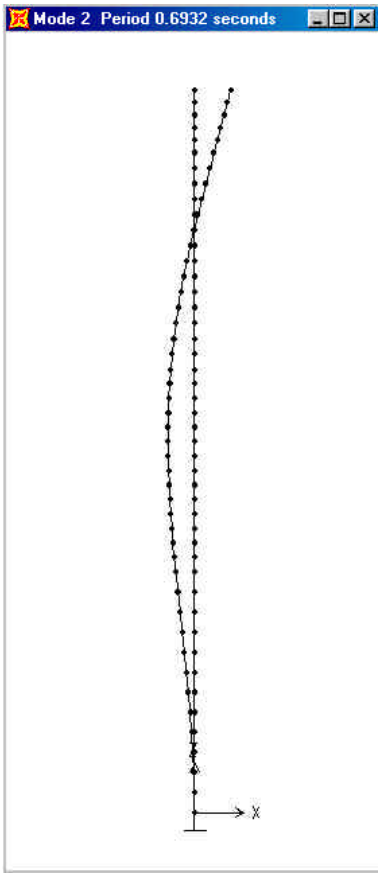

Second mode of natural frequency

$$f = \frac{1}{T} = \frac{1}{0.6932} = 1.44 \text{ Hz}$$

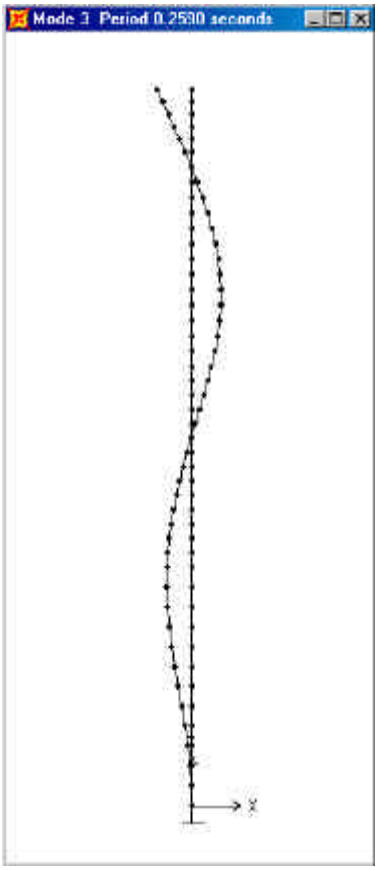

Third mode of natural frequency

$$f = \frac{1}{T} = \frac{1}{0.2590} = 3.86 \text{ Hz}$$

Figure 2.4 a The three lowest modes of natural frequencies calculated for the VEAB chimney.

These calculated natural frequencies might be compared with observed values for the actual structure. The natural frequency was determined from observations of oscillations in the first mode using a theodolite. Average values was:

0.287 Hz	1996-05-03
0.283 Hz	1996-10-29

In Section 3.7.2, the first mode of natural frequencies for the four years of measurements is presented. Based upon an evaluation of the vast amount of recorded data the average value of the first mode of natural frequency for the measurement period 1997 through 2000 was 0.288 with a total variation of ± 0.005 Hz.

Thus the observed natural frequency, based on two different ways of measurement and observed over a long period of time, corresponds well with the calculated value of 0.282 Hz.

2.4.2 Vortex shedding

According to [3] the critical wind velocity at vortex shedding is calculated as

$$v_{cr} = \frac{f \cdot d}{St} \quad \text{.....(2.5)}$$

where f = Natural frequency (0.282 Hz used in this section)
d = Diameter
St = Strouhal number (Equation 1.2), 0.2 at ordinary vortex shedding and lower if any lock-in phenomena occur

In Table 2.4 a the critical wind velocities for the three lowest natural frequencies are found.

Table 2.4 a The critical wind velocity for the three lowest modes for the VEAB chimney. Strouhal number assumed to 0.2. Calculated values for natural frequencies have been used.

	Critical wind velocity for first mode (Hz)	Critical wind velocity for second mode (Hz)	Critical wind velocity for third mode (Hz)
At chimney shell d = 2.3 m	3.24 m/s	16.6 m/s	44.4 m/s
At damper unit d = 2.8 m	3.95 m/s	20.2 m/s	54.0 m/s

In Section 3.2.3.2 the mean wind velocity at 90 m height was calculated to 34.2 m/s. Critical wind velocity for both first and second mode is of interest for vortex shedding phenomena because their magnitude is less than the mean wind velocity.

According to [3] the equivalent load during vortex shedding may be calculated as

$$w_{eq} = m_{tr} \cdot p_{cr} \cdot d \cdot \frac{p}{d_m} \quad \text{.....(2.6)}$$

where m_{tr} = Shape factor for cross wind oscillations
p_{cr} = Wind velocity pressure (Pa)
d = Diameter (m)
d_m = Logarithmic decrement, assumed to 0.07 for the VEAB chimney with active dampers

Further the wind velocity pressure p_{cr} is calculated as

$$p_{cr} = 0.5 \cdot r \cdot v_{cr}^2 \quad \text{.....(2.7)}$$

where r is assumed equal to 1.25 kg/m^2 [3].

m_{tr} is a function of the Reynold number, which is defined in Equation 1.1

In Table 2.4 b equivalent load during vortex shedding are found for the VEAB chimney.

Table 2.4 b Equivalent loads during vortex shedding.

	d (m)	v_{cr} (m/s)	*Re*	m_{tr}	p_{cr} (Pa)	w_{eq} (N/m)
Shell plate	2.3	3.24	$4.97 \cdot 10^5$	0.2	6.56	135
At damper	2.8	3.95	$7.37 \cdot 10^5$	0.2	9.75	245

Some comments about this model and values of the temperature dependent variables will be discussed later in Section 6.

It is important to note that the VEAB chimney do not satisfy the restrictions in [3] for applicability of the code model. The restrictions are:

$$\frac{h}{d} \leqslant 30 \quad \text{.....(2.8)}$$

$$y_{max} \leqslant 0.06 \cdot d \text{ for the load } 1.3 \cdot w_{eq} \quad \text{.....(2.9)}$$

where y_{max} = Top deflection amplitude (m)

The maximum top deflection range during vortex shedding was calculated by the manufacturer to $2 \cdot 133.6 = 273$ mm. The corresponding bending stress at the chimney base was calculated to 11.6 MPa. For the VEAB chimney the slenderness h/d = 39 which means that the restrictions for the applicability of the load model of the code [3] is exceeded.

2.4.3 Elastic energy

To get an estimation of the energy added to the oscillating chimney the beam elastic energy is calculated.

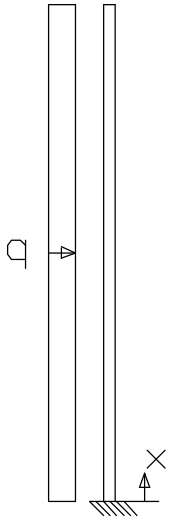

Figure 2.4 b A distributed load on a fixed cantilever beam.

Modulus of elasticity

$E = 21 \cdot 10^4$ MPa

Height of the VEAB chimney

H=90 m

Bending moment in the beam loaded by a distributed load

$$M_b(x) = q \cdot (H - x) \cdot \frac{(H - x)}{2} = \frac{q}{2} \cdot (H - x)^2 \quad \text{.....(2.10)}$$

The VEAB chimney outer diameter is

D=2.3 m

Plate thickness varies according to Table 2.2 a.

Moment of inertia varies as

$$I(x) = \frac{p}{64} \cdot \left[D^4 - (D - 2 \cdot t)^4 \right] \quad \text{.....(2.11)}$$

The beam elastic energy is described as

$$W = \int_0^H \left(\frac{(M_b(x))^2}{2 \cdot E \cdot I(x)} \right) \cdot dx \quad \text{.....(2.12)}$$

For each part with a constant shell thickness the moment of inertia is constant. The integral is therefore calculated separately for each part with constant shell thickness. The total beam elastic energy is then calculated by superposition. The part integration will be

$$W_{\text{part}} = \frac{1}{2 \cdot E \cdot I_{\text{part}}} \int_{h_1}^{h_2} (M_b(x))^2 \cdot dx = \frac{q^2}{8 \cdot E \cdot I_{\text{part}}} \int_{h_1}^{h_2} (H - x)^4 \cdot dx$$

$$W_{\text{part}} = \frac{q^2}{8 \cdot E \cdot I_{\text{part}}} \left[-\frac{1}{5} \cdot (H - x)^5 \right]_{h_1}^{h_2}$$

$$W_{\text{part}} = \frac{q^2}{40 \cdot E \cdot I_{\text{part}}} \left[(H - h_1)^5 - (H - h_2)^5 \right] \quad \text{.....(2.13)}$$

The numerical results are shown in Table 2.4 c.

Table 2.4 c Numerical integration of the beam elastic energy. It is assumed that $q=w_{eq}=135$ N/m, the equivalent load during vortex shedding of the VEAB chimney according to Section 2.4.2.

Part no	1	2	3	4	5	6	7	Total
h_1 (m)	0.0	5.0	12.5	20.0	30.0	42.6	55.2	
h_2 (m)	5.0	12.5	20.0	30.0	42.6	55.2	90.0	
t (m)	0.018	0.016	0.014	0.012	0.010	0.008	0.006	
I (m^4)	0.0840	0.0749	0.0657	0.0564	0.0472	0.0378	0.0284	
W (Nm)	37.9	47.5	36.8	34.7	24.7	10.8	4.5	197

This means that a distributed load of 135 N/m corresponds to a bending energy of 197 Nm for a half oscillating cycle. The period of the oscillations is $T = \frac{1}{f} = \frac{1}{0.288} \approx 3.5$ s.

2.5 Time history of the VEAB chimney

The VEAB chimney was erected in late November to early December 1995. It was snowy weather and the temperature was a couple of degrees below zero Celsius.

During the first winter period after erection several persons made observations of oscillations with large top deflections of the chimney. The potential for fatigue problems were first pointed out in a report by the second author. During the spring of 1996 cracks were found. Therefore an extensive crack examination program was carried out during the late summer and early autumn of 1996. A large number of cracks were found, examined and repaired.

One important explanation to the unacceptable top deflections was that the damper was mal-functioning. It was repaired but questions still remained if there could be other explanations for the large oscillations. Therefore an extensive data collecting system was installed intended to continuously monitor and record the response of the structure to wind loads. The data collecting system has been in continuous operation since mid December 1996 until 2001.

In December 1998 some additional cracks were found at locations not examined before. A couple of design changes were made. As part of the action to ensure a safe design the original foundation ring was modified. On top of the gussets an additional ring was added aimed to reduce stress concentrations at the horizontal welds between shell and gusset plates. The same action was taken at the connection ring at the flanged splice on the 30 m level.

3. Observed and recorded behaviour of the VEAB chimney

3.1 Observation of mal-functioning of the chimney

3.1.1 Observations of large oscillations

During the first nine months of the chimney in operation oscillations with large top deflections were observed. Observations of some witnesses during the first winter period December 1995 to April 1996 were later documented and are briefly related below.

The first working day after Christmas 1995 the temperature was about -20 °C with a sunny clear sky. A supervisor discovered that the chimney top oscillated with an amplitude approximately equal to the diameter and sounded like a chime of bells with a frequency of about one second period. He estimated the magnitude of the top deflection from measurements on the chimney shadow. His understanding was that the sound originated from movements between the outer and inner pipe. At 10.30 to 12.30 h the top chimney shadow moved about 4 m at the top of the power plant building. The chimney oscillated in west/east direction. The smoke from the older concrete chimney was almost above the new one or a little to the west. At 14.00 to 15.00 h the chimney again oscillated in a similarly manner. At 17.00 to18.00 h it oscillated again but not as much as before. The supervisor estimated that the chimney oscillated from Christmas 1995 or April 1996 one or two days a week with total top deflection amplitude of 0.5 to1.0 m.

A building worker observed on the first working day after Christmas 1995 that the chimney oscillated with a top amplitude equal to about the diameter. Later during the winter the same building worker, working on the power plant roof, observed the chimney to oscillate with amplitude of about 0.5 m at roof level.

Another building worker also made observations of the oscillations the same day as the supervisor. The top deflection amplitude was not quantified. After that he saw the chimney oscillate several times but not as much as on the first day.

Several design engineers and one structural engineer at a nearby engineering office of the Fläkt Industri AB located about 600 m NW of the chimney observed from their windows during the first working day after Christmas 1995 that the chimney oscillated violently. The structural engineer estimated the top amplitude to about half the diameter. The conditions for estimating the magnitude of the oscillations were good because the new steel chimney is almost in line with an older concrete chimney as viewed from the engineering office windows.

Two other structural engineers at a separate engineering office of the Fläkt Industri AB located about 1 km NW of the chimney observed from their windows the chimney to oscillate drastically during several times in January and February 1996. By levelling relative to a wall they estimated the top amplitude to be about half the diameter.

3.1.2 Initial observations of cracks and causes

According to the manufacturer a documented quality control was made before the shipping of the chimney and there where no detected cracks when it left the workshop. Personnel from the manufacturer as well as external testing personnel were involved in the quality inspection and testing.

Because of the observed behaviour of the VEAB chimney an inspection was made in May 1996 by the second author acting as a consultant for VEAB. At the foundation level cracks were found at the weld toes to the gusset plates. Both the maximum bending moment from wind loads and the large stress concentration at fillet welds at top of gusset plates to shell at chimney coincided. The appearance of these cracks indicated that the cause was fatigue.

The main explanation for the cracks was that one of the three guiding bars for friction masses of the damping pendulum at the top of the chimney was to long and therefore resting on the bottom friction plate. The pendulum movements were partly restrained. Apparently the damper gave only limited damping action until it was adjusted in September 1996.

3.1.3 Detailed examination of cracks

As a result of the initial observations of cracks at the base a detailed examination of cracks was made using magnetic particle and eddy current testing techniques. A description of the detailed examination of cracks is found in appendix J. The first author conducted and participated in all inspections and investigations and performed all evaluations.

Cracks were found at foundation ring gusset plates, at flanged erection splice gusset plates at 30 m level and at top and bottom of connecting gas duct vertical gussets. In Figure 3.1 a typical cracks for vertical gusset plates at foundation ring and vertical gusset plates at flanged erection splice at 30 m level are found. (a*)* denotes the initiation point at the weld toe where the angle at several welds was too sharp. (b*)* denotes the initiation point at the weld root. (1) shows the propagation direction for the weld toe initiated cracks. (2*)* and (3*)* shows the propagation direction for the centre of weld-initiated cracks. The most common type of crack was (1*)*.

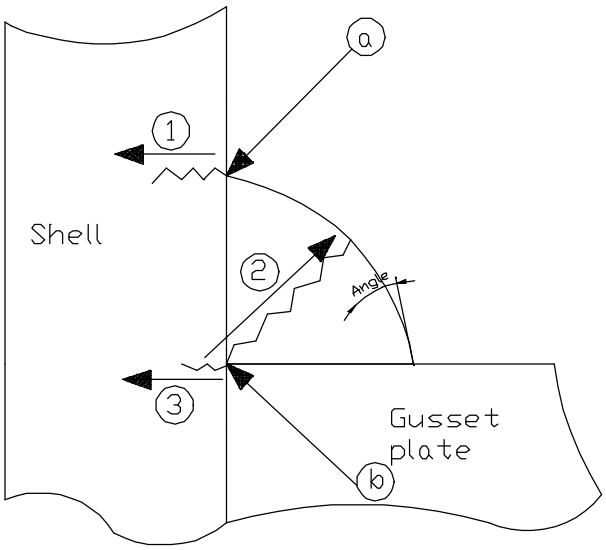

Figure 3.1 a Typical cracks at horizontal fillet welds at top of gusset plates to shell at chimney

At 12 of the 40 outside gusset plates and 37 of the 40 inside gusset plates at foundation level cracks were indicated. At 30 m level almost all of the gusset plates had some kind of a linear indication, probably from cracks. At both locations the crack lengths varied from 2 to 20 mm and the depths 1 to 3 mm, except at (2*)* according to Figure 3.1 a where some of the cracks at foundation level went through the weld. A picture of a typical weld is found in Figure 3.1 b.

← Crack at the weld toe
← Crack in centre of weld

Figure 3.1 b A weld after 1.5 mm of grinding.

At the weld toe of the horizontal welds at ends of the vertical plate reinforcements five cracks were found as shown in Figure 3.1 c.

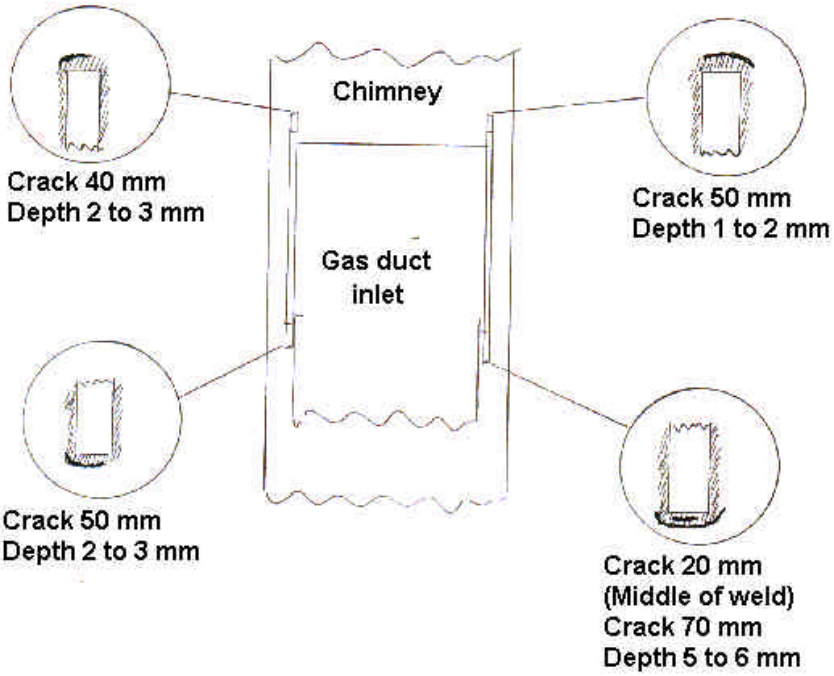

Figure 3.1 c Detected cracks at gas duct inlet.

3.1.4 Summary of cracks

All detected cracks had started either from an sharp and unacceptable weld toe or from root defects as shown in Figure 3.1 a. The weld roots had often remaining slag and cavities. The weld quality did not satisfy the code requirements for the weld qualities used in the design calculations. Most of the horizontal welds at top of gusset plates at foundation level and 30 m level were damaged by cracks observed after only a few months of service of the chimney.

3.1.5 Notches not available for examination

A number of potential points for fatigue crack initiation were not available for examination, such as welds at support gusset plates for inner pipe and guiding U-beams for inner pipe between the inner and outer shell. Therefore knowledge about their condition is unknown.

3.1.6 Repair of the damaged welds

All welds with indicated cracks were repaired and once again examined by the magnetic particle method. This was made immediately after the testing.

3.2 Data recording system

3.2.1 General

Because doubts remained about the reliability of the damper even after the adjustment in September 1996 it was decided that oscillations of the structure had to be monitored and stored by a data recording system. The data recording system consists of three main parts, the strain gauges, the wind data transmitters and the computer.

The data recording system was created primarily for studying the influence of first mode oscillations with respect to fatigue strength. Daltek Probator, Sweden, was responsible for developing and installing the data recording system.

3.2.2 Strain gauges

On the shell plate inside the stack at 4 m height above the concrete foundation strain gauges were applied at 16 points symmetrically in circumferential direction. The section at 4 m level was chosen in order to avoid influence of local stress concentrations from gusset plates at the chimney base and from the inlet to the gas duct. The inside chimney location was selected for weather protection reasons. The opposite strain gauges were coupled in pairs, bridges. For access and serviceability of the strain gauges a platform was built inside the chimney at 3 m height. Initially the recording system was aimed at monitoring the chimney behaviour for a few months. The results obtained from such a short period were not convincing. Therefore the monitoring period was extended. The first installation of the strain gauge system was aimed for a short period. Thus, the selected glue for the strain gauges was not aimed for long-term use.

The accuracy of the recorded values from the strain gauges were estimated to 1 percent.

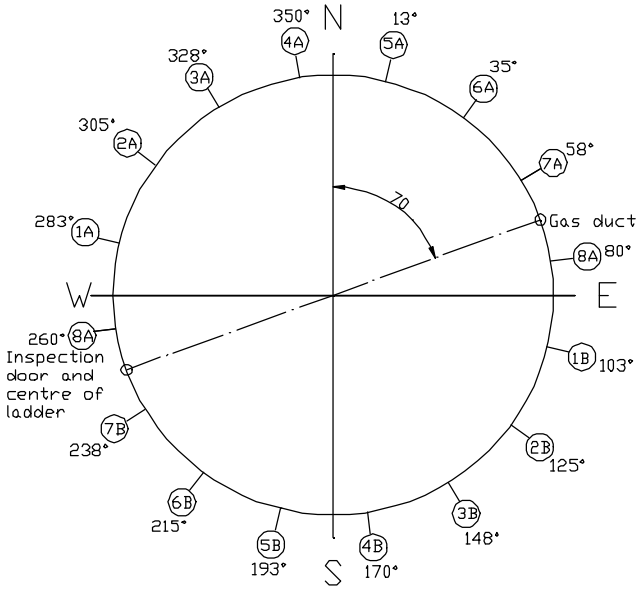

Figure 3.2 a Designation and orientation of strain gauges and locations relative to gas duct, inspection door and ladder of the VEAB chimney.

3.2.3 Wind data transmitter

3.2.3.1 General

Figure 3.2 b The VEAB Sandvik plant. To the right Sandvik II unit and the 90 m steel chimney. A balloon shows location of the wind data transmitter on top of the power plant building of the Sandvik II unit.

The wind data transmitter, wind monitor 05103 Young, was installed on the top of the power plant building on a 5 m height pole. The height of the power plant building roof is 40 m above ground level. The horizontal distance between the wind data transmitters and the VEAB chimney is 43 m. Therefore all recorded wind data refer to a 45 m height above ground level and a point 43 m approximately north of the VEAB chimney. This is to be compared with the height of the chimney, 90 m above ground level.

The distance between the VEAB chimney and the old concrete chimney, to the left in Figure 3.2 b is about 110 m or approximate 50 times the VEAB chimney diameter. It is much larger than 15 times the diameter, below which interaction between two equal chimneys may become significant [3], [9]. Furthermore the distance between the old concrete chimney and the VEAB chimney (new steel chimney) are drastically different. Thus as stated in Section 2.1, interaction between the two chimneys should be insignificant.

Figure 3.2 c The wind data transmitters on the Sandvik II unit roof.

Because of the small distance between the power plant outer roof and the wind data transmitter some form of turbulent boundary layer disturbances in the recorded wind data may be expected.

The wind data transmitter signals were also used by VEAB for their plant planning and for monitoring environmental conditions.

3.2.3.2 Correction for wind at 90 m height

The wind mean velocity varies with height according to [3]

$$v_{mk}(z) = v_{ref} \cdot \sqrt{C_{exp}(z)} \quad \text{.....(3.1)}$$

where the exposure factor is

$$C_{exp}(z) = \left[b \cdot \ln\left(\frac{z}{z_0} \right) \right]^2 \quad \text{for } z > z_{min} \quad \text{.....(3.2)}$$

For the VEAB chimney, topographical category II that is similar to the code definition [3] of an open terrain with small obstacles.

Reference wind velocity and terrain related parameters for topographical category II is [3]

$v_{ref} = 24$ m/s, $b = 0.19$, $z_0 = 0.05$ and $z_{min} = 4$ m

The height correction factor n_{corr} for wind at height h_2 but measured at height h_1 above ground level will be

$$n_{corr} = \frac{v_{mk}(h_2)}{v_{mk}(h_1)} \quad \text{.....(3.3)}$$

Table 3.2 a Exposure factor, wind mean velocity and height correction factor to 90 m height for some heights.

Height (m)	C_{exp}	v_{mk} (m/s)	n_{corr}
10	1.01	24.2	1.41
45	1.67	31.0	1.10
90	2.03	34.2	1.00

Wind data presented in this report have been corrected with the correction factor n_{corr} in Table 3.2 a.

3.2.3.3 Influence of distance between chimney and wind data transmitter

Because of the distance of 43 m between the chimney and the wind data transmitter wind data were not measured at the same time as oscillations of the chimney. The wind mean values for both wind velocity and direction were calculated at three arithmetic mean values 10s, 1 min and 10 min. As found from Figure 3.2 d below error influence will be limited because the time to create mean values will have greater influence on the results than the elapsed time for wind transferring from chimney to wind data transmitters or reverse.

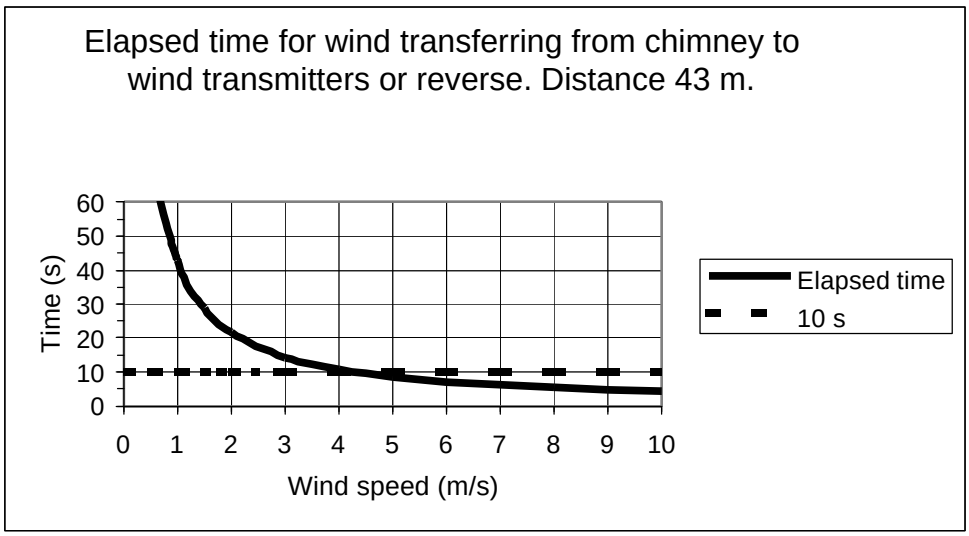

Figure 3.2 d Elapsed time for wind transferring from chimney to wind data transmitter.

Distance between chimney and transmitter is 43 m. Therefore, in this report no correction was made to account for the distance between chimney and wind data transmitter.

3.2.4 Recording computer

The measurement equipment was based on a Pentium 100 MHz personal computer equipped with a data collecting card with 16 analogue input ports and a separate card for signal conditioning. At the time of installation it was a modern personal computer. Collection of data, control and control of alarm functions were made by a computer program, a virtual instrument especially developed for this project. Daltek Probator AB, Sweden developed the LabVIEW application and was responsible for both program installation and hardware.

Both the strain gauges and the wind velocity and direction transmitter equipment were connected to the computer. The computer was located in a partly heated and completely weather-protected building intended for exhaust gas environmental control instruments. A locked cabinet prevented the computer from unauthorized curiosity.

Figure 3.2 e The recording computer in its cabinet.

Figure 3.2 f The recording computer.

The measurement program collected data continuously and supervised eight signals from the eight strain gauge bridges and two signals from the wind data transmitter (velocity and direction). On the computer screen a virtual instrument presented some output data. An example is shown in Figure 3.2 g.

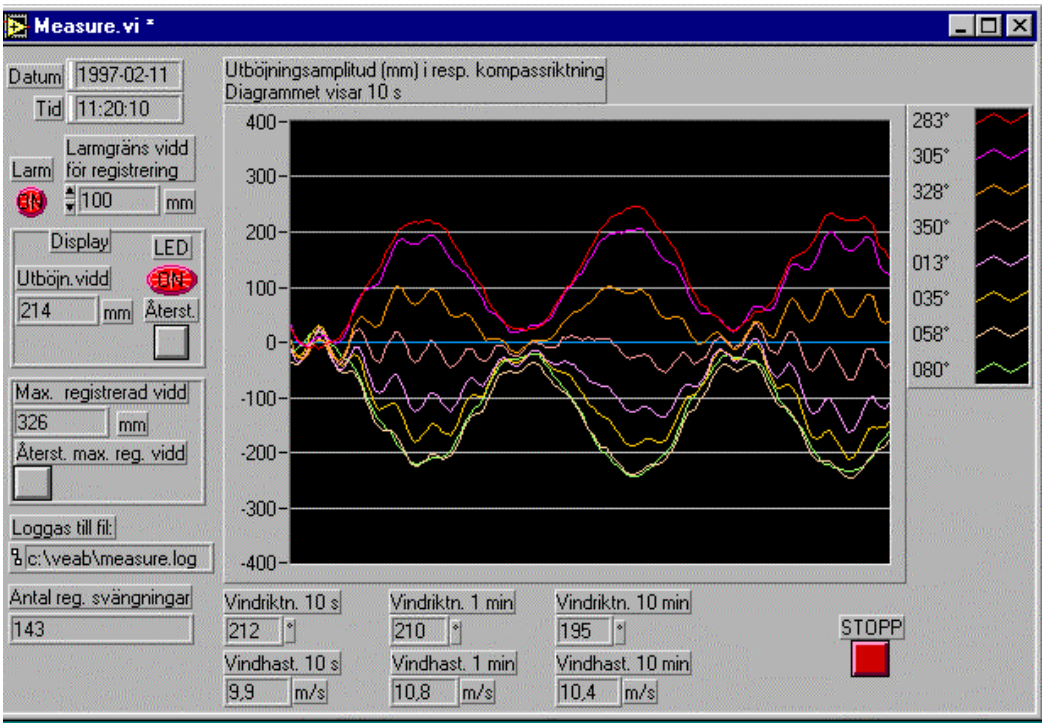

Figure 3.2 g The virtual instrument for recording and supervising the chimney.

The terminology in Swedish of the virtual instrument screen as exemplified in Figure 3.2 g is as follows:

Larmgräns vidd för registrering	If the chimney top deflection range in any direction exceeds this limit value the actual data was stored on the computer hard disk. The virtual lamp Larm was lit only when the top deflection range exceeds the limit value
Display	Actual chimney maximum top deflection range in any direction. The virtual lamp LED was lit once the limit value was exceeded. It has to be switched off by pushing the button Återst.
Max. registerad vidd	Maximum recorded top deflection range was shown. The value has to be set to zero by pushing the button Återst. Max registrerad vidd.
Loggas till fil	Shows name of file to which all recordings were stored.
Antal reg. svängningar	Shows number of recorded registrations since last restart of the program.
Vindriktn. 10s, Vindriktn. 1min, Vindriktn 10 min	Shows wind direction values in 360 degrees according to Figure 3.2 a. Mean values were calculated over a period of 10s, 1 min and 10 min.
Vindhast. 10s, Vindhast. 1 min, Vindhast. 10 min	Shows wind velocity values in m/s. Mean values were calculated over a period of 10s, 1 min and 10 min.
Stopp	A button for stopping the program when copying recorded results.
Utböjningsamplitud (mm) i resp. kompassriktning	This diagram shows the actual amplitude in real time for all eight strain gauge bridges. Results for the last 10 s were shown as default value. For some screen plots other values have been used.

The following data was stored in the recording file, see example in Figure 3.2 b.

1. The number of the recording since last stop of the computer program.
2. Year
3. Month
4. Day
5. Hour
6. Minute
7. Second as an integer
8. Top deflection range for direction 1 as an integer (mm)
9. 2
10. 3
11. 4
12. 5
13. 6
14. 7
15. 8
16. Mean wind velocity 10 s
17. 1 min
18. 10 min
19. Mean wind direction 10 s
20. 1 min
21. 10 min

Table 3.2 b An example from the recorded measurement files.

4449	1997	6	27	16	9	38	81	118	141	155	145	120	78	61	5.2	5	5	270	247	228
4450	1997	6	27	16	9	41	94	144	176	182	165	125	73	48	5.6	4.9	4.9	273	247	229
4451	1997	6	27	16	9	44	99	153	182	186	171	132	79	53	5.6	4.8	4.9	259	247	229
4452	1997	6	27	16	9	48	99	153	186	188	174	133	74	48	6.6	4.7	4.9	254	247	229
4453	1997	6	27	16	9	51	104	164	190	192	164	123	70	47	5.8	4.5	4.9	239	245	229
4454	1997	6	27	16	9	54	114	158	174	168	147	110	58	56	5.7	4.5	4.9	235	242	229
4455	1997	6	27	16	9	58	121	183	210	213	181	129	66	61	5.7	4.4	4.9	222	239	229
4456	1997	6	27	16	10	1	83	146	186	197	185	146	85	52	6.9	4.6	4.9	219	235	229
4457	1997	6	27	16	10	4	94	148	171	168	145	109	61	45	6.5	4.7	4.9	220	236	229

3.2.5 Calculation of top deflection range

Signals from all strain gauge bridges and wind data transmitters were read with a sampling frequency of 1000 values per second. With an interval of 67 ms five samples were collected and mean values were calculated. With actual parameters for the strain gauges, strains were calculated every 67 ms.

From the strains, chimney top deflection range was calculated with the following relationships and Equation 4.6.

$$s = E \cdot e$$

$$y = \frac{s}{0.087} = \frac{E \cdot e}{0.087} \quad \text{.....(3.4)}$$

(s and E in MPa and y in mm)

From the bending moment the bending stress is calculated as:

$$s = \frac{M_b}{W_b}$$

$$W = \frac{I}{\frac{d}{2}}$$

$$s = \frac{M_b}{\frac{2 \cdot I}{d}} \quad \text{.....(3.5)}$$

where
s = Bending stress at level of strain gauges (4 m level)
E = Modulus of elasticity
e = Strain at level of strain gauges (4 m level)
M_b = Bending moment at level of strain gauges (4 m level)
W_b = Section modulus (4 m level)
I = Moment of inertia (4 m level)
d = Diameter

3.2.6 Verification of the equipment

During the installation of the data recording system calibrations were made. A/D and D/A transducers were calibrated in the LABVIEW system. Signals from wind data transmitters were checked. Strains for calculating top deflections were checked using a model chimney with an equal strain gauge as on the chimney. An additional theodolite check of the

deflections to those obtained from the strain gauges was made during the damping tests in August 1997 (see Section 3.3.1). Both deflection range and frequency were checked and compared with computer results.

3.2.7 Procedures

A limit value for recording the results was set to 100 mm equivalent top deflection range to ensure a reasonable amount of recorded data. This means that all results where the maximum range was less than 100 mm were truncated except during the damping tests.

During the first months the computer was checked twice a week. Later the interval was increased to once a week, twice a month and finally once a month. All data results were then transferred to another computer where the evaluations were made. Maximum values were checked and the evaluation computer programs were run (Appendix H). The results were sorted and fatigue damage was calculated.

3.2.8 Operating experiences

The strain gauge equipment started to operate in December 1996 and operated without any problem until January 2000. Two of the strain gauges, no 1 and 3, then started to present unrealistic values and almost immediately became short-circuited. A decision was immediately taken that all strain gauges should be replaced with new ones and that a long-term glue should be used. Fortunately the strain gauge no 4, which was unharmed, had given the largest ranges for the first three years of measurements. Therefore the data recording system could operate satisfactory and deliver trustworthy recordings with only a short break for the installation of the new strain gauges.

During the recording period there were also some small interruptions in recording of data caused by short interruption of the plant electricity. Other interruptions were some minutes each time when the recorded data was transferred from the recording computer to data diskettes. The recording program was always shut off on such occasions.

The recording system has been in operation 99.8 percent of the time during the measurement years.

During the month of July in 1998 the “Larmgräns vidd för registrering” (see section 3.2.4) by a mistake was set to 200 mm instead of the intended value 100 mm. Therefore ranges below 200 mm were truncated that month. There was no correction made for this.

Unfortunately the strain gauges were damaged in the spring of 2001 (see Section 6.6).

3.3 Behaviour of the mechanical damper

3.3.1 Observation of behaviour of chimney with and without damper

3.3.1.1 Introduction

Tests were performed to determine the damping properties of the VEAB chimney, that is, the logarithmic decrement of the chimney with the mechanical damper. The chimney was initially forced to deflect and the resulting free sway of the chimney was recorded. Comparison tests were also made for the chimney with the mechanical damper in a locked position.

The damping test was repeated a number of times in order to get a good mean value of the logarithmic decrement, and to get some understanding of the variability in the measurements.

The damping tests were made in August 1997 in fairly calm weather. The wind was below 6 m/s (10-minute mean) during all tests performed. The test instances were selected in order to avoid influence of aerodynamic damping from gust wind during the damping tests.

3.3.1.2 Setup for Damping tests

A 20 mm nylon rope was attached to the top of the chimney and connected to a wheel loader located approximately 150 m away from the chimney in southward direction. The wheel loader pulled the rope until a desired deflection was obtained. Using a mechanical device the rope was abruptly disconnected close to the wheel loader and the chimney started to oscillate freely. A catch rope was connected to the pulling rope in order to prevent the rope from swaying uncontrolled. The setup for damping measurements is shown in Figure 3.3 a and 3.3 b.

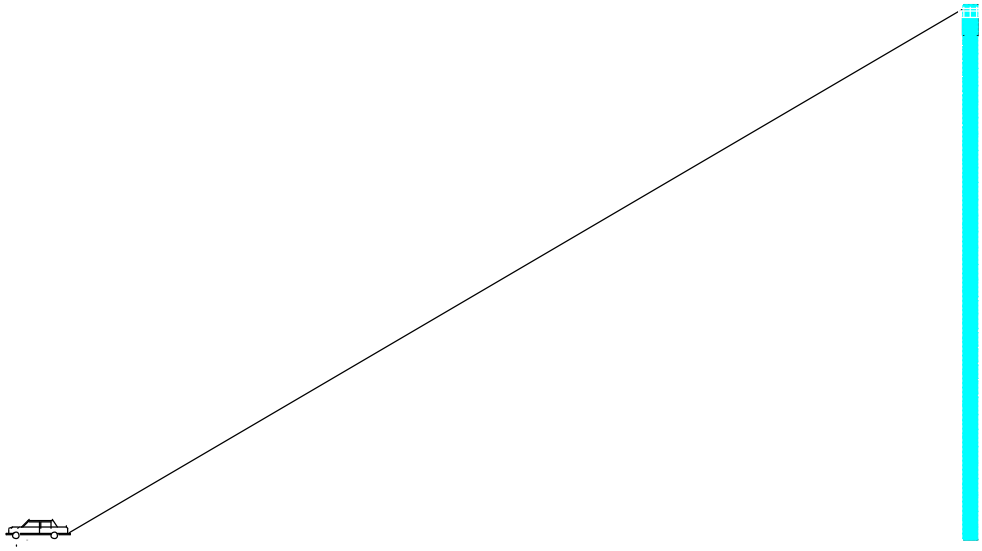

Figure 3.3 a Setup of damping measurements for VEAB chimney – view

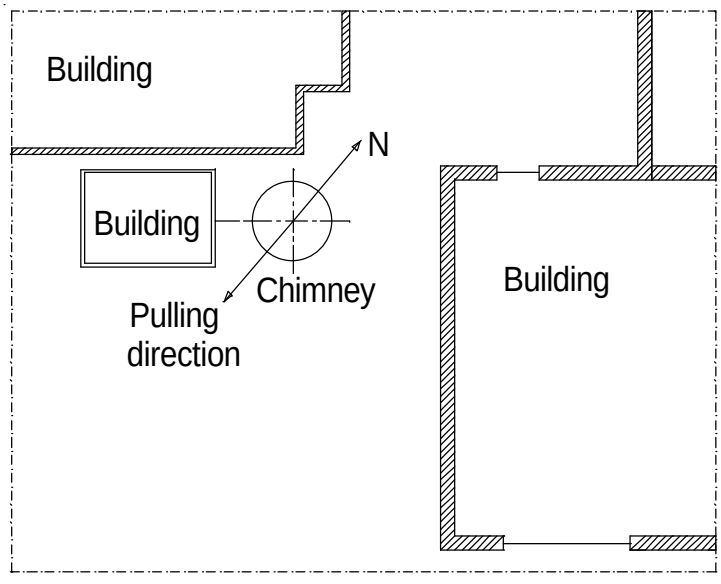

Figure 3.3 b Setup of damping measurements for VEAB chimney - plan

The top of the chimney was forced to deflect a maximum distance of 200 mm for a free mechanical damper and 100 mm for the chimney the comparison test with locked damper. This limit was used in order to secure that the damping device would not be harmed in any way. The normal recording program to determine oscillations from wind and other actions was in effect during the damping tests.

Deflections at the top of the chimney were calculated from recordings of the strain gauges attached to the chimney (see Section 3.2), which had been calibrated to the top deflections. Deflections of the chimney were checked also using a theodolite. These visual observations showed good agreement with the recordings obtained from the strain gauges.

Similar measurements of damping of other slender structures have been reported in the literature, see for instance [2].

During the course of the damping measurements the wind velocity and direction were recorded using the wind indicator located on the top of the adjacent power plant building at 45 m height above ground and at a distance of approximately 43 m from the chimney (see Section 3.2.3.1). The wind velocity during the damping tests was very low, and in no instances exceeded 6 m/s (10-minute mean) or 8 m/s (10 s mean). The wind direction was approximately the same as the pulling direction in the damping tests.

3.3.1.3 Recordings

A total number of 20 tests were performed to verify the damping of the chimney. Tests # 1 through 16 refer to the chimney with the mechanical damper acting in normal operation. Tests # 17 through 20 refer to the chimney with a locked damper.

The data was collected using strain gauge readings and the recording computer described previously (se Section 3.2).

It should be observed that recordings refer to *variations* in actions, in this case deflection *range* rather than the deflection itself. This is because the recording system was designed to verify performance of the chimney with respect to fatigue, where *variation* of stress, that is, stress range, is of utmost importance. Where required, deflection itself has been evaluated from the deflection-range data, as discussed below.

Some examples of screen plots showing the parts of the oscillation behaviour during the damping tests are shown in Figures 3.3 c, 3.3 d and 3.3 e.

The recorded natural frequency (first mode) of the chimney with the mechanical damper in normal operation was 0.253 Hz. For the chimney with locked damper the recorded natural frequency was 0.258 Hz.

The natural frequency obtained from the damping tests differ by 10 percent from the natural frequency calculated theoretically for the chimney considering the actual distribution of stiffness and mass along the chimney, see Section 2.4.1 and from that measured 0.288 Hz, see Section 3.7.2.

One explanation could be that the first cycles of time history for the two mass damped systems have an irregular behaviour. This explanation is supported by the irregular curve for the first cycles as shown in the screen plots in Figures 3.3 c, 3.3 d, 3.3 e and in Appendix C.

Another explanation could be that the damper may have been tuned by the manufacturer of the chimney during the days of damping tests. A definite explanation for this discrepancy has not been found. Thus natural frequency was about the same with and without an acting damper.

All recordings from the damping tests have been collected in Appendix C. A data file with results from the recording program is shown in tables. Some explanations and support lines have been included there to facilitate the interpretation of the data.

In Appendix C is also plotted the Deflection Range (that is, twice the deflection) as a function of the order of the oscillation cycle.

Furthermore, in Appendix C is shown a screen plot of the virtual recording instrument for all damping tests. In evaluating the results it should be observed that the recording limit of 100 mm means that a few cycles at the end of the course of sway action may not be registered.

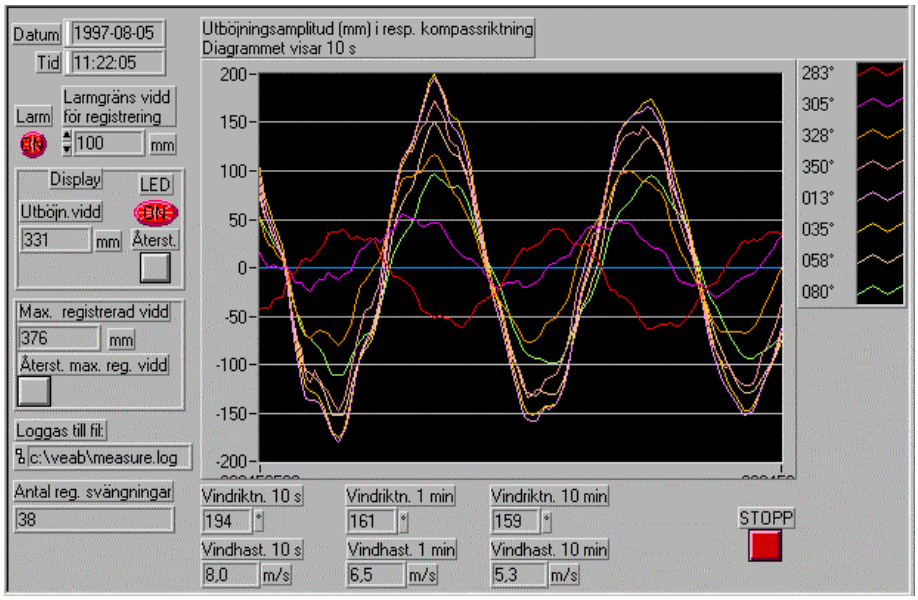

Figure 3.3 c Screen plot of first oscillations after loosening the pulling rope, test no 1 of chimney with mechanical damper in normal operation.

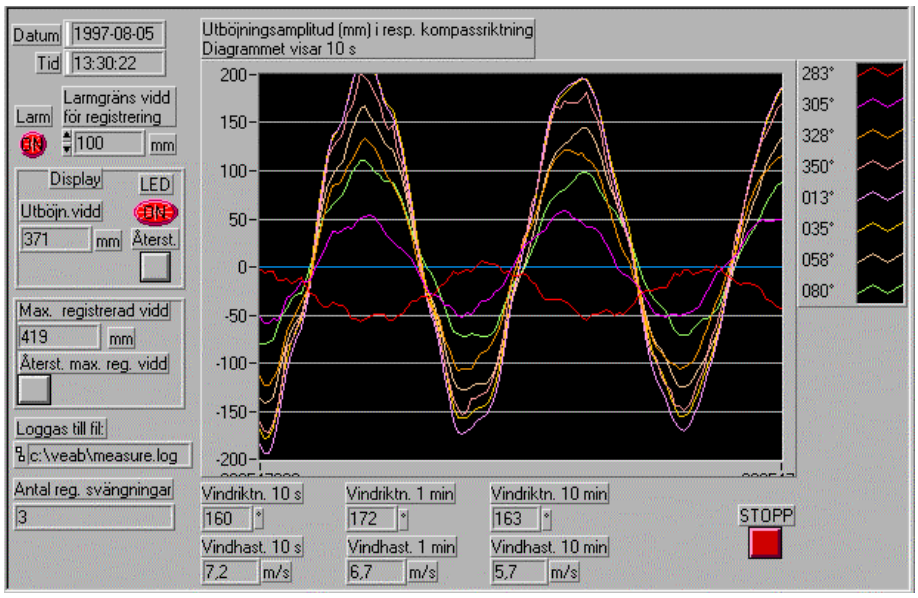

Figure 3.3 d Screen plot of first oscillations after loosening the pulling rope, test no 4 of chimney with mechanical damper in normal operation.

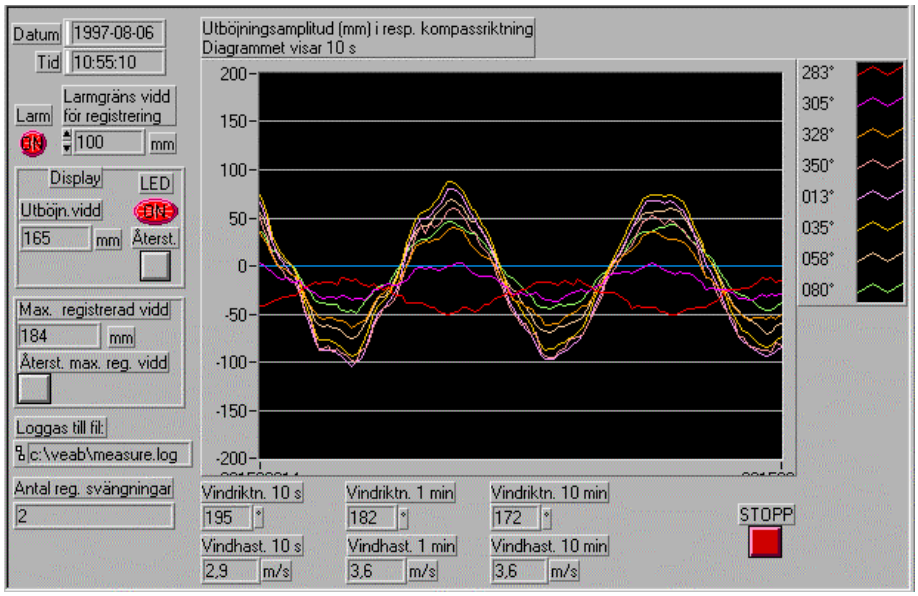

Figure 3.3 e Screen plot of first oscillations after loosening the pulling rope, test no 17 of chimney with locked mechanical damper.

3.3.1.4 Error when calculating logarithmic decrement from recorded deflection range

All measurements and the calculations of logarithmic decrement were based on the *deflection range* that is, not the deflection itself. This will cause an error in the calculated value of the logarithmic decrement. The magnitude of this error is calculated in the following.

Symbols in this section, such as w , differ from those used in others sections.

For a free single degree of freedom system with viscous damping less than critical the deflection y is found from [10]

$$y = C \cdot e^{-z \cdot w_n \cdot t} \cdot \sin\left(w_d \cdot t + q\right) \quad \text{.....(3.6)}$$

where

C	=	An arbitrary constant
z	=	Relative damping
w_n	=	The undamped natural frequency
w_d	=	The damped natural frequency
t	=	Time
q	=	The phase angle

$$d = \frac{2 \cdot p \cdot z}{\sqrt{1 - z^2}}$$

$$w_n = 2 \cdot p \cdot f$$

$$w_d = w_n \cdot \sqrt{1 - z^2}$$

where

f = Natural frequency
d = Logarithmic decrement

For the VEAB chimney the typical values are

$f = 0.288$ Hz , the observed natural frequency according to Section 3.7.2
$d = 0.07$ for functioning damper and 0.04 for mal-functioning damper, the observed logarithmic decrement according to Section 3.3.1.6

Inserting these typical values into the parameter expressions will yield (the number of digits required is large to obtain the required accuracy)

$z = 0.0111$ (0.0065 for malfunctioning damper)
$w_n = 1.809557$ rad/s
$w_d = 1.809446$ rad/s

With the selected phase angle 90 degrees the deflection may be written

$$y = C \cdot e^{-0.02009 \cdot t} \cdot \sin\left(1.809446 \cdot t + \frac{p}{2}\right) \quad \text{.....(3.7)}$$

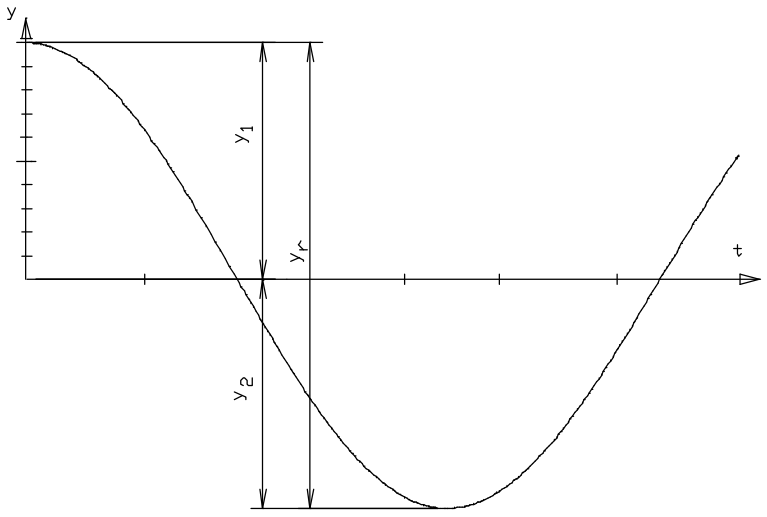

Figure 3.3 f Deflection as a function of time.

With y_1, y_2 and y_r as defined in Figure 3.3 f and the phase angle $\theta = 90$ degrees we achieve

$$y_r = y_1 + y_2$$

$$y_1 = \left| C \cdot e^{-\zeta \omega_n 0} \cdot \sin\left(\omega_d \cdot 0 + \frac{\pi}{2}\right) \right|$$

$$y_2 = \left| C \cdot e^{-\zeta \omega_n \frac{0.5}{f}} \cdot \sin\left(\omega_d \cdot \frac{0.5}{f} + \frac{\pi}{2}\right) \right|$$

$$\frac{y_2}{y_1} = e^{-\zeta \pi \frac{0.5}{f}} \cdot \sin\left(2 \cdot \pi \cdot f \cdot \sqrt{1-\zeta^2} \cdot \frac{0.5}{f} + \frac{\pi}{2}\right) \approx e^{-\zeta \pi \frac{0.5}{f}} = e^{-0.06054\pi} = 0.9413$$

$$y_r = y_1 + 0.9413 \cdot y_1$$

$$y_1 = \frac{y_r}{1.9413} = 0.5151 \cdot y_r$$

$$y_r = \frac{y_2}{0.9413} + y_2$$

$$y_2 = \frac{y_r}{1 + \frac{1}{0.9413}} = \frac{y_r}{2.062} = 0.485 \cdot y_r$$

In the evaluation we use the amplitude

$$y = \frac{y_r}{2}$$

and get an error of

$$\Delta = 1 - \frac{\frac{y_r}{2}}{y_1} = 1 - \frac{\frac{y_r}{2}}{0.5151 \cdot y_r} = 1 - 0.971 = 0.029$$

This means that the evaluation procedure using range instead of amplitude will result in a 3 percent underestimation of the correct result. The results could have been corrected for this, however the correction is small compared to other uncertainties and has therefore been neglected.

3.3.1.5 Evaluation of Logarithmic Decrement

The logarithmic decrement d was calculated from Equations 3.8.

$$d = \ln(y_n / y_{n+k}) / k \quad \text{.....(3.8)}$$

where

y_n = Deflection for the first oscillation considered
y_{n+k} = Deflection for the final oscillation considered
k = Number of oscillations considered

The first, and in some instances also the second, oscillation after loosening the pulling rope were disregarded in evaluating the logarithmic decrement. This is because the start of the deflection history may be non-linear, and causing the computer evaluation program to make an incorrect calculation of the deflection range for the first and second oscillation.

Mean values of the logarithmic decrement $d_{ave\,k}$ were obtained for each 20 damping tests from this starting value until the deflection falls below the value of 100 mm, that is, a deflection range of 200 mm. This would lead to 6 to 12 oscillations being considered for the chimney with the damper in normal operation, and 3 to 9 oscillations for the chimney with locked damper. By averaging over a number of oscillations the influence of damping due to action of any gust winds or irregularities in the action of the damper during the tests should be minimized.

Alternate calculations of the logarithmic decrement were made applying a set of three consecutive oscillations (that is, with n running from first to final value considered and $k = 3$) to study the variation in the logarithmic damping as obtained in the test. Figure 3.3 g shows an example of such an alternate calculations. From studying such variations it was concluded that the variation was not significant and should be caused by various irregularities due to the fact that the tests were made under field conditions. Data for such alternative calculations are included in Appendix C.

The results of the 20 damping tests performed are summarized in Table 3.3 a. ”Initial deflection range” in the table equals the sum of the initial deflection at the moment of loosening the pulling rope and the following minimum value of the deflection, see Figure 3.3 h. “Number of oscillations k” refers to the number considered in determining the logarithmic decrement $d_{ave\,k}$ given in the final column of Table 3.3 a.

Examples of deflection range as a function of time for two of the 20 tests performed are shown in Figure 3.3 h and 3.3 i. The first diagram is for tests with the mechanical damper in normal operation and the third for a test with a locked damper.

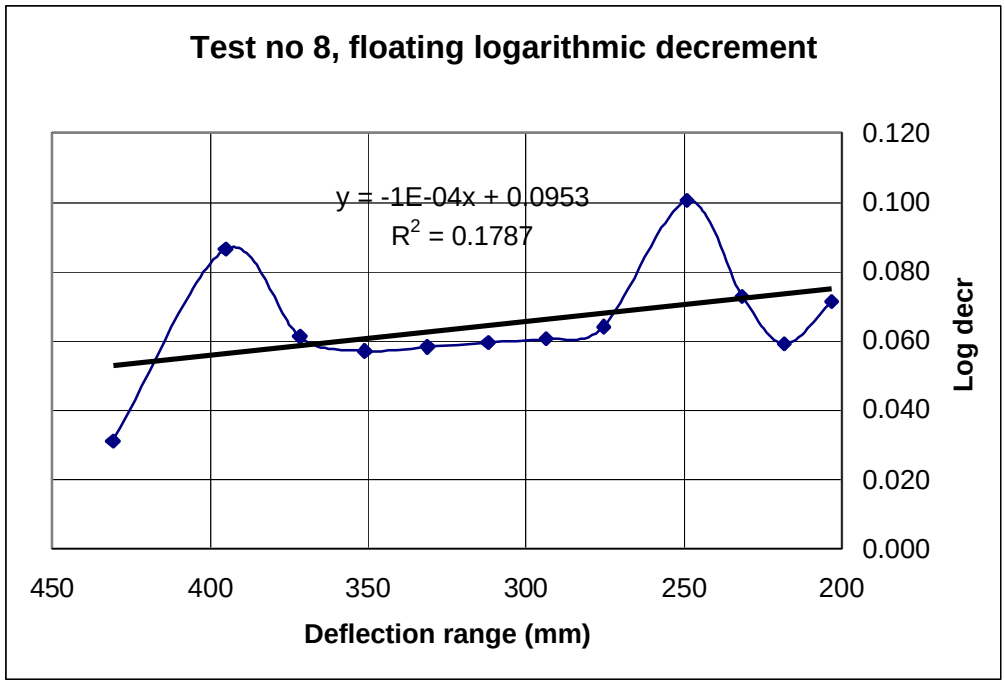

Figure 3.3 g Example of variation in recorded logarithmic decrement d determined for three consecutive oscillations. Test no 8.

Table 3.3 a Conditions and results from 20 tests of damping of VEAB chimney

Test #	Time of test	Initial deflection range (mm)	Wind velocity (m/s) 10 s	1 min	10 min	Wind direction (degrees, 0 / 360) 10 s	1 min	10 min	Number of oscill. k	Logarithmic decrement d_{avek}
Chimney with mechanical damper in normal operation, date 97-08-05										
1 *	11.22	376	8.0	6.5	5.3	194	161	159	6	0.072
2 **	12.55	304	5.0	4.7	2.9	168	172	118	7	0.064
3	13.04	425	4.5	6.4	4.8	179	170	173	10	0.057
4	13.30	419	7.2	6.7	5.7	160	172	163	8	0.070
5	13.34	422	5.2	5.7	5.6	173	169	164	9	0.062
6	13.38	394	4.9	6.2	5.6	136	152	162	6	0.098
7 ***	13.41	382	6.3	4.8	5.6	156	154	164	6	0.081
8	16.45	507	4.3	3.6	3.1	181	187	169	12	0.065
9	16.55	415	3.3	3.7	3.3	219	191	184	10	0.068
10	16.59	411	4.3	3.5	3.4	170	193	186	7	0.070
11	17.01	421	3.7	3.8	3.5	168	172	185	7	0.078
12 **	17.04	445	2.3	3.1	3.5	171	172	182	9	0.068
13	20.31	445	3.6	2.9	2.5	170	169	172	10	0.063
14 **	20.36	426	1.9	2.7	2.7	185	173	172	6	0.068
15	20.40	397	3.4	2.7	2.8	157	165	170	8	0.068
16 **	20.44	382	2.7	3.3	3.1	168	155	164	7	0.071
Mean				4.0			168		0.070	
Standard deviation										0.009
Chimney with locked mechanical damper, date 97-08-06										
17	10.55	184	2.9	3.6	3.6	195	182	172	4	0.038
18	10.58	202	2.4	2.5	3.8	210	191	175	9	0.031
19	11.04	191	4.8	5.8	3.9	184	182	175	5	0.056
20	11.09	185	3.7	3.3	3.9	137	131	170	3	0.048
Mean				3.8			173		0.043	
Standard deviation										0.011

Notes to table:

* A technician was standing on the platform at the top of the chimney during the test.

** During the course of oscillations one or two irregularities were obtained. These oscillations were disregarded in determining the mean logarithmic decrement d_{avek} given in the table.

*** The pulling rope fractured near the top of the chimney instead of at the wheel loader.

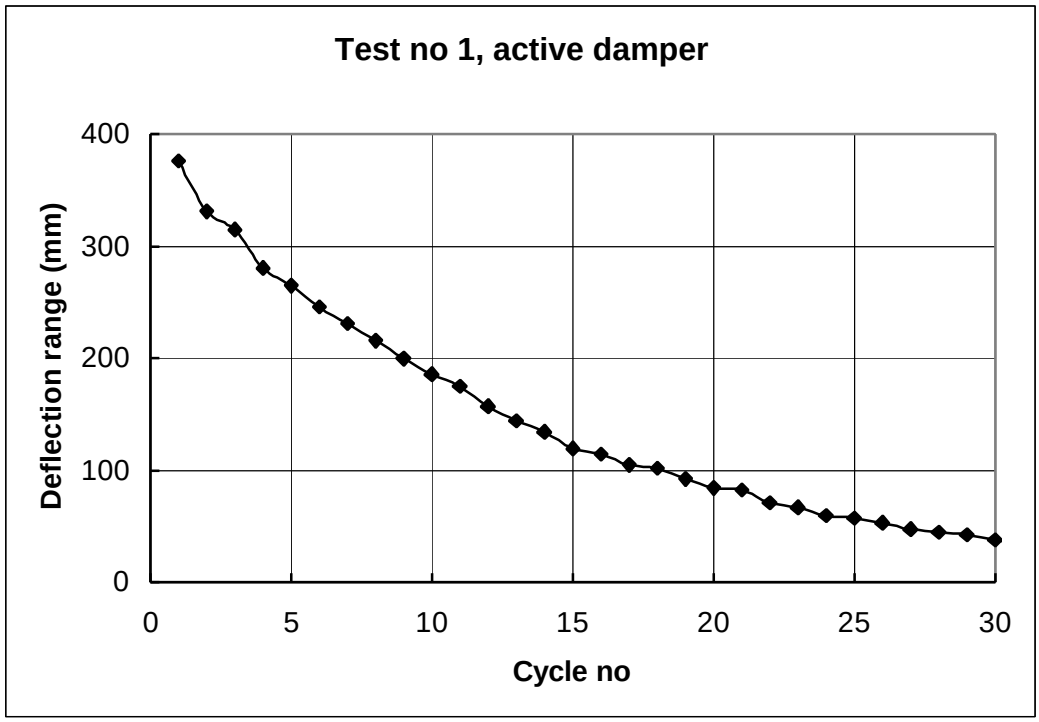

Figure 3.3 h Deflection range as a number of time (cycle number). Test no 1 with mechanical damper in normal operation. One cycle corresponds to approximately 3.5 s.

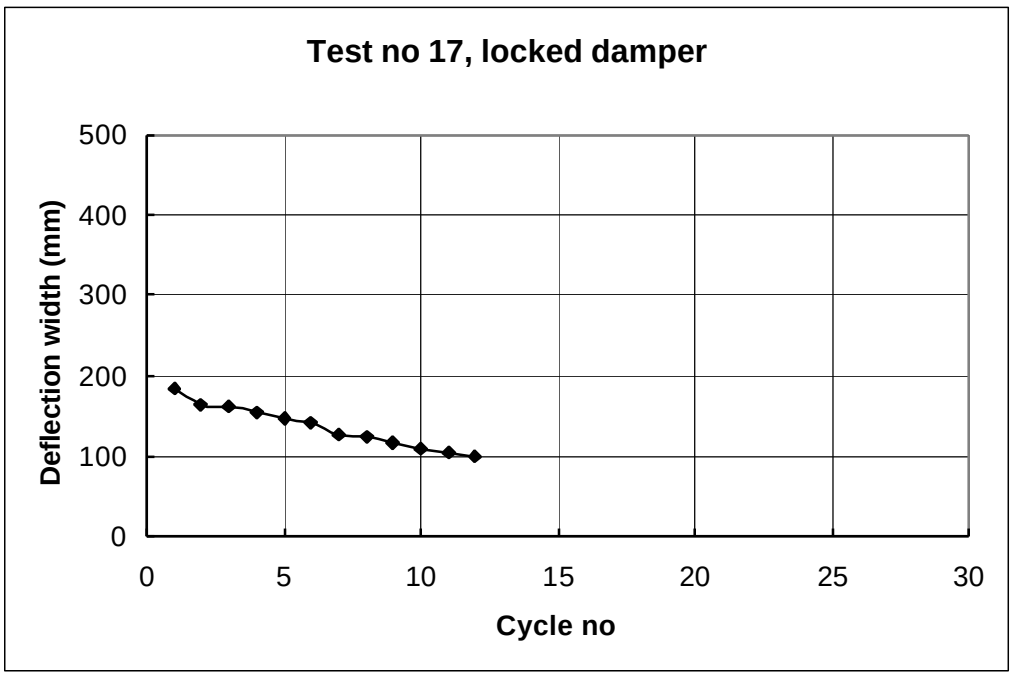

Figure 3.3 i Deflection range as a number of time. Test no 17 with locked damper. One cycle corresponds to approximately 3.5 s.

Further examples are found in Appendix C.

The recorded damping expressed as logarithmic decrement d consists of three parts:

$$d = d_a + d_m + d_d \quad \text{..... (3.9)}$$

where

d_a = aerodynamic damping
d_m = mechanical damping of the chimney, without damper
d_d = mechanical damping of the damper

The mean recorded logarithmic decrement for the chimney with the mechanical damper in normal operation is 0.070. The logarithmic decrement in the 16 tests performed varies from 0.057 to 0.098.

The mean recorded logarithmic decrement for the chimney with a locked damper is 0.043. The logarithmic decrement variation in the four tests performed varies from 0.031 to 0.056.

Thus, the recorded logarithmic decrement of the chimney with the mechanical damper in normal operation was 63 percent higher than for the chimney with a locked damper. This beneficial effect was smaller than could be expected, considering the fact that a theoretical study performed by the supplier of the chimney claimed a tenfold increase in the logarithmic decrement when adding the mechanical damper to the chimney. The probable cause for this is discussed in Section 3.3.2.5.

3.3.1.6 Discussion of results

The recorded logarithmic decrement d =0.043 is somewhat higher than the range 0.02 to 0.03, to be used for design of normal steel chimneys with installations, such as internal ducts, ladder etc. as given in [3], [5]. This increase in damping may at least partly be caused by some beneficial action from the mechanical damper, although it was locked to minimise such action and from effective damping of non-structural elements.

The mechanical damper will increase the mean value of the logarithmic decrement of the chimney d =0.07 over the normal upper design value of 0.03 [3], [5] by a factor of 2.3.

The relatively large variation in the logarithmic decrement obtained in the repeated tests, expressed as a standard deviation of about 0.01, could be due to at least three reasons, listed here in the order of estimated importance:

1) Accidental variations in the action of the mechanical damper

2) Disturbances from variations in environmental conditions, mainly aerodynamic damping due to variations in wind velocity and wind direction, due to the fact that these tests were made under field conditions

3) Inaccuracies in the recording system.

The recorded logarithmic decrement of the VEAB chimney, with the mechanical damper in normal operation, agrees well with the damping assumed in the design calculations prepared by the chimney supplier, but was considerably smaller than could be expected from a theoretical study.

In [11] a full scale damping test for a 45 m chimney with a tuned damper was made. As in our damping tests the damper was both locked and unlocked. The logarithmic decrement was found to be 0.019 with locked damper and 0.5 to 0.6 with unlocked damper. Compared to the VEAB chimney the damping arrangement as reported in [11] appears much more efficient.

3.3.2 Theoretical study of chimney behaviour with and without damper

3.3.2.1 Model

Ruscheweyh has presented a simplified calculation model for a chimney provided with a tuned pendulum mass damper [6]. In the model, damping from the mass damper k_1 was neglected. This model has been extended in this section to account for the effect of the mass damper k_1.

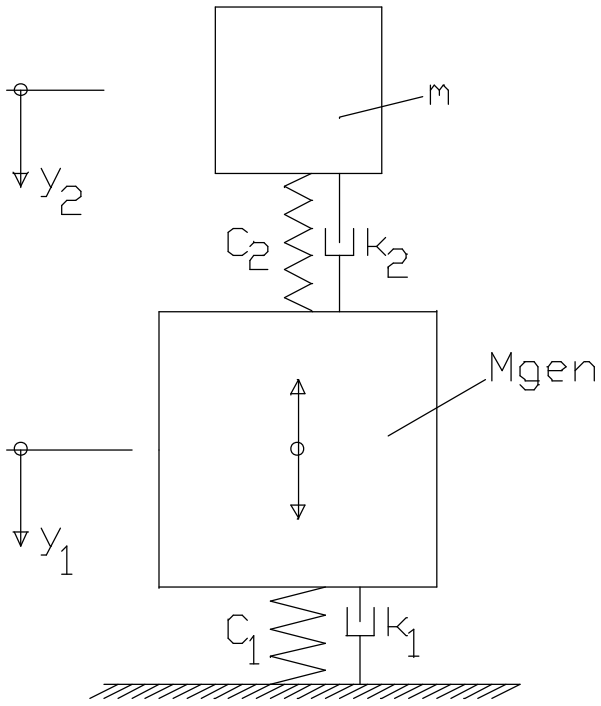

Figure 3.3 j Model of a two mass spring and damper system

$$M_{gen}\frac{d^2y_1}{dt^2} + c_1 \cdot y_1 + c_2 \cdot (y_1 - y_2) + k_1 \cdot \frac{dy_1}{dt} + k_2 \cdot (\frac{dy_1}{dt} - \frac{dy_2}{dt}) = F \cdot \sin(w \cdot t) \quad \text{.....(3.10)}$$

$$m \cdot \frac{d^2y_2}{dt^2} + c_2 \cdot (y_2 - y_1) + k_2 \cdot (\frac{dy_2}{dt} - \frac{dy_1}{dt}) = 0 \quad \text{.....(3.11)}$$

where M_{gen} = Generalised mass of the chimney
m = Damper pendulum mass

F = Amplitude for vortex shedding force

y_1 = Deflection of chimney
y_2 = Deflection of pendulum mass

c_1 = Chimney stiffness
c_2 = Damper stiffness

k_1 = Chimney damping
k_2 = Damper damping

v_1 = Velocity for M_{gen}
v_2 = Velocity for m

a_1 = Acceleration for M_{gen}
a_2 = Acceleration for m

w = Angular frequency of vortex shedding

The differential equations were rewritten as finite difference equations and solved for a large number of small time steps with a computer program. Accuracy and convergence was checked by changing the time steps.

Start values are v_{10}, v_{20}, y_{10} and y_{20} where the second index means time zero.

The finite differences may be written

$$\frac{\Delta(\frac{\Delta y_1}{\Delta t})}{\Delta t} = \left[-(c_1 + c_2) \cdot y_{10} + c_2 \cdot y_{20} - k_1 \cdot \frac{\Delta y_{10}}{\Delta t} - k_2 \cdot \frac{\Delta y_{10}}{\Delta t} + k_2 \cdot \frac{\Delta y_{20}}{\Delta t} + F \cdot \sin(w \cdot t) \right] \cdot \frac{1}{M_{gen}} \quad \text{.....} \quad (3.12)$$

$$\frac{\Delta(\frac{\Delta y_2}{\Delta t})}{\Delta t} = \left[c_2 \cdot y_{10} - c_2 \cdot y_{20} + k_2 \cdot \frac{\Delta y_{10}}{\Delta t} - k_2 \cdot \frac{\Delta y_{20}}{\Delta t} \right] \cdot \frac{1}{m} \quad \text{.....} \quad (3.13)$$

$$a_1 = \frac{\Delta(\frac{\Delta y_1}{\Delta t})}{\Delta t} \quad \text{.....} \quad (3.14)$$

$$a_2 = \frac{\Delta(\frac{\Delta y_2}{\Delta t})}{\Delta t} \quad \text{.....} \quad (3.15)$$

$$\Delta v_1 = a_1 \cdot \Delta t \quad \text{.....} \quad (3.16)$$

$$\Delta v_2 = a_2 \cdot \Delta t \quad \text{.....} \quad (3.17)$$

$$v_1 = v_{10} + \Delta v_1 \quad (3.18)$$

$$v_2 = v_{20} + \Delta v_2 \quad (3.19)$$

$$\Delta y_1 = v_1 \cdot \Delta t \quad (3.20)$$

$$\Delta y_2 = v_2 \cdot \Delta t \quad (3.21)$$

$$y_1 = y_{10} + \Delta y_1 \quad (3.22)$$

$$y_2 = y_{20} + \Delta y_2 \quad (3.23)$$

Critical wind velocity at vortex shedding is calculated according to Equation 2.5 and wind velocity pressure according to Equation 2.7.

A computer program, see Appendix H, has been developed which takes into consideration all variables above. It also deals with the wind turbulence by allowing a randomised relative level of the amplitude for vortex shedding force and the frequency of the vortex shedding. The program is capable of creating a dynamic response for a frequency spectrum and a time history.

3.3.2.2 Input data

The following data was used as input data for this theoretical study of the damped system.

Generalised mass, M_{gen}	12 460 kg *)
Damper pendulum mass, m	$0.1 \cdot 12\,460 = 1\,246$ kg *)
Observed natural frequency, f_{e1} see Section 3.7.2	0.288 Hz
Optimum damper frequency tuning according to [6]	$f_{e2} = \frac{1}{1+0.1} \cdot f_{e1} = 0.262$ Hz (3.24)

For determining the stiffness of the VEAB chimney an equivalent load, calculated according to Section 2.4.2, was applied on the complete height of the chimney in the same FE calculation as in Section 2.4.1. The results are shown in Figure 3.3 k.

*) Data given by the manufacturer of the chimney. See also chapter 2.3.2.

For a cantilever beam loaded by a distributed load the deflection is

$$d_q = \frac{q \cdot L^4}{8 \cdot E \cdot I} \quad \text{.....(3.25)}$$

For a cantilever beam loaded by a point load at distance L the deflection is

$$d_F = \frac{F \cdot L^3}{3 \cdot E \cdot I} \quad \text{.....(3.26)}$$

The distributed load, when the complete chimney height is assumed to be loaded by vortex shedding loads according to Table 2.4 b is

$$q = m_{tr} \cdot p_{cr} \cdot d = 0.2 \cdot 6.56 \cdot 2.3 = 3.0 \text{ N/m} \quad \text{.....(3.27)}$$

The point load replacing the distributed load will be

$$d_F = d_q \quad \Rightarrow$$

$$F = \frac{3}{8} \cdot q \cdot L = \frac{3}{8} \cdot 3.0 \cdot 90 = 102 \text{ N} \quad \text{.....(3.28)}$$

Point load for calculating stiffness when q=135 N/m according to Table 2.4 b is used

$$F = \frac{3}{8} \cdot q \cdot L = \frac{3}{8} \cdot 135 \cdot 90 = 4556 \text{ N} \quad \text{.....(3.29)}$$

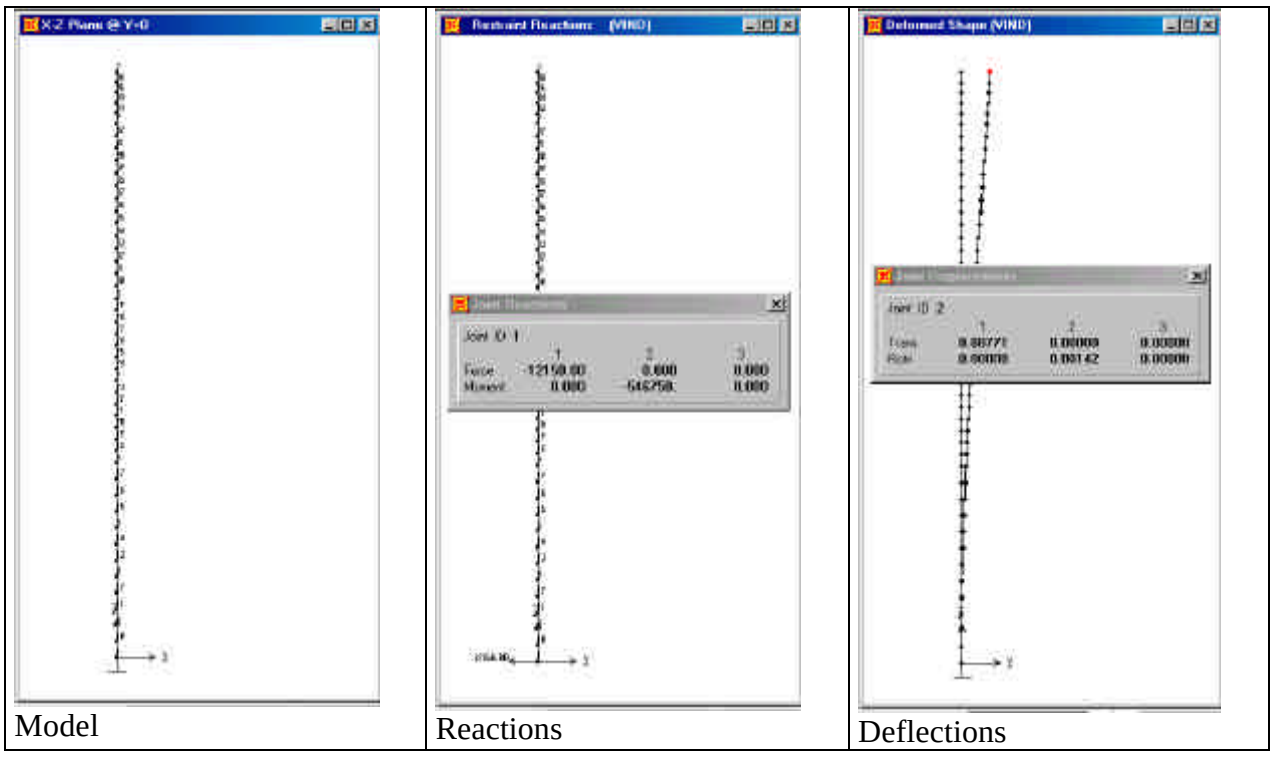

Model | Reactions | Deflections

Figure 3.3 k Deflections of the chimney loaded by vortex shedding.

Chimney stiffness

$$c_1 = \frac{4\,556}{0.0877} = 52\,000 \text{ N/m} \quad \text{.....(3.30)}$$

Damper stiffness

$$c_2 = m \cdot (2 \cdot p \cdot f_{e2})^2 = 1\,246 \cdot (2 \cdot p \cdot 0.262)^2 = 3\,372 \text{ N/m} \quad \text{.....(3.31)}$$

Logarithmic decrement according to [12]

$$d_1 = \ln\left(\frac{y_{10}}{y_1}\right) = \frac{2 \cdot p \cdot V_1}{\sqrt{1 - V_1^2}} \quad \text{.....(3.32)}$$

$$2 \cdot V_1 = \frac{k_1}{\sqrt{c_1 \cdot m}} \quad \text{.....(3.33)}$$

$$d_2 = \ln\left(\frac{y_{20}}{y_2}\right) = \frac{2 \cdot p \cdot V_2}{\sqrt{1 - V_2^2}} \quad \text{.....(3.34)}$$

$$2 \cdot V_2 = \frac{k_2}{\sqrt{c_2 \cdot M_{gen}}} \quad \text{.....(3.35)}$$

where z = The fraction of critical damping or relative damping

From Equations 3.33 through 3.35 the logarithmic decrement of the chimney 0.04 corresponds to a damping of k_1=324 kg/s. Similarly the logarithmic decrement of the pendulum damper 0.03 corresponds to a damping of k_2=19 kg/s.

From a comparison study the time step found to be acceptable considering convergence and precision is

$\Delta t = 0.001 \text{ s}$

Start values for dynamic response calculations during vortex shedding at time 0:

$y_{10} = 0$
$y_{20} = 0$
$v_{10} = 0$
$v_{20} = 0$

The density of air was assumed to 1.25 kg/m^3.

The actual wind is neither constant in frequency nor magnitude. The model applied in the computer program was therefore created to consider a randomised turbulence vortex shedding frequency and amplitude for vortex shedding force. Both with and without the 50 percent randomised turbulence vortex shedding frequency and amplitude for vortex shedding force were applied in the computer program. According to Section 3.4, 50 percent is a reasonable value for both frequency and magnitude. In the following calculations Figures 3.3 p and 3.3 q show two examples.

When calculating the dynamic response the frequency step used in the finite difference calculation has been 0.01 Hz.

Start values for the damping test calculations at time 0:

y_{10} = 200 mm
y_{20} = 0
v_{10} = 0
v_{20} = 0

The corresponding amplitude for vortex shedding force was then F=0.

3.3.2.3 Dynamic response during vortex shedding

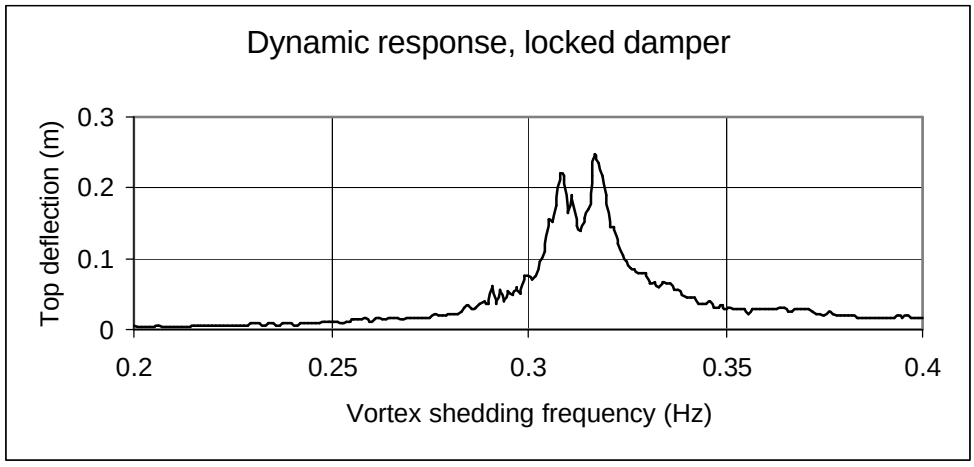

Figure 3.3 l Dynamic response of top amplitude deflection during vortex shedding and a locked (mal-functioning) damper. Both vortex shedding frequency and vortex shedding force were randomised by 50 percent. The vortex shedding force varies with the oscillating frequency. Maximum top amplitude was calculated to 0.248 m (the maximum point in the diagram) deflection at vortex shedding frequency 0.317 Hz.

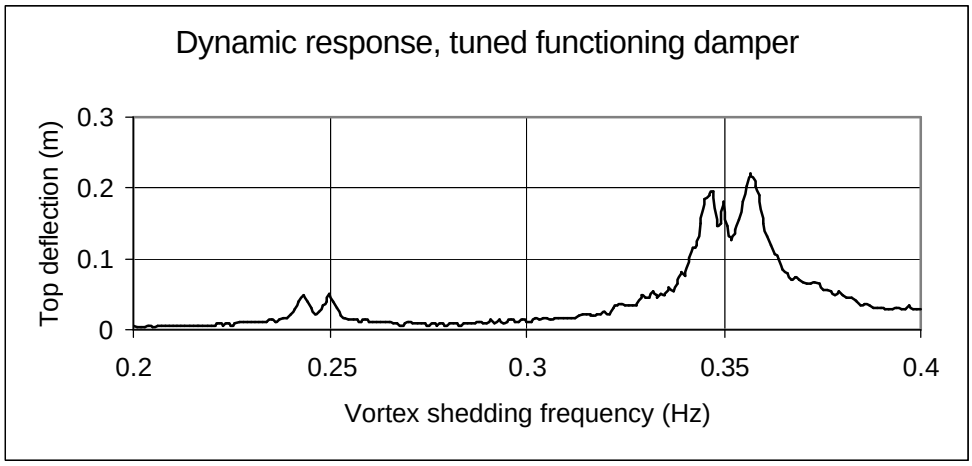

Figure 3.3 m Dynamic response of top amplitude deflection during vortex shedding and a tuned functioning damper. Both vortex shedding frequency and critical wind velocity during vortex shedding were randomised to 50 percent. The vortex shedding force varies with the oscillating frequency. Maximum top amplitude deflection was calculated to 0.220 m at vortex shedding frequency 0.357 Hz.

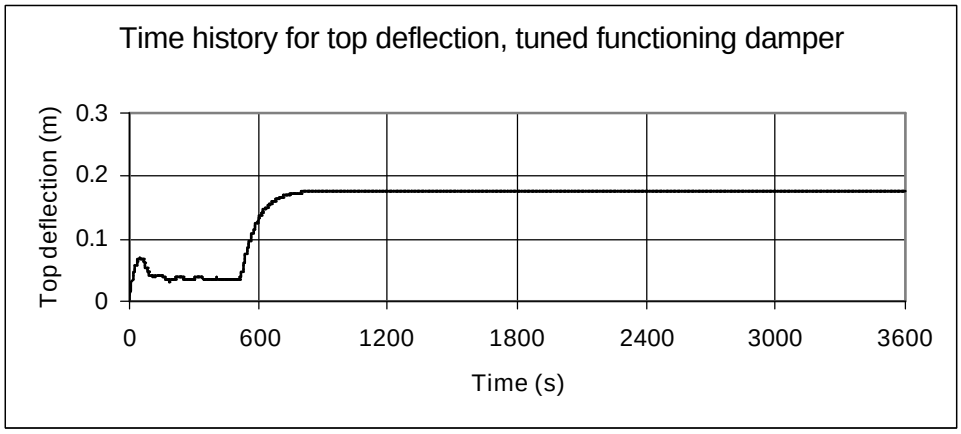

Figure 3.3 n Time history of top amplitude deflection at the vortex shedding frequency f=0.357 Hz and a tuned functioning damper. Neither vortex shedding frequency nor critical wind velocity during vortex shedding was randomised.

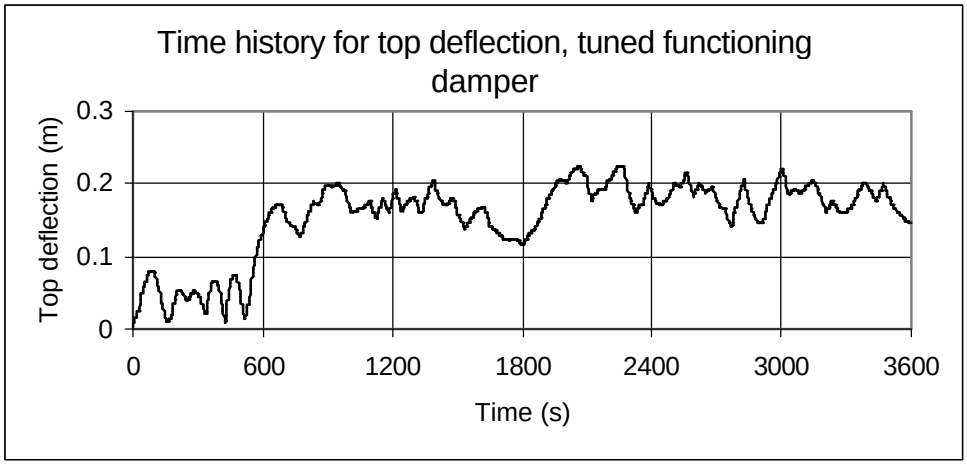

Figure 3.3 o Time history of top amplitude deflection at the vortex shedding frequency f=0.357 Hz and a tuned functioning damper. Both vortex shedding frequency and critical wind velocity during vortex shedding were randomised by 50 percent according to figure 3.3 p and 3.3 q.

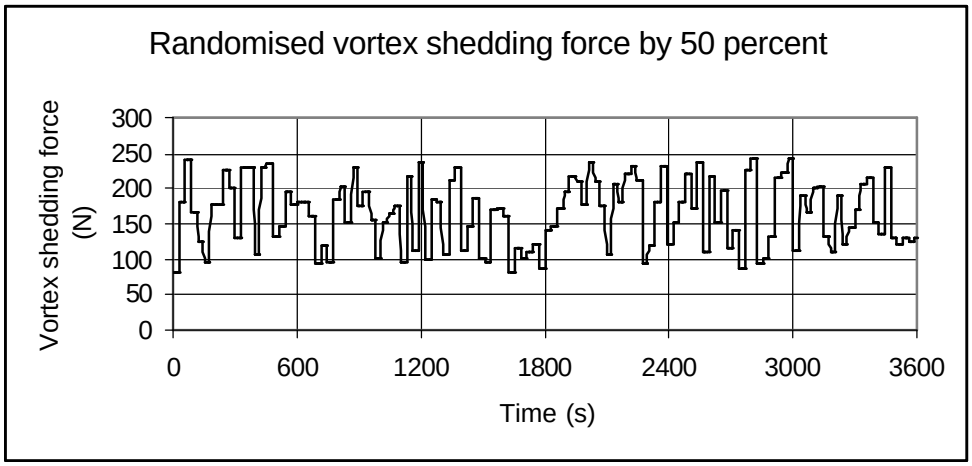

Figure 3.3 p The 50 percent-randomised vortex shedding force used for Figure 3.3 o.

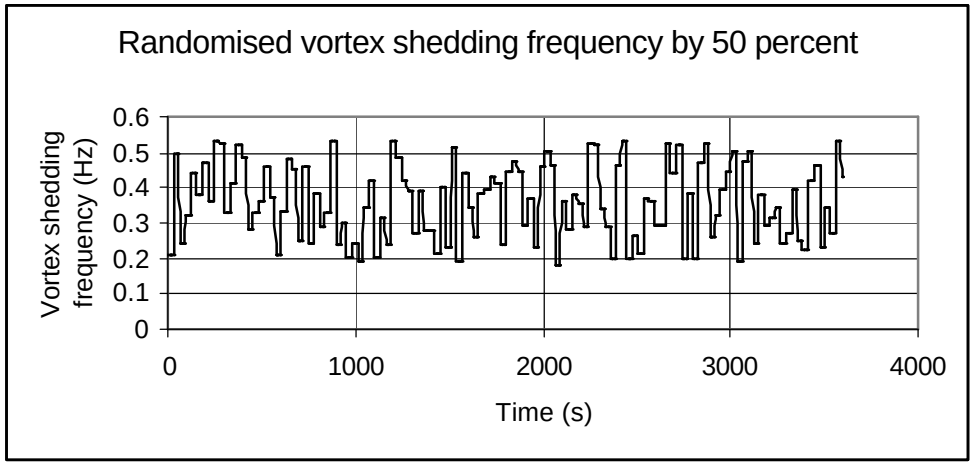

Figure 3.3 q The 50 percent-randomised vortex shedding frequency used for Figure 3.3 o.

3.3.2.4 Dynamic response during vortex shedding and a mistuned damper

To study the influence of an error in the tuning of the damper it is assumed that the first mode of natural frequency is 0.34 Hz instead of the correct value 0.288 Hz (Section 3.7.2).

The frequency tuning is calculated to

$$f_{e2} = \frac{1}{1+0.1} \cdot f_{e1} = \frac{1}{1.1} \cdot 0.34 = 0.31 \text{ Hz} \quad \text{.....(3.36)}$$

This means that the damper stiffness will be

$$c_2 = m \cdot (2 \cdot p \cdot f_{e2})^2 = 1246 \cdot (2 \cdot p \cdot 0.31)^2 = 4727 \text{ N/m} \quad \text{.....(3.37)}$$

Similar calculations as in Section 3.3.2.3 are performed with the new damper stiffness.

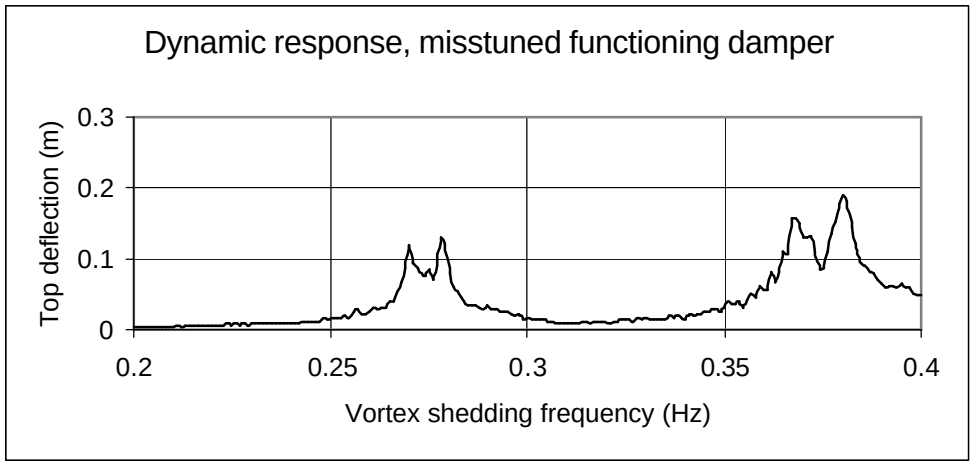

Figure 3.3 r Dynamic response of top amplitude deflection during vortex shedding force and a mistuned functioning damper (frequency f_2=0.31 Hz). Both vortex shedding frequency and critical wind velocity during vortex shedding were randomised by 50 percent. The vortex shedding force varies with the oscillating frequency. The tuned damper to be compared with this one was found in Figure 3.3 m. Maximum top amplitude was 0.191 m at vortex shedding frequency 0.380 Hz.

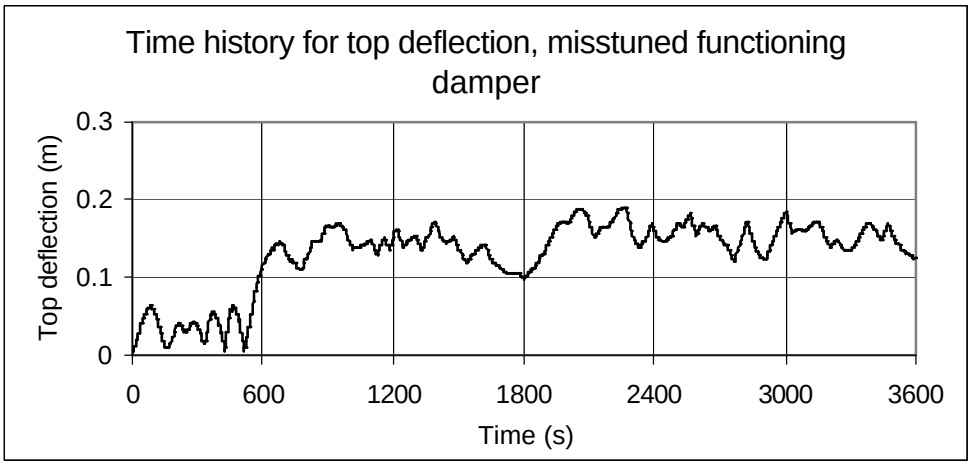

Figure 3.3 s Time history of top amplitude deflection at the oscillating frequency f=0.380 Hz, a variable vortex shedding force and tuned functioning damper (frequency f_2=0.31 Hz). Both vortex shedding frequency and critical wind velocity during vortex shedding were randomised by 50 percent. This was the case of a functioning damper. The tuned damper to be compared with this one is found in Figure 3.3 n and 3.3 o.

3.3.2.5 Influence of the geometrical limitations of the damper house

As shown in Section 2.3.2, Figure 2.3 h and 2.3 j the space in damper house is limited and the pendulum mass angle movement is therefore limited to approximately 1.2 degrees. The maximum possible relative amplitude movement in horizontal direction is 75 mm. By plotting the deflection for the pendulum mass it is obvious that the damper unit is not able to act in the way as intended. That was also an explanation to the surprisingly low damping value delivered by the damper unit. A reasonable assumption was that the damper units damping was achieved by a combination of the limited pendulum movement, the stroke of the damper friction and/or pendulum mass against the vertical damper unit walls and the energy losses in the chain movements. Therefore the above-presented model still could be valid for principle calculations.

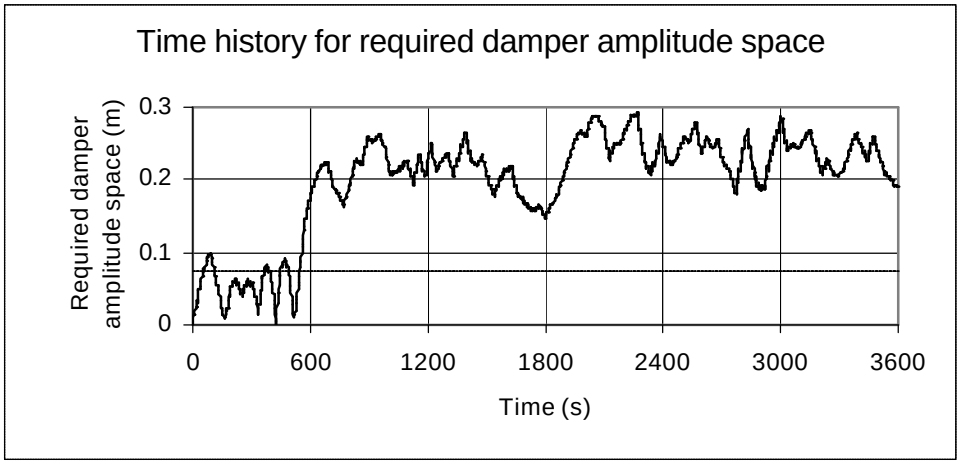

Figure 3.3 t Time history of required free functioning damper amplitude space at the vortex shedding frequency f=0.357 Hz, a variable vortex shedding force and tuned frequency f_2=0.262 Hz. Both vortex shedding frequency and critical wind velocity during vortex shedding were randomised by 50 percent. The horizontal line show available damper space, 75 mm. Figure 3.3 o shows the time history diagram for the chimney mass.

3.3.2.6 Influence of lock-in effects

Because of lock-in phenomena the amplitude could increase considerably because the vortex shedding starts at lower wind velocities, and the chimney continues to oscillate with the same frequency as the vortices were separated from the chimney. It is well known that the Strouhal number could be reduced to half its normal value because of lock-in effects. The wind velocity will be doubled and the wind pressure increases by a factor of four. Slender structures are more sensitive for lock-in phenomena, see for instance [26]. The probability for conditions causing this type of lock-in are low, but a chimney does have a lot chances during its long lifetime. Therefore lock-in phenomena could be dangerous for slender chimneys. This is one of the reasons for the limitation of the applicability of the equivalent load in [3] and [24].

3.3.2.7 Accelerations

From the solutions of the finite difference equations, accelerations of the chimney mass and the accelerations of the damper mass were calculated. The magnitude of the damper mass accelerations is of great importance. The damper mass acceleration must be greater than the friction force between damper friction mass and the damper house bottom.

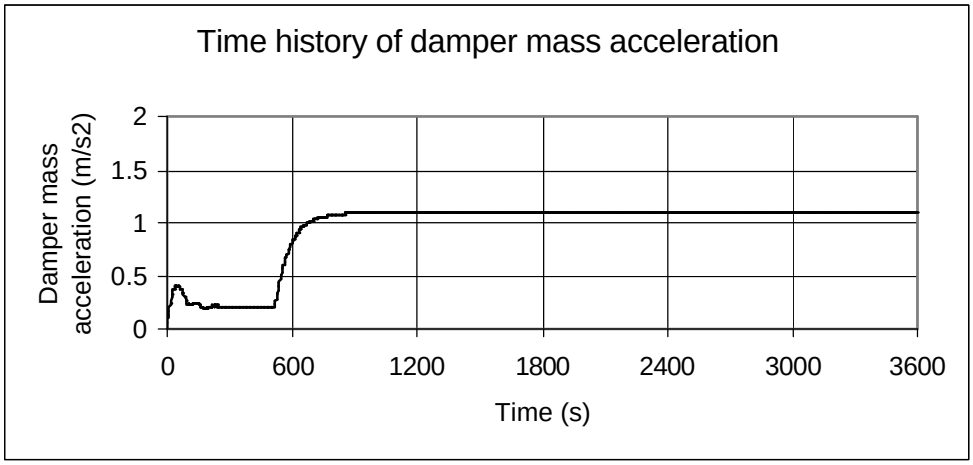

Figure 3.3 u Time history of damper mass acceleration at the vortex shedding frequency f=0.357 Hz, tuned frequency f_2=0.262 Hz and a functioning damper. Neither vortex shedding frequency nor critical wind velocity during vortex shedding was randomised. Figure 3.3 n shows the corresponding time history diagram for the top amplitude deflection.

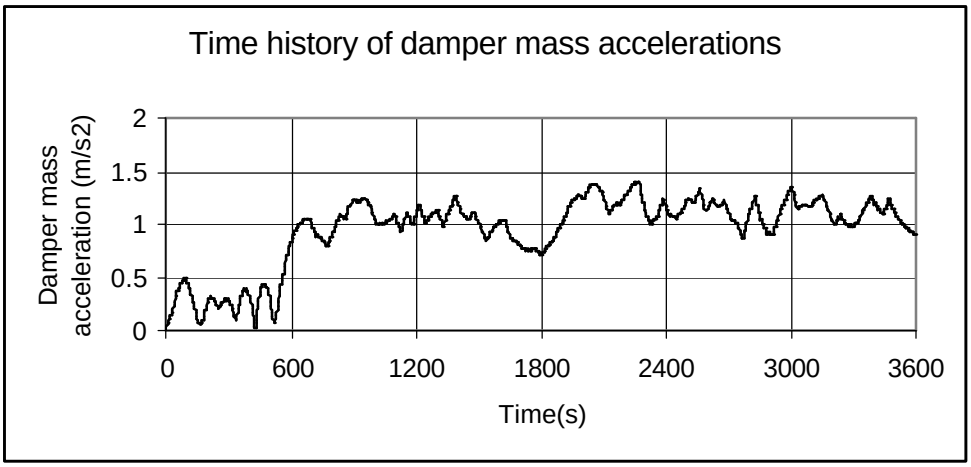

Figure 3.3 v Time history of damper mass acceleration at the vortex shedding frequency f=0.357 Hz, a variable vortex shedding force, tuned frequency f_2=0.262 Hz and a functioning damper. Both vortex shedding frequency or critical wind velocity during vortex shedding were randomised to 50 percent. Figure 3.3 o shows the corresponding time history diagram for the top amplitude deflection.

By comparing figure 3.3 u and 3.3 v it is found that the mean damper mass acceleration is about 1 m/s^2. The resulting horizontal force will be about 1200 N (pendulum mass 1246 kg). If the friction masses weight is about 40 kg the maximum required friction force according to Equation 2.4 will be approximately 120 N. Therefore it is obvious that there will be enough acceleration for activating the friction masses.

3.3.2.8 Calculation the damping measurement conditions

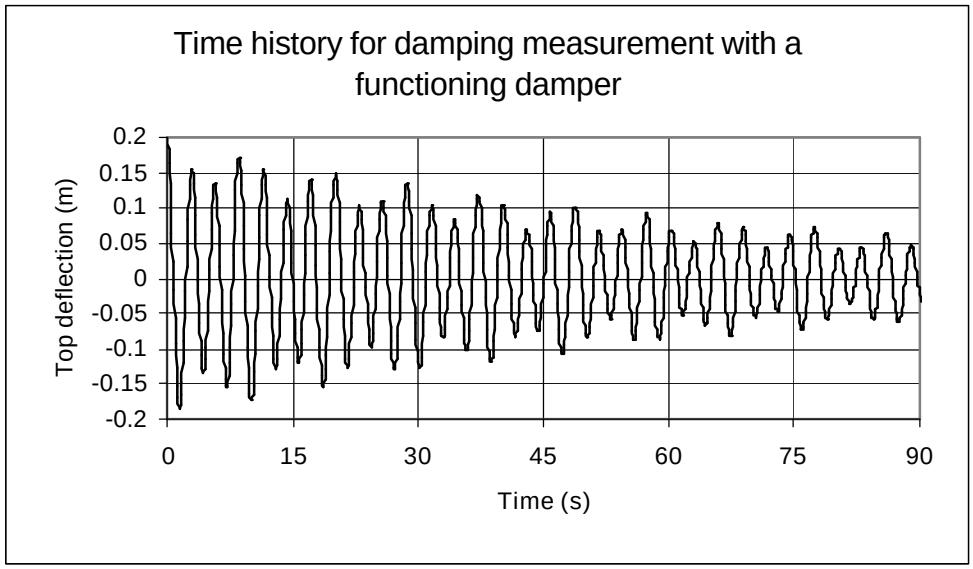

Figure 3.3 w Time history of damping test with a functioning damper. The figure could be compared with Figure 3.3 h representing the corresponding damping test.

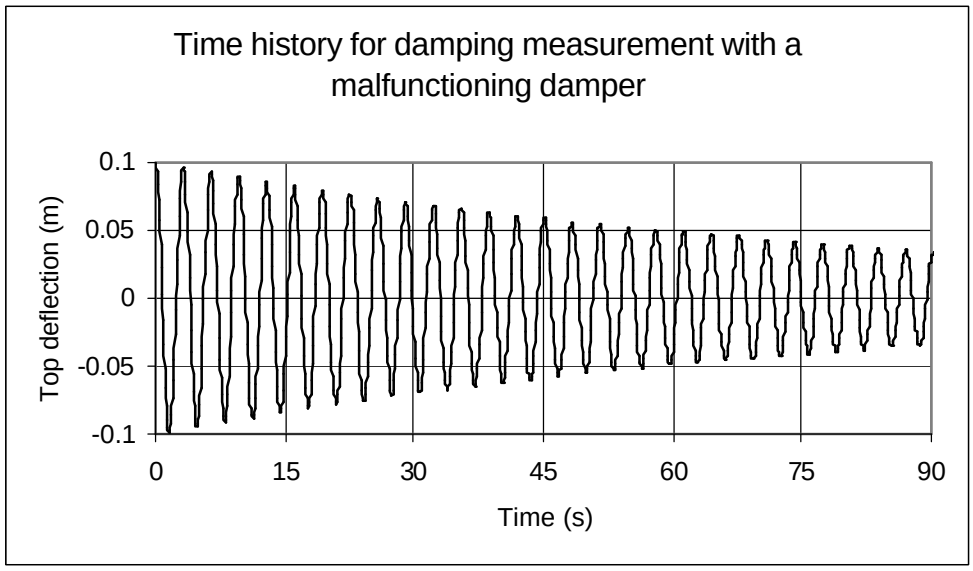

Figure 3.3 x Time history of damping test with a mal-functioning damper. The damper stiffness was assumed to zero and the chimney damper mass were added to the generalised mass. Thus the damper mass will be neglected. The figure could be compared with Figure 3.3 i, representing the corresponding damping test.

3.3.3 Comparison between observations and theoretical study

The solutions for the dynamic response, Equation 3.10 and 3.11, show a similar behaviour in the solutions as in [6], [13] and [14].

It is important to note that the model does not include any advanced fluid mechanical behaviour.

According to the theory a sudden and quick increase of the top amplitude deflection will occur. From the recorded data given in Section 3.4 a similar behaviour is observed. A very quick increase of the top amplitude deflection and often an almost equal decrease was observed. The quick decrease was explained by the turbulent behaviour of the wind. The recorded data also show that the wind quickly and often change both velocity and direction. Thus the model only is limited sensitive to relatively large randomised changes in frequency or vortex shedding force, large amplitude deflection during vortex shedding will only occur for short periods at a time. This corresponds also well to the recordings according to Section 3.4.

There were some deviations between theory and damping measurements that mainly may be explained by the fact that theory comes to the conclusion that there is not enough horizontal space in the damper house. Thus the damper produces less damping than expected.

Figure 3.3 l for the mal-functioning damper show a top deflection range of 496 mm. No lock-in effects are included. If we assume a lock-in on the wind velocity of two times the top deflection range will increase with a factor four to about 2000 mm. The calculations will then roughly confirm the observations noted in Section 3.1 and studied further in an estimated load spectrum in Section 4.2 and reverse.

Figures 3.3 m, 3.3 n and 3.3 o for the functioning damper show a top deflection range of approximately 400 mm. With the same discussion as for the mal-functioning damper it seems reasonable to expect a top deflection range of approximately 1600 mm for the functioning damper and the same weather conditions.

It is worth noting that the mistuned damper in Figure 3.3 r and 3.3 s gives a little less top deflection amplitude as compared to the tuned damper, but the vortex shedding frequency is larger.

The accelerations are found to be large enough to overcome the friction forces between the damper friction masses and the damper house bottom friction plate.

For the simulation of the damping tests, Figure 3.3 w and 3.3 x corresponding to the damping tests, Figure 3.3 h and 3.3 i are found except for one behaviour. Figure 3.3 w shows two superimposed oscillations, which could not be found in Figure 3.3 h. The superimposed oscillations show the sum of oscillations of the both masses. This difference was an additional argument to that only a minority of the damping is achieved from the friction masses. The major part is probably achieved from friction losses in the chains etc.

The theoretical study supports the statement made in Section 3.3.1.6 that the VEAB chimney damper is a not an optimum damper device.

3.4 Recorded dynamic properties of the chimney

From the recorded results, about two million loggings, all periods where the top deflection range exceeds 267 mm have been identified. According to Section 4.1 maximum deflection ranges during vortex shedding was calculated as $2 \cdot 133.6 = 267$ mm, the vortex shedding top deflection range calculated by the manufacturer. Typical for vortex shedding is that several large oscillations follow after each other in time. Typical for gust wind is that only one or a few large oscillations follow after each other in time. By plotting all identified results on the computer screen and truncating all periods where only a few cycles follow in time the results according to Table 3.4 a and 3.4 b remains.

Table 3.4 a Number of occasions per month where top deflection range exceeds 267 mm for more than a few cycles. Year numbers are vertical to the left and month number horizontal at top.

Year/ Month no	1	2	3	4	5	6	7	8	9	10	11	12
1997	0	8	9	5	5	4	4	0	9	0	0	0
1998	1	6	2	2	3	7	20	11	0	4	0	1
1999	12	4	0	4	3	2	11	2	1	3	5	10
2000	4	0	7	0	6	9	4	3	0	3	1	0

Table 3.4 b Relative time for the chimney when top deflection range exceeds 267 mm. Year number are vertical to the left and month number horizontal at top.

	1	2	3	4	5	6	7	8	9	10	11	12	Total
1997	0,000000	0,000870	0,000639	0,000259	0,000110	0,000295	0,000311	0,000005	0,000542	0,000009	0,000017	0,000005	0,000255
1998	0,000063	0,000185	0,000014	0,000075	0,000468	0,000331	0,001692	0,000758	0,000009	0,000183	0,000000	0,000065	0,000320
1999	0,000350	0,000418	0,000000	0,000215	0,000165	0,000578	0,000855	0,000067	0,000041	0,000079	0,000206	0,001174	0,000346
2000	0,000444	0,000019	0,000342	0,000004	0,000245	0,000446	0,000120	0,000226	0,000025	0,000262	0,000060	0,000027	0,000185
Total	0,000214	0,000370	0,000249	0,000138	0,000247	0,000413	0,000745	0,000264	0,000155	0,000133	0,000071	0,000318	0,000277

The differences between the two tables were due to that all cycles when top range deflection exceeds 267 mm was included in Table 3.4 b. In Table 3.4 a the top range deflections less than a few cycles were truncated.

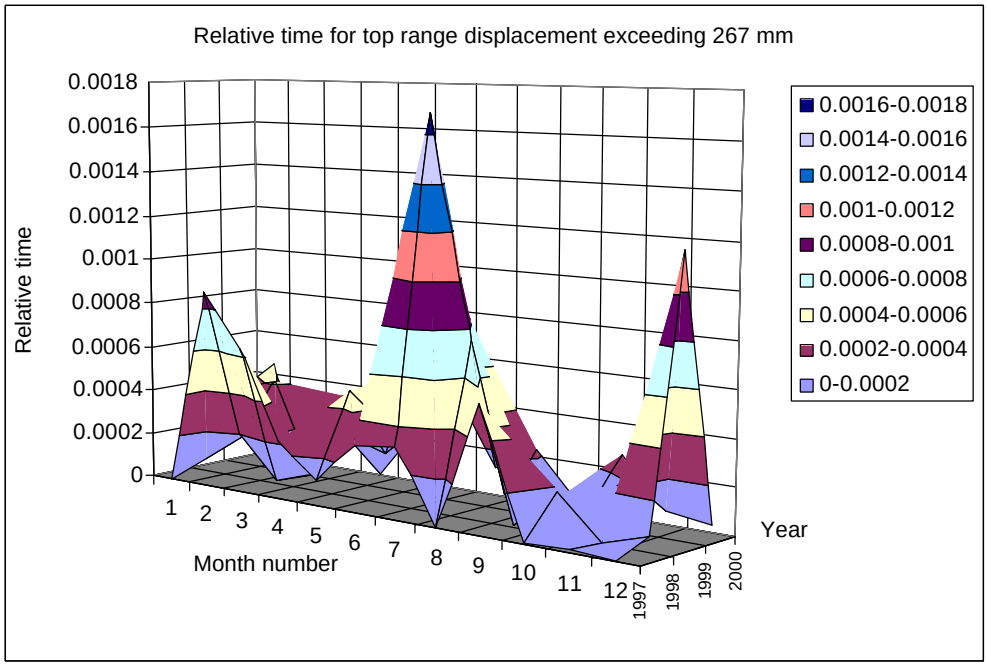

Figure 3.4 a Relative time of the measure period for the chimney when top deflection range exceeds 267 mm.

It is well known, as described in for instance [1], that it is more probable for huge laminar vortex shedding induced oscillations to occur during cold winter days with cold laminar airflow. From Figure 3.4 a show large top range deflections during the winter time but in the middle of the summer the largest amount of oscillations occurred. This was not expected. Obviously large vortex-shedding oscillations could to be expected also during summer periods.

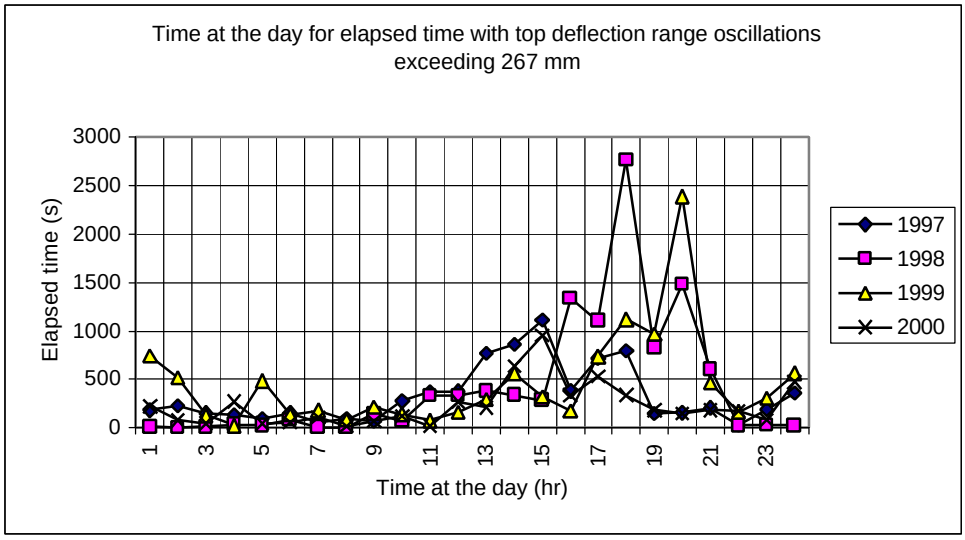

Figure 3.4 b Time at the day for elapsed time with top deflection range oscillations exceeding 267 mm.

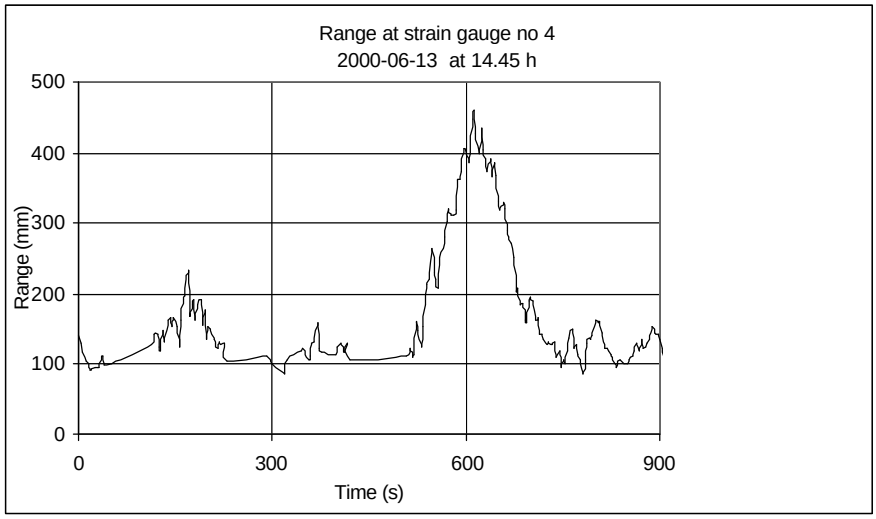

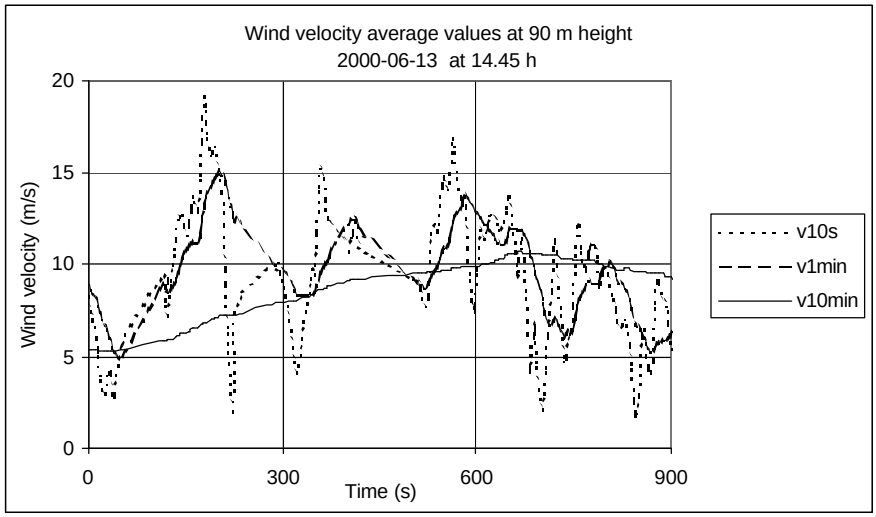

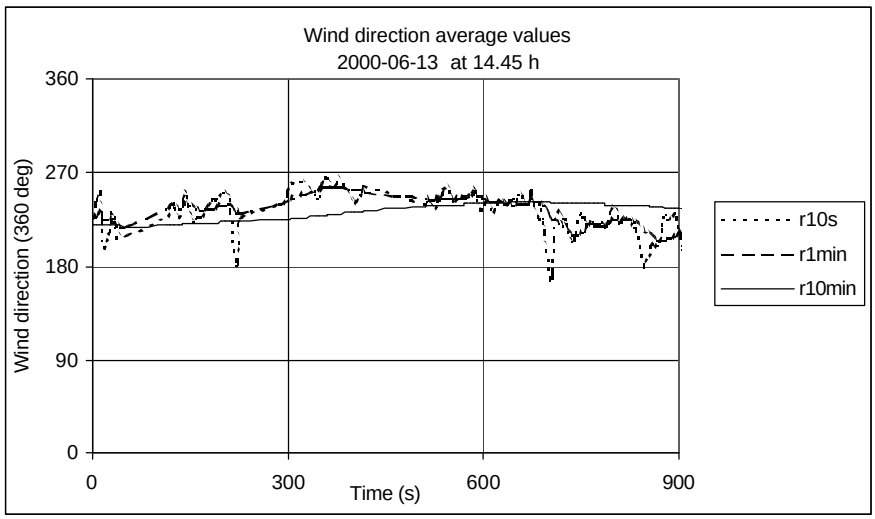

Figure 3.4 c A typical vortex shedding behaviour with a rather long period of large deflection ranges. Range, wind velocity and wind direction were plotted as a function of time. Wind velocity and wind direction were calculated as mean values over 10 seconds, 1 minute and 10 minutes.

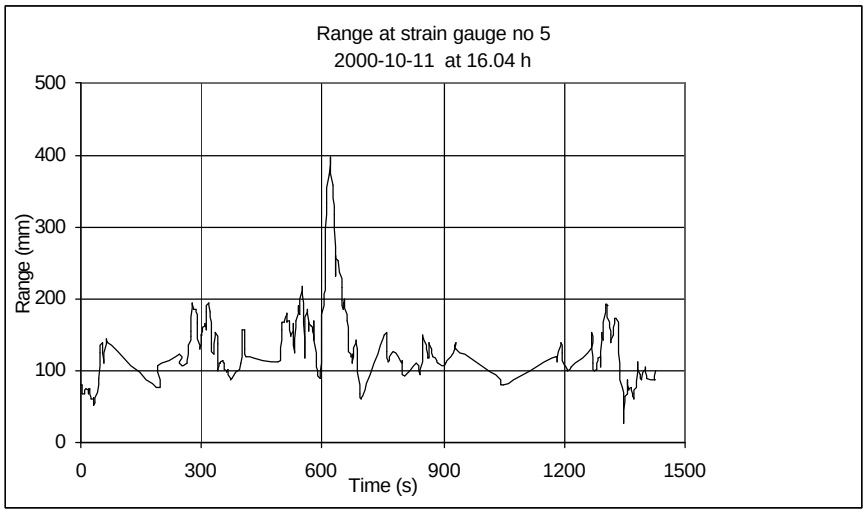

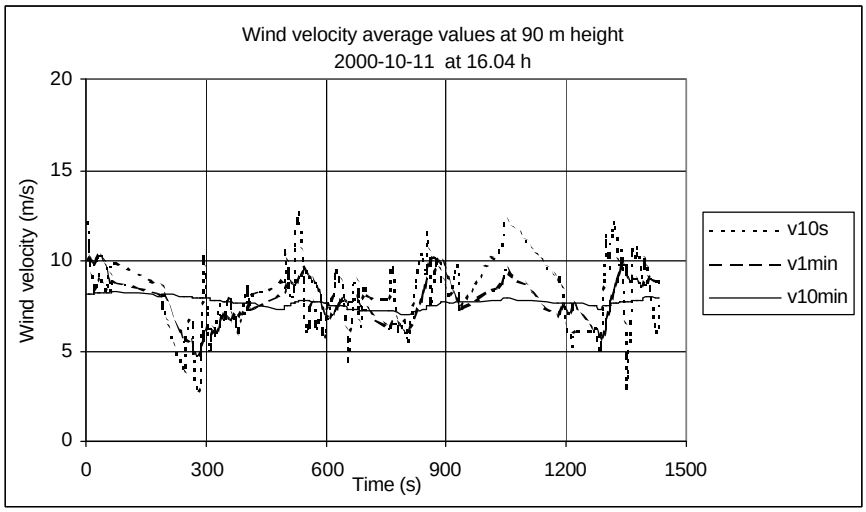

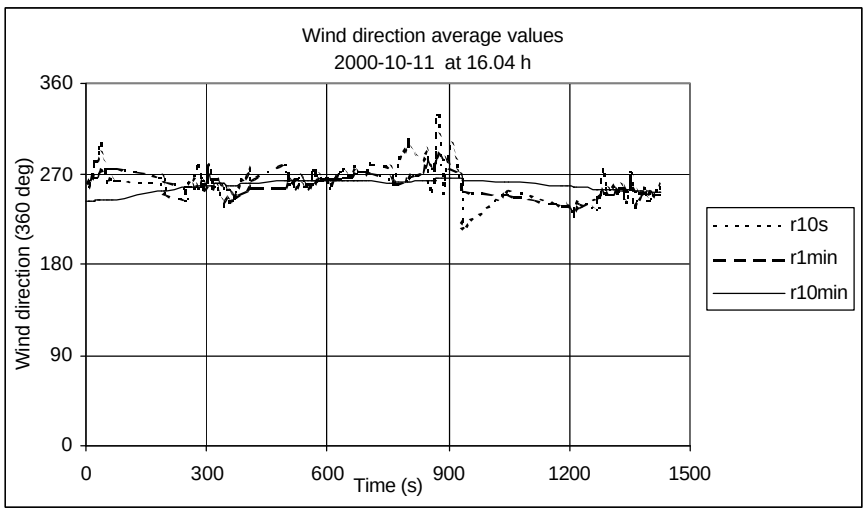

Figure 3.4 d A typical vortex shedding behaviour with a short period of large deflection ranges. Range, wind velocity and wind direction were plotted as a function of time. Wind velocity and wind direction were calculated as mean values over 10 seconds, 1 minute and 10 minutes.

In Appendix I all identified periods with the criteria top deflection range exceeding 267 mm for the year 2000 were plotted (see also Table 3.4 a and 3.4 b).

A typical time history response during vortex shedding was an immediate increase from small deflection ranges to large deflection ranges. The large deflection ranges continues for typically about 100 seconds and decrease immediate again.

It was also obvious that large deflection ranges occur even if the turbulence intensity of the wind velocity is relatively large. About 50 percent turbulence intensity is typical if defined as 10 seconds mean value divided by 10 min mean value. The magnitude of 10 min mean values seems to be most important for vortex shedding. The time required to obtain stationary top deflection range during vortex shedding is > 10 minutes according to Section 3.3.2.

From Table 3.4 b it is found that the VEAB chimney oscillates with a top deflection range exceeding 267 mm (mainly vortex shedding) for 0.028 percent of the time or about ten hours during the four-year observation period discussed in this report. This corresponds to about 80 000 cycles ($\frac{30 \text{ year of service}}{4 \text{ recording years}} \cdot 10 \frac{\text{hours}}{4 \text{ years}} \cdot 60 \frac{\text{minutes}}{\text{hour}} \cdot 60 \frac{\text{second}}{\text{minute}} \cdot 0.288\text{Hz} = 77760$) above the design value for the top deflection range of 267 mm during a 30-year service life.

3.5 Observed wind properties

3.5.1 Wind pressure and top deflection range, anthill diagrams

For the measurement period wind pressure and top deflection range anthill diagrams are plotted for the VEAB chimney. Dynamic wind pressure is assumed to follow $p_{dyn} = 0.5 \cdot r_{Air} \cdot v_{10\,\mathrm{min}}{}^{2}$ where $v_{10\,\mathrm{min}}$ is mean wind speed calculated over 10 minutes and r_{Air} = air density based on daily mean values for temperature according to Section 3.8. All recorded data for the four years 1997 through 2000 are read, sorted monthly, calculated and finally plotted in anthill diagrams by a couple of computer programs (Appendix H). The plotting was made in the Auto Cad dxf drawing format. In this section a typical selection of periods are presented. If maximum top deflection range was less than 100 mm the recording was truncated and dots were plotted for wind pressure nor deflection range.

Additional plots are found in Appendix F.

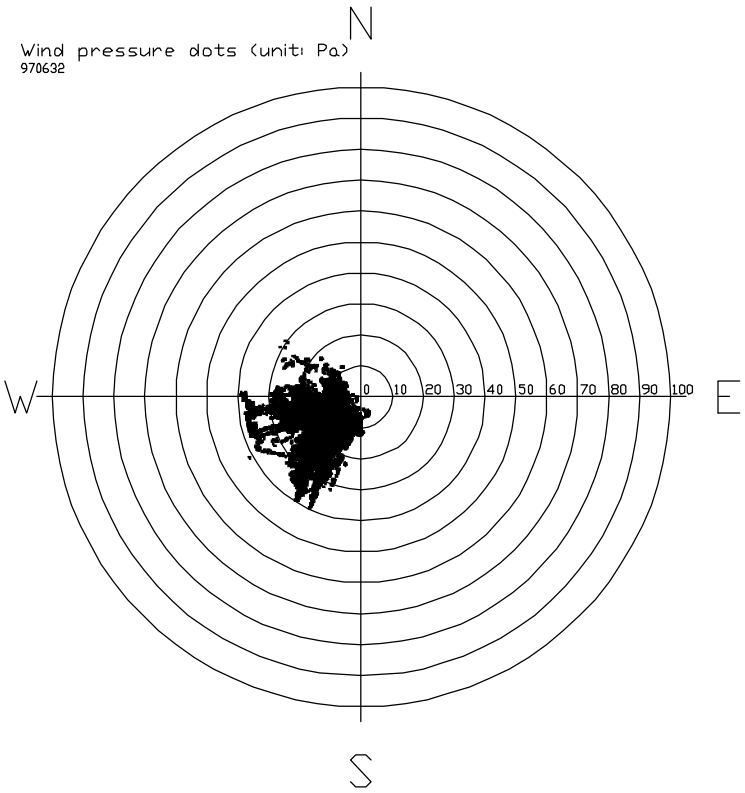

Figure 3.5 a Wind pressure anthill diagram for June 1997.

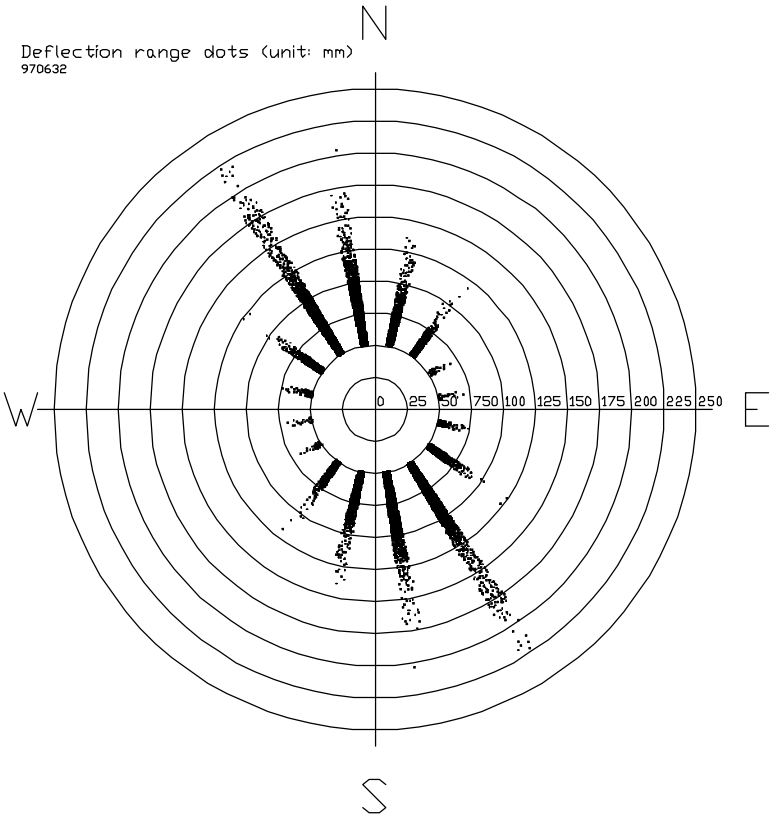

Figure 3.5 b Top deflection range anthill diagram for June 1997.

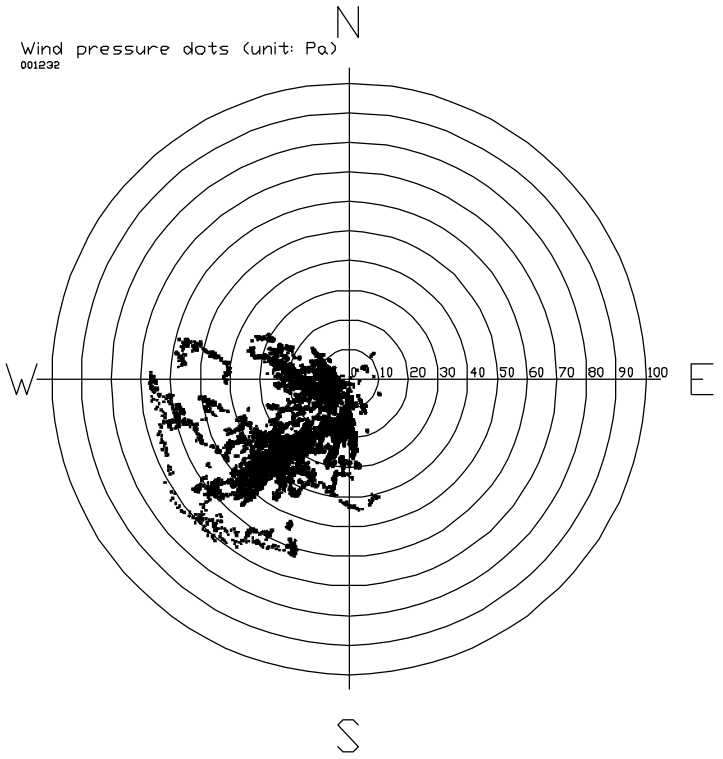

Figure 3.5 c Wind pressure anthill diagram for December 2000.

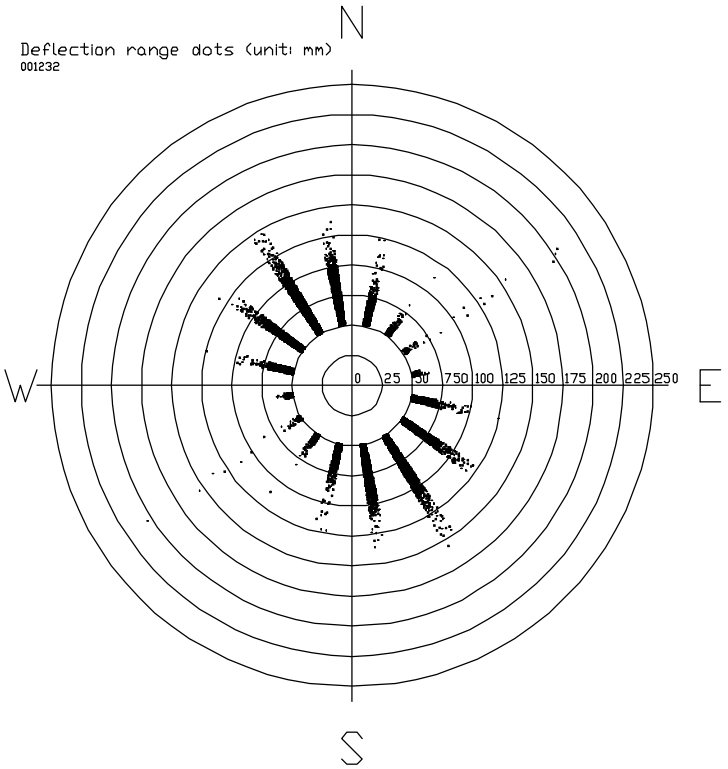

Figure 3.5 d Top deflection range anthill diagram for December 2000.

3.5.2 Accumulated wind pressure and accumulated top deflection range diagrams

Similarly as in Section 3.5.1 and for the same months the sum of wind pressure (10 minutes mean values) times number of cycles and the sum of top deflection range times number of cycles are plotted. Wind pressure times number of cycles is a measure of the applied wind energy. Top deflection range times number of cycles is a measure of the accumulated deflection energy. Finally some summary plots are given.

In Appendix F additional diagrams are found.

The mean angle between wind pressure times number of cycles and deflection range times number of cycles is about 67 to 90 degrees. The chimney oscillates with an angle almost perpendicular to the wind direction. The year 1999 above is typical and all other recorded years show the same behaviour. It is obvious that the dominating oscillations for the VEAB chimney are in NNW direction and that the dominating wind causing those oscillations blows from SW direction.

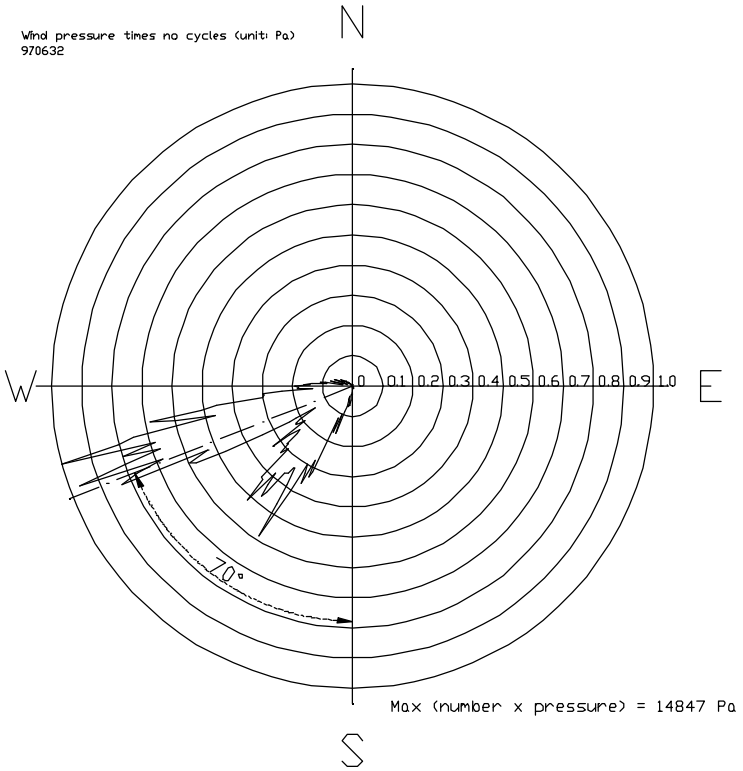

Figure 3.5 e Sum of wind pressure times number of cycles for June 1997.

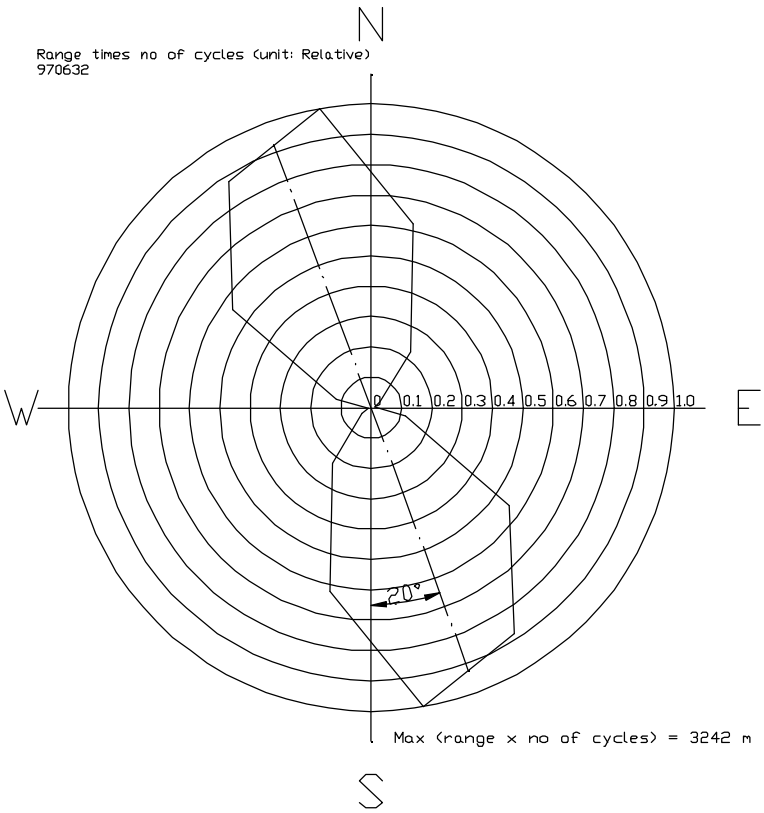

Figure 3.5 f Sum of top deflection range times number of cycles for June 1997.

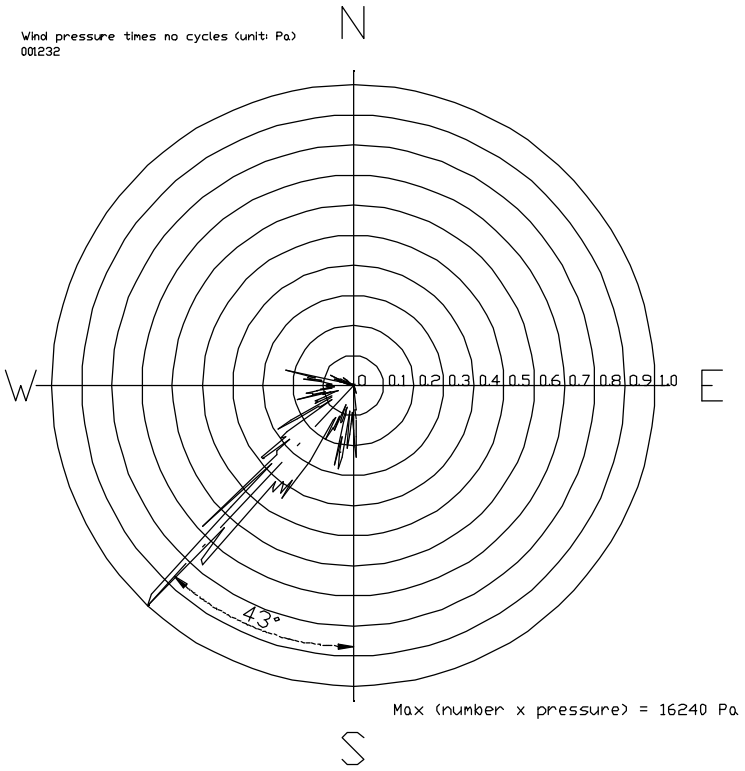

Figure 3.5 g Sum of wind pressure times number of cycles for December 2000.

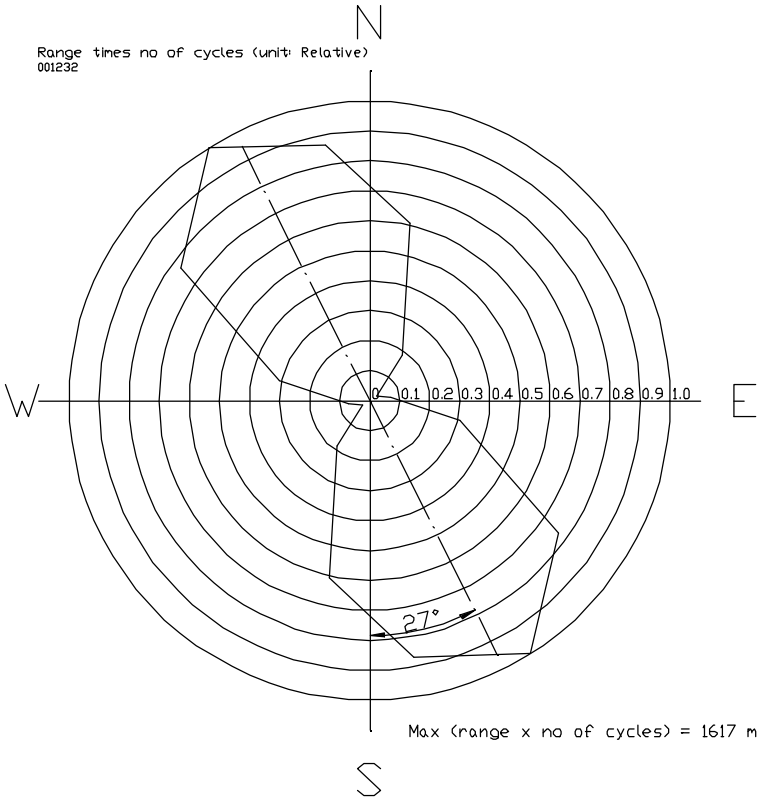

Figure 3.5 h Sum of top deflection range times number of cycles for December 2000.

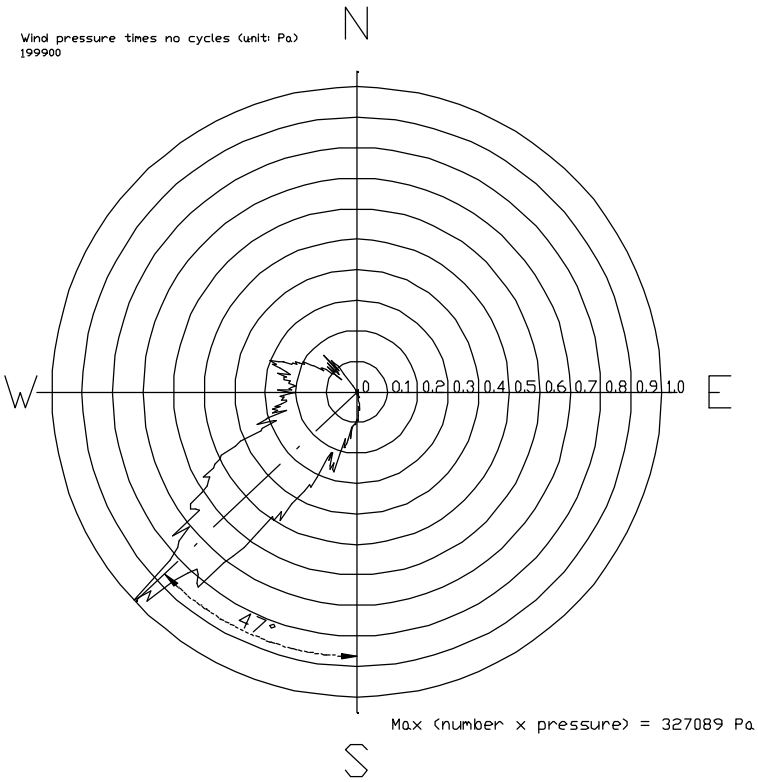

Figure 3.5 i Sum of wind pressure times number of cycles year 1999.

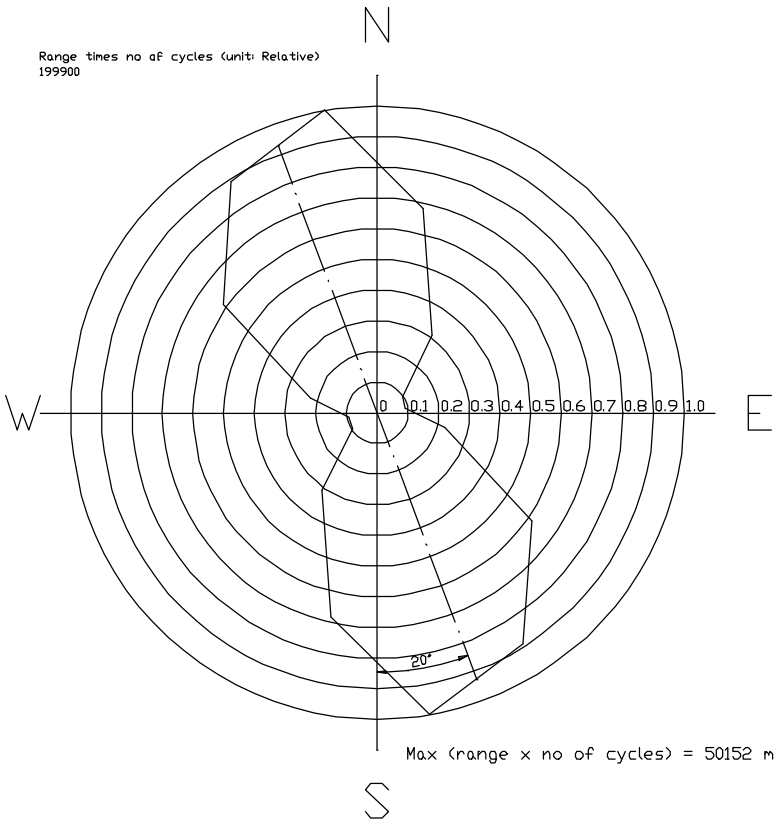

Figure 3.5 j Sum of top deflection range times number of cycles for year 1999.

3.5.3 Elastic energy diagrams

Similar as in Section 3.5.2 and for the same months the elastic energy diagrams, calculated according to Section 2.4.3 are plotted for the VEAB chimney.

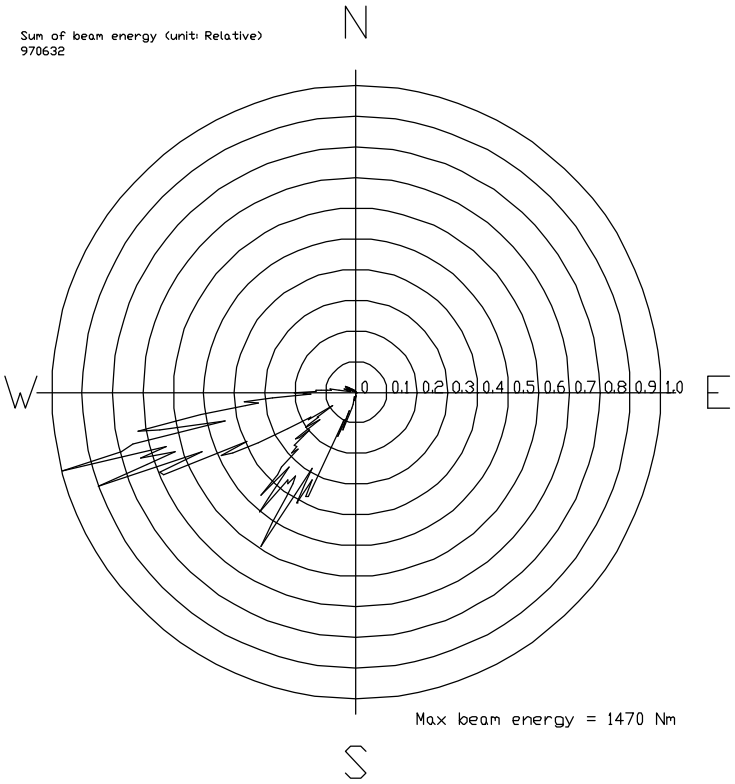

Figure 3.5 k Elastic energy diagram for June 1997.

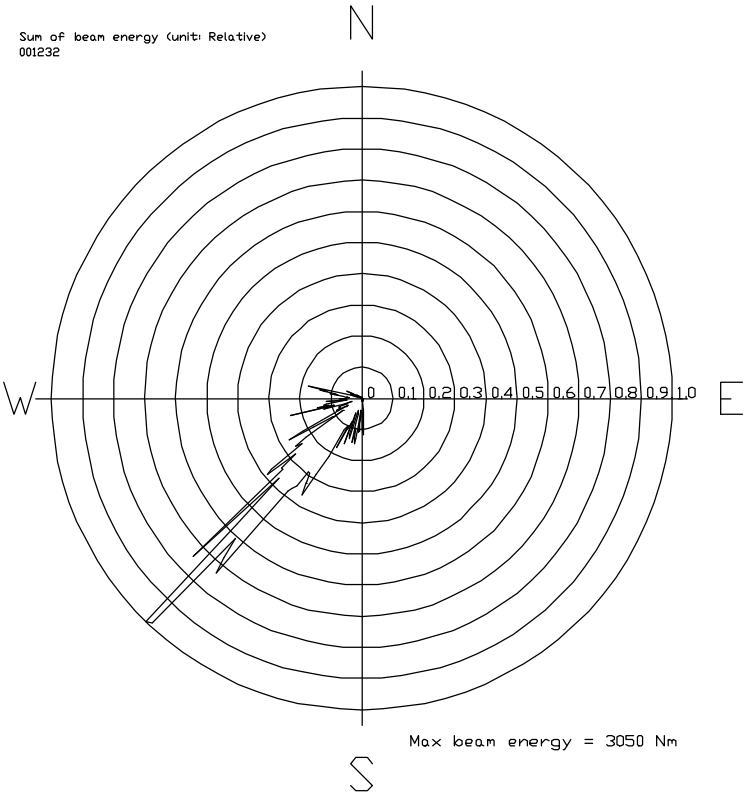

Figure 3.5 l Elastic energy diagram for December 2000.

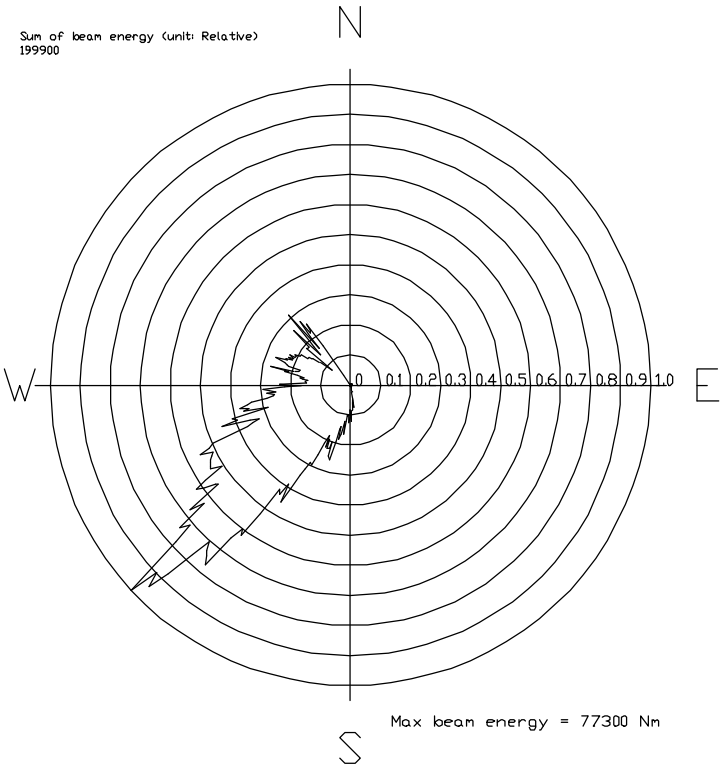

Figure 3.5 m Elastic energy diagram for the year of 1999.

3.5.4 Anthill diagrams for wind pressure at Växjö A station

Swedish Meteorological and Hydrological Institute, SMHI, administrates a net of observation stations for meteorological and hydrological observations all over Sweden. The closest station to the VEAB plant is Växjö A, located at latitude 56° 51´ and longitude 14° 50´, about four km south of the plant. Height above sea level at the observation station is about 199 m. A slope in northern direction and a sea separate the Växjö A station and the VEAB plant.

All wind data in this section origin from SMHI and Växjö A. The wind velocity is measured at 10 m height above the ground. A 360-degree compass has been used. 0 or 360 degrees means that the wind blows from the north, 90 degrees means that the wind blows from east and so on.

In Appendix F diagrams for some additional periods are found.

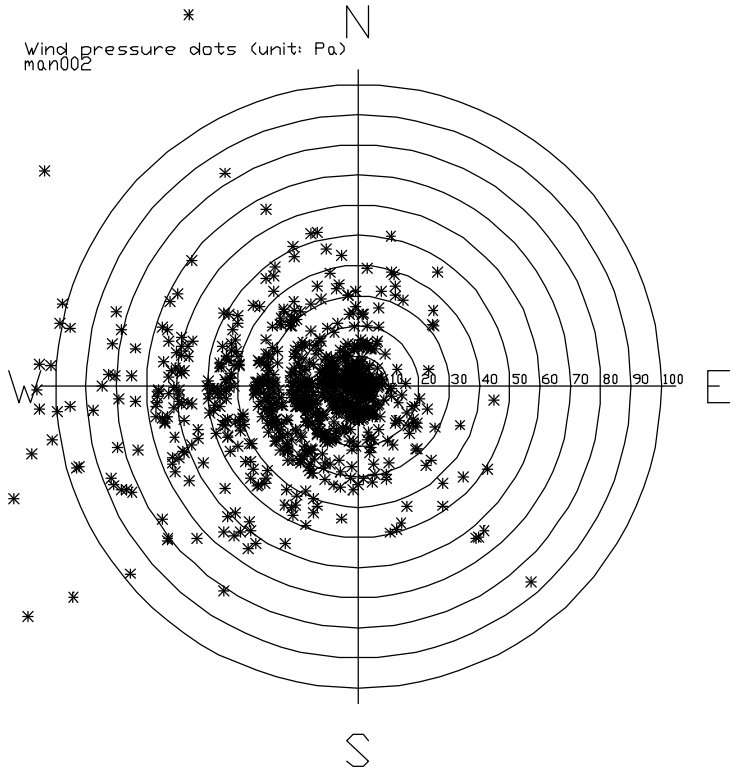

Figure 3.5 n Wind pressure anthill diagram for February 1997 to 2000 at SMHI Växjö A observation station.

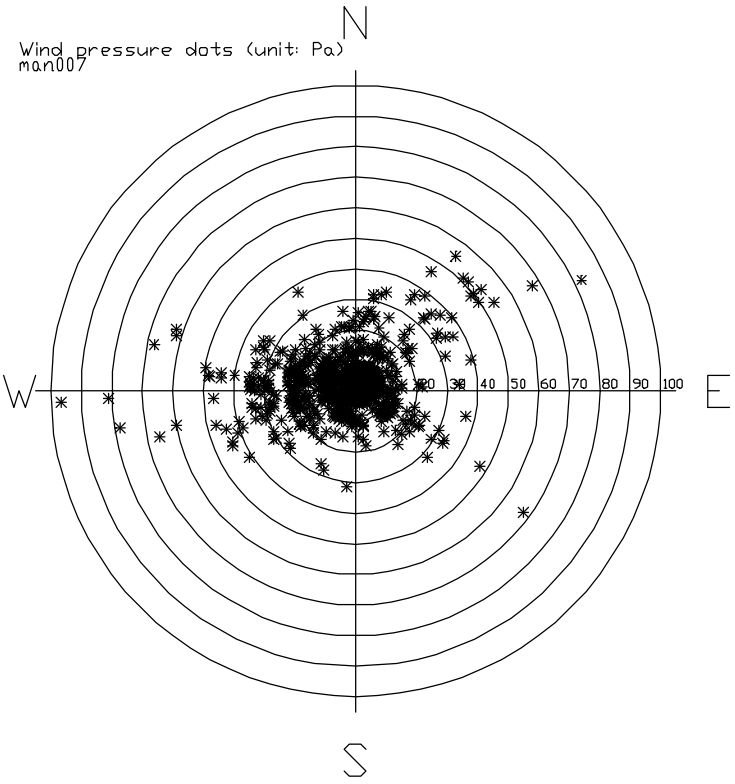

Figure 3.5 o Wind pressure anthill diagram for July 1997 to 2000 at SMHI Växjö A observation station.

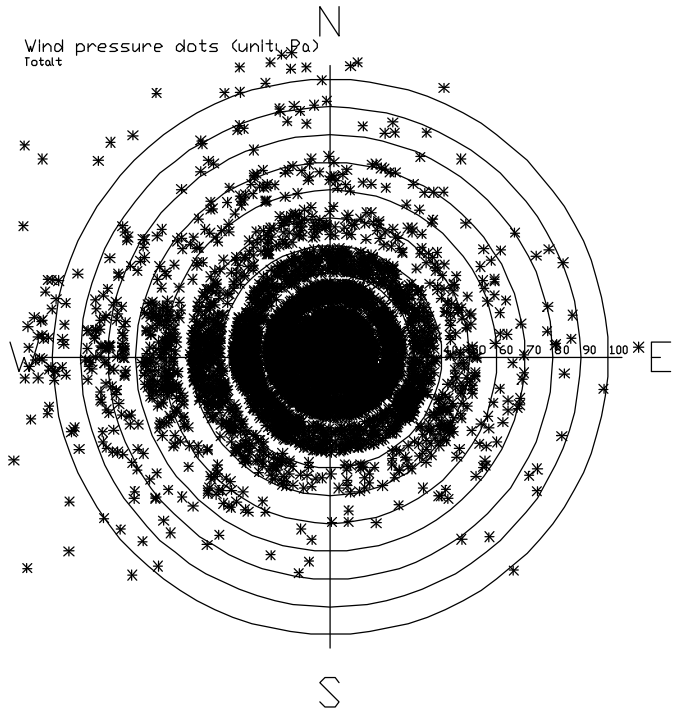

Figure 3.5 p Wind pressure anthill diagram for 1997 to 2000 at SMHI Växjö A observation station.

3.5.5 Deflection and wind velocity anthill diagrams

To study the combination of deflection and wind speeds, anthill diagrams for maximum top deflection as a function of wind velocity at 10 min mean values are plotted for the VEAB chimney. Below two typical anthill diagrams are shown in Figures 3.5 q and 3.5 r.

In Appendix F more diagrams are found.

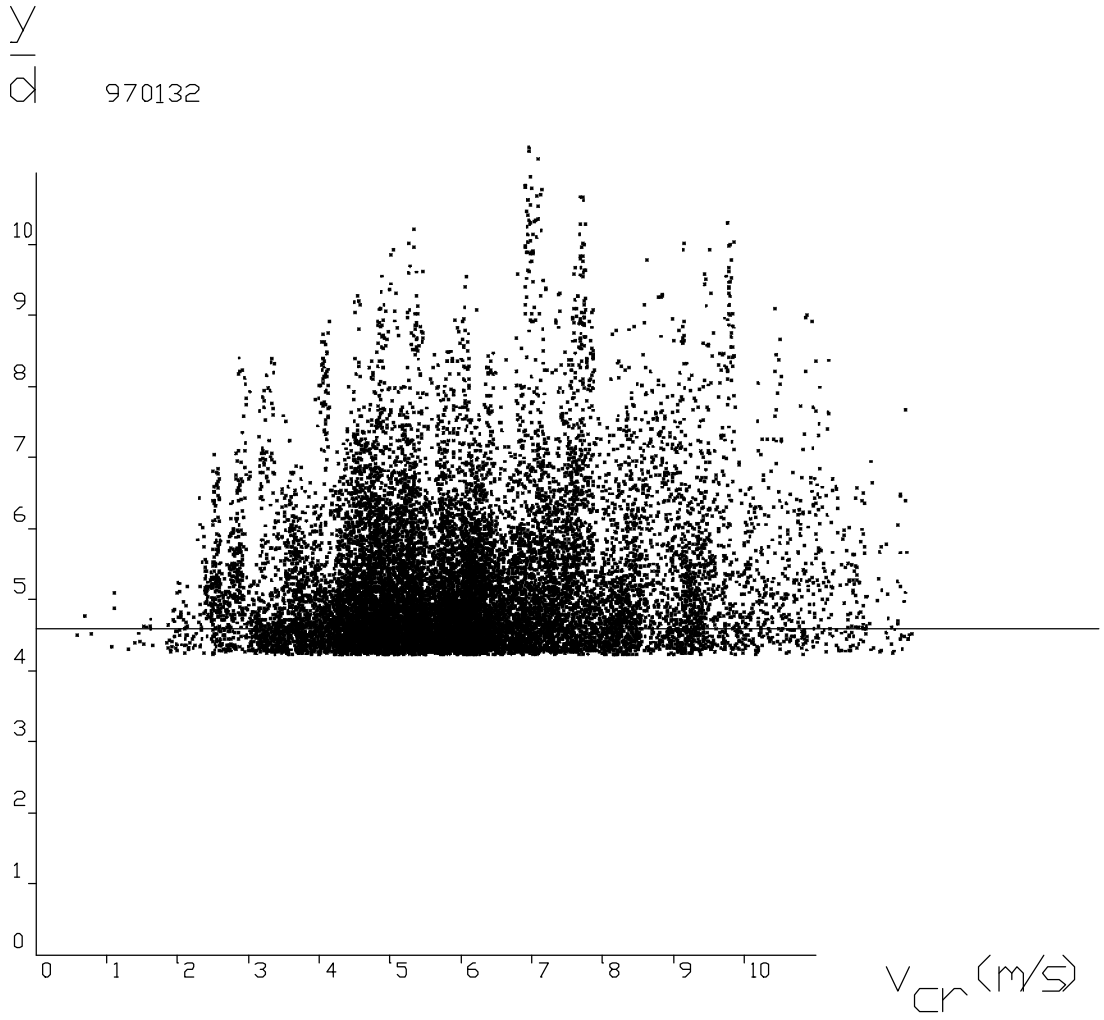

Figure 3.5 q Maximum top range deflection as a function of wind velocity (10 min mean values). Horizontal axis is wind velocity in m/s and vertical axis is 100 times top range deflection divided by diameter. The horizontal line corresponds to y/d = 0.06/1.3, which is the limit load for applicability of the equivalent load model for vortex shedding in [3]. The actual period is January 1997.

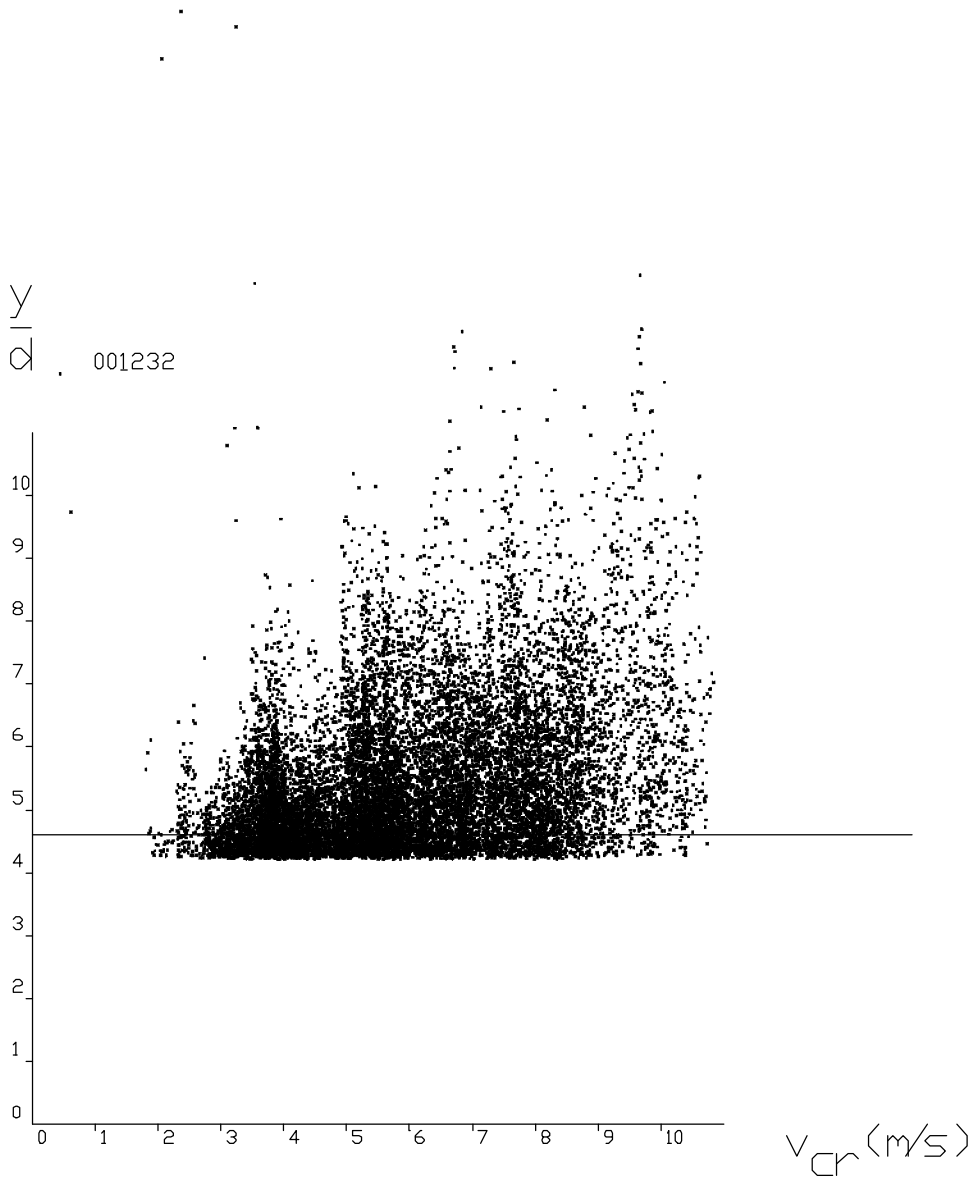

Figure 3.5 r Maximum top range deflection as a function of wind velocity (10 min mean values). Horizontal axis is wind velocity in m/s and vertical axis is 100 times top range deflection divided by diameter. The horizontal line corresponds to $y/d = 0.06/1.3$, which is the limit load for applicability of the equivalent load model for vortex shedding in [3]. The actual period is December 2000.

3.5.6 Wind turbulence anthill diagrams

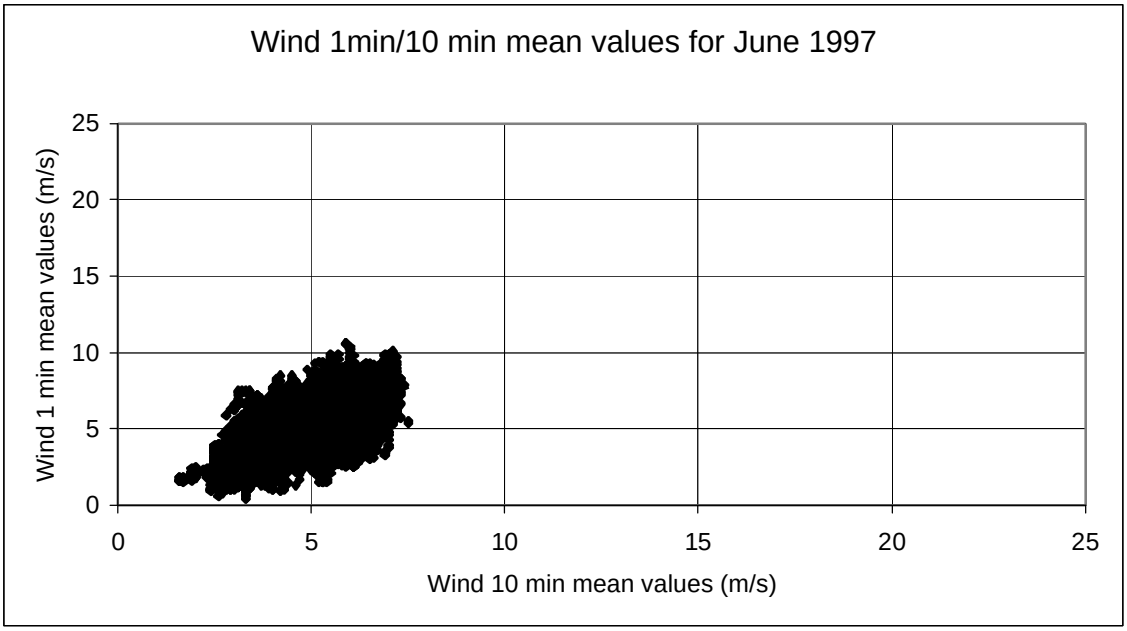

Figure 3.5 s Wind 1 min mean values as a function of wind 10 min mean values for June 1997.

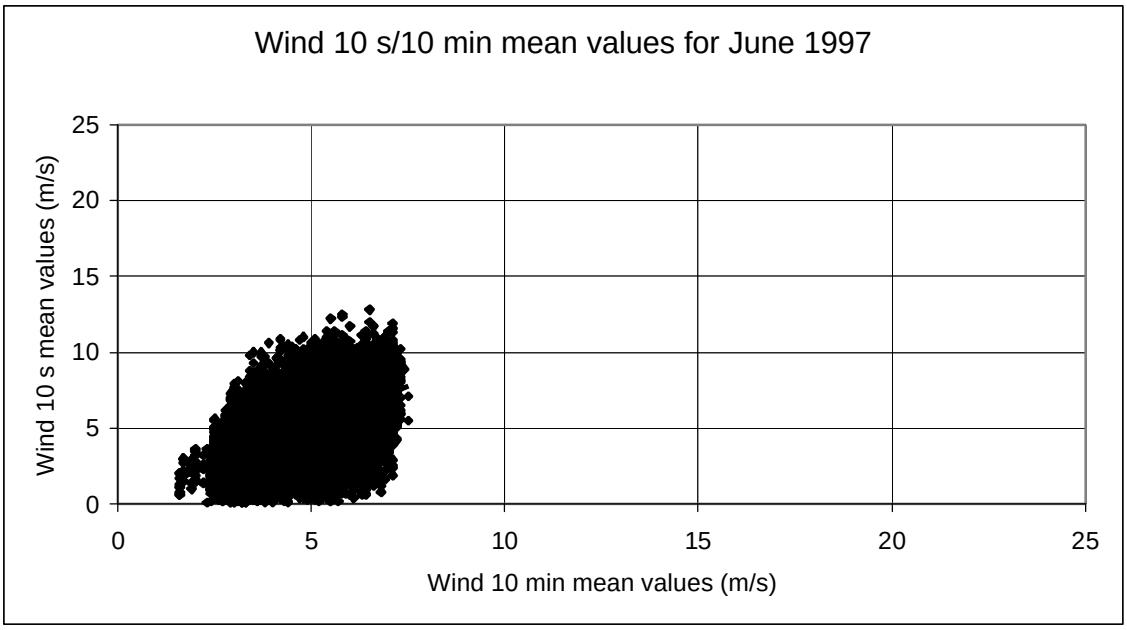

Figure 3.5 t Wind 10 s mean values as a function of wind 10 min mean values for June 1997.

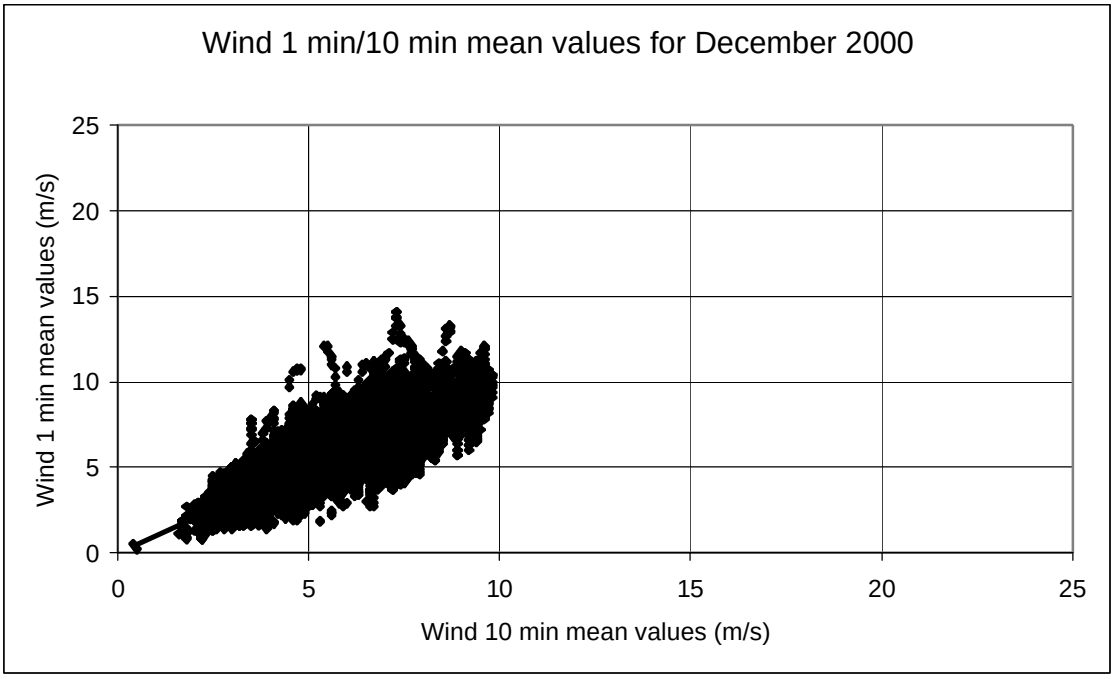

Figure 3.5 u Wind 1 min mean values as a function of wind 10 min mean values for December 2000.

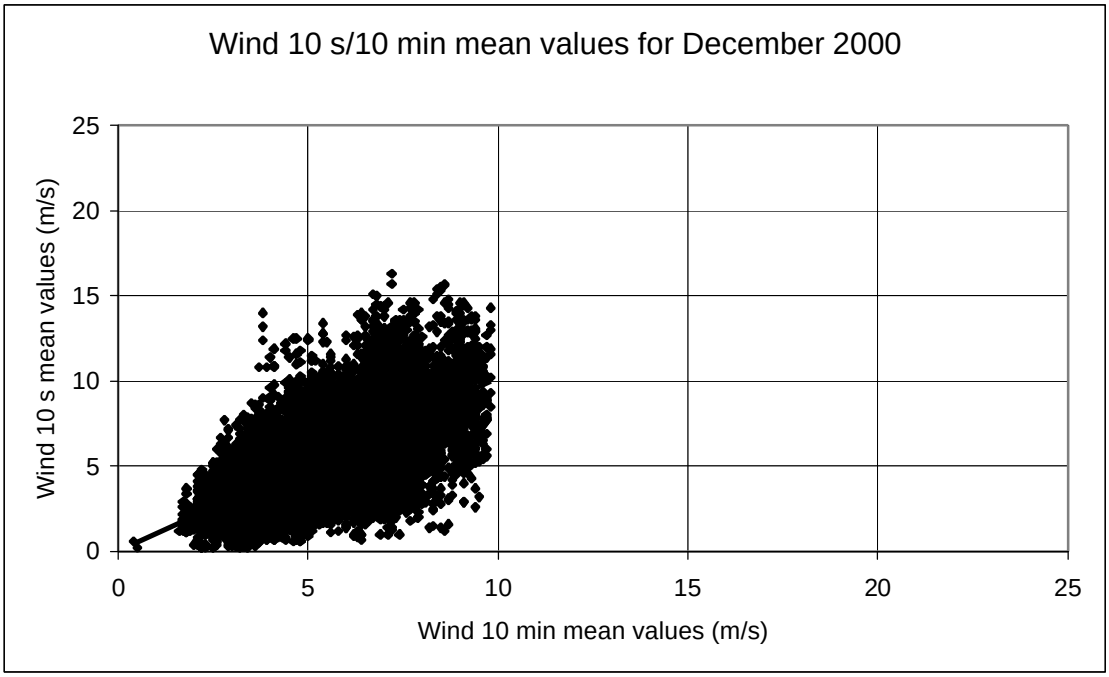

Figure 3.5 v Wind 10 s mean values as a function of wind 10 min mean values for December 2000.

3.5.7 Load spectra

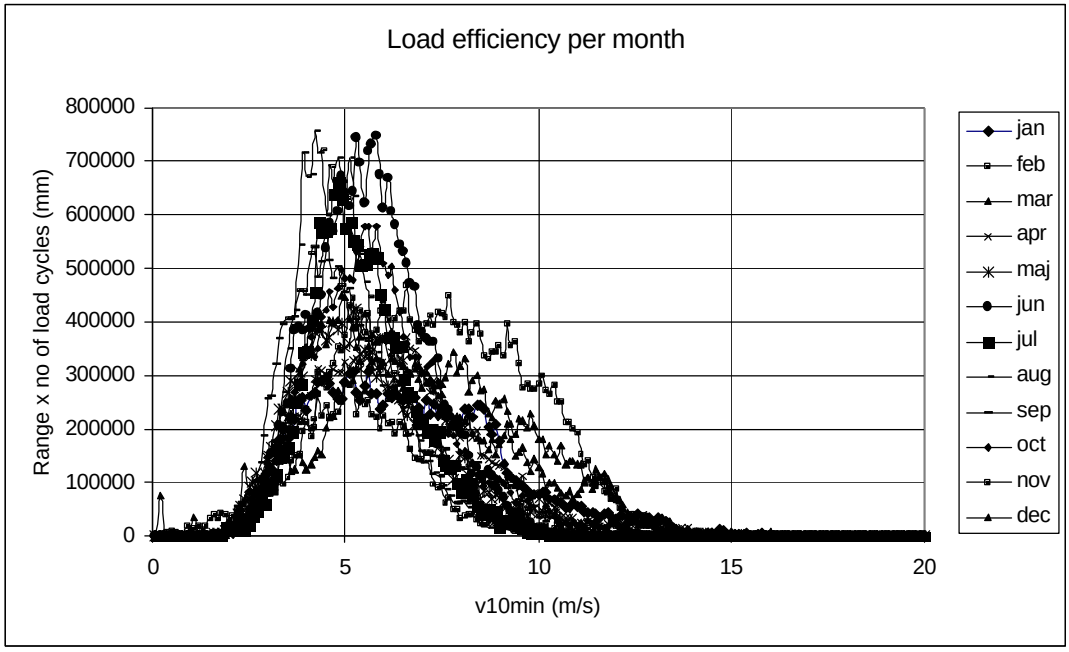

Figure 3.5 w Top range deflection times number of load cycles as a function of 10 minutes wind velocity mean value per month for the recording period.

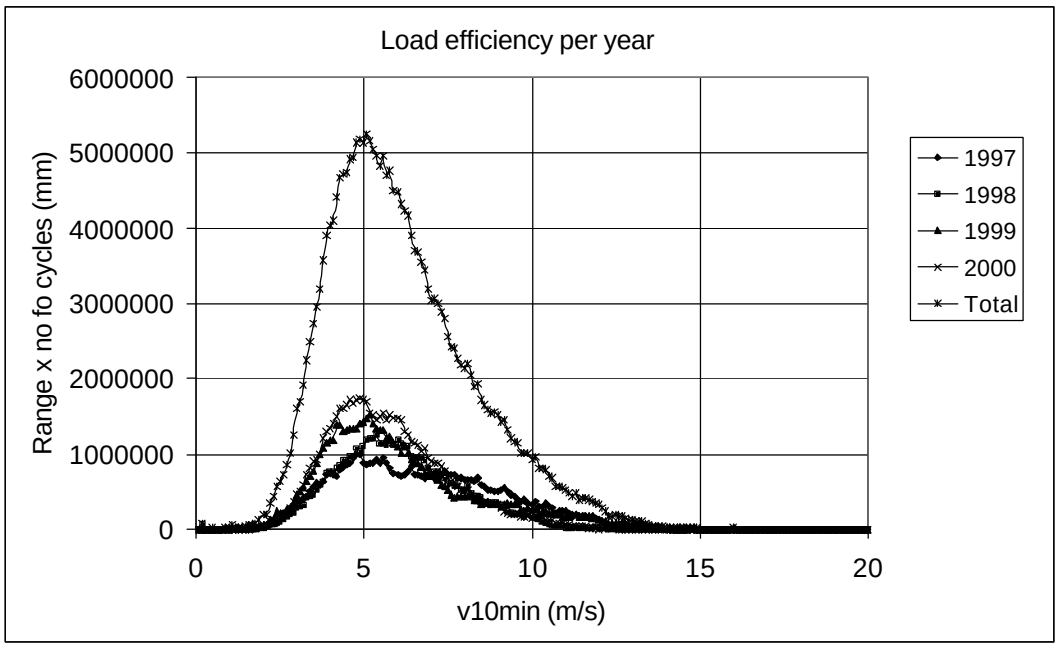

Figure 3.5 x Top range deflection times number of load cycles as a function of 10 minutes wind velocity mean value per year for the recording period.

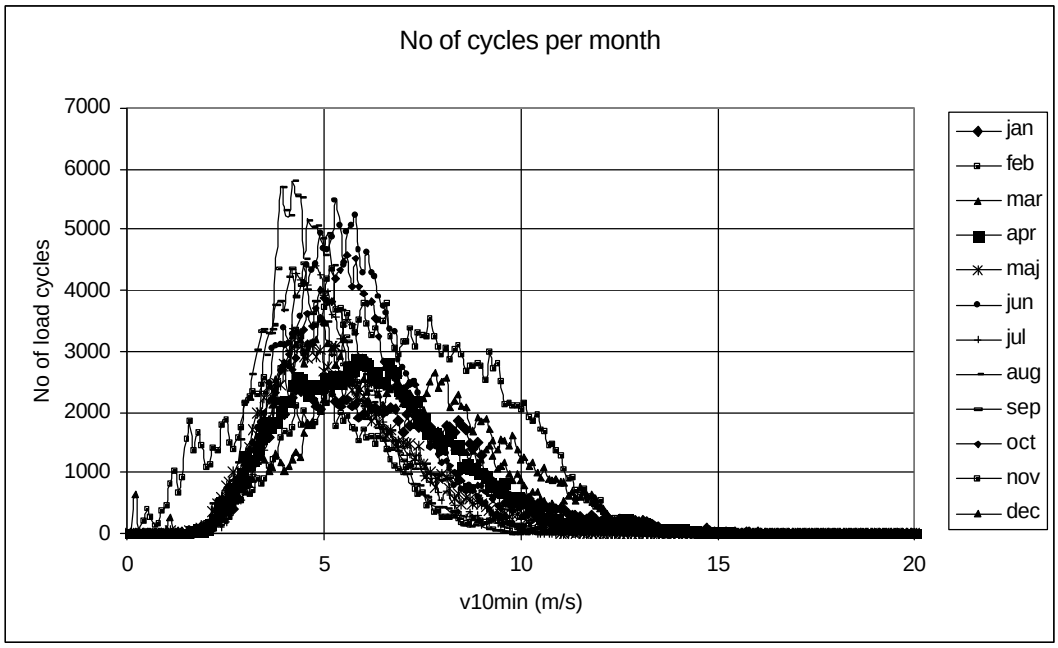

Figure 3.5 y Number of cycles per month as a function of 10 minutes wind velocity mean value per month for the recording period.

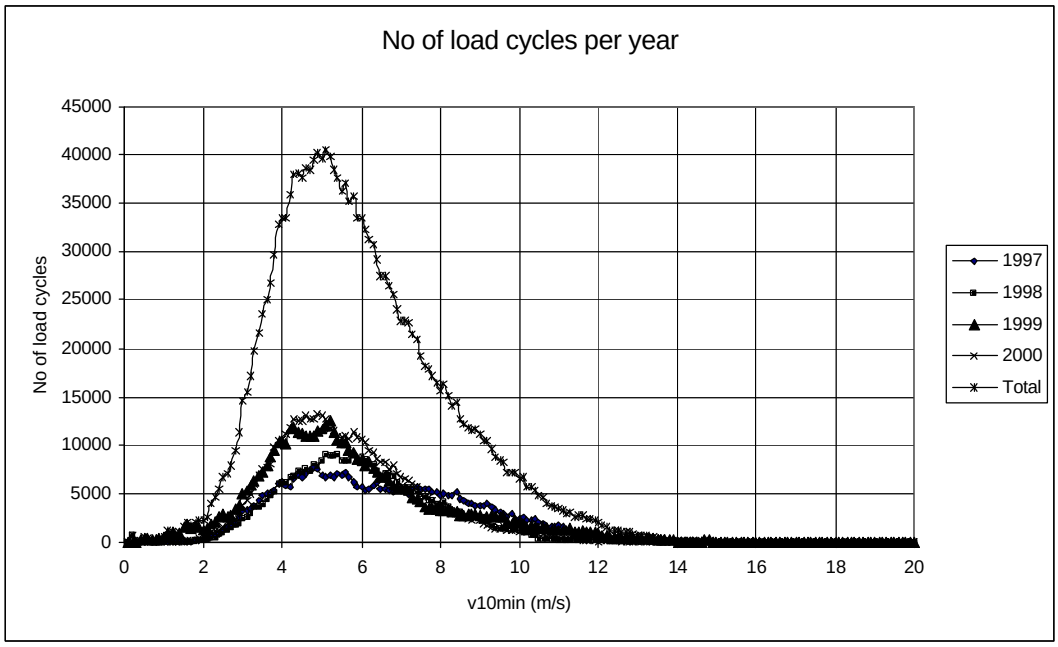

Figure 3.5 z Number of cycles per month as a function of 10 minutes wind velocity mean value per year for the recording period.

From Figure 3.5 *a* "mass centre" of the wind load was found to v_{10min} =6.32 m/s at 1.75 10^6 cycles. It means 0.44 10^6 cycles per year or 13.1 10^6 cycles per 30 year. Shape factor in this reverse calculation was 0.2.

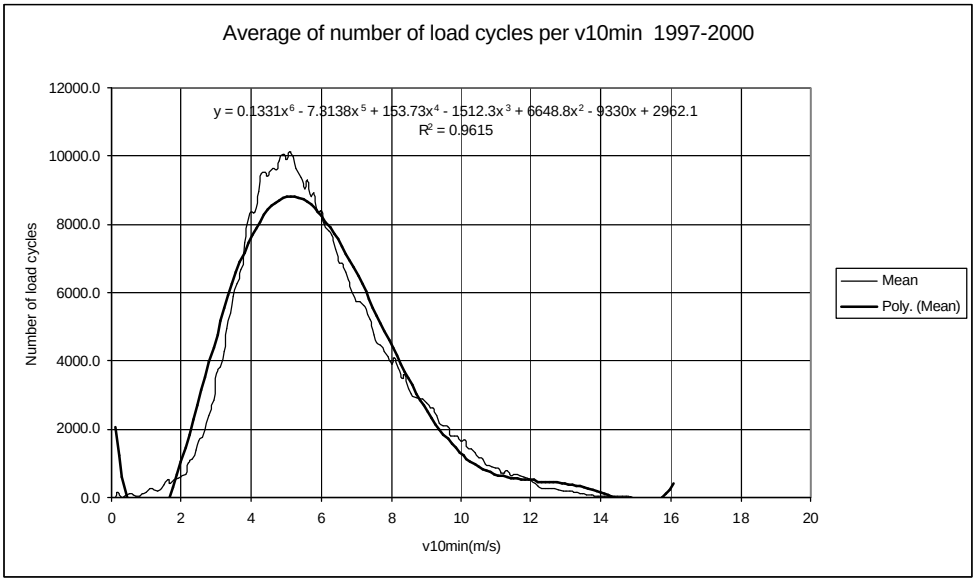

Figure 3.5 *a* Number of cycles per month as a function of 10 minutes wind velocity mean value per year for the recording period.

Critical wind velocity for vortex shedding has been calculated in Table 2.1 b to 3.24 m/s at the diameter 2.3 m (the chimney shell except at damper house) and 3.95 m/s at the diameter 2.8 m (at the damper house with a height of 3.35 m). The damper house height was only a little more than the diameter. Therefore its influence will be limited.

From [3] the number of load cycles during vortex shedding may be calculated from

$$n_v = 1.2 \cdot 10^7 \cdot t \cdot f_0 \cdot P(v) \quad \text{.....(3.38)}$$

where The factor 1.2 includes influence of different wind velocity directions and that an amount of time is required for building up vortex shedding oscillations

f_0 = Natural frequency

$P(v)$ = Probability for that mean wind velocity during one year occurs in the interval between v_{cr} and $\varepsilon\, v_{cr}$ where v_{cr} is the critical wind velocity for resonance vortex shedding oscillations.

P(v) is assumed to be a Rayleigh distribution.

$$P(v) = e^{\left[-\left(\frac{v_{cr}}{v(z)}\right)\right]} - e^{\left[-\left(\frac{e \cdot v_{cr}}{v(z)}\right)\right]} \quad \text{.....(3.39)}$$

$$v(z) = v_0 \cdot \sqrt{C_{exp}(z)} \quad \text{.....(3.40)}$$

where $v(z)$ = Yearly mean wind velocity at the height z
v_0 = The modal value of the distribution, 5.5 m/s
e = 1.25 but the difference between e and $e\, v_{cr}$ should be at least 2 m/s

v_{cr} is defined in Section 2.4.2. C_{exp} is defined and found from Table 3.2 a to 2.03.

Numerical values for the VEAB chimney gives

$v(z)$ = 7.83 m/s
$P(v)$ = 0.204
n_v = $0.7 \cdot 10^6$ oscillations per year or $21 \cdot 10^6$ oscillations for a 30 year period

The wind velocity found is twice the value achieved if the code [3] is extrapolated outside its limits but the number of cycles is less. In Figure 6.3 b the spectra for top deflection (functioning damper) is shown for both the recordings and some codes.

The wind vortex shedding load on the VEAB chimney is $\frac{13.1 \cdot 10^6 \cdot 6.32^2}{21 \cdot 10^6 \cdot 3.24^2} = 2.4$ times larger than what will be assumed from calculations according to [3] when limit restrictions are neglected (gust wind is not considered).

In Figure 3.5 β cumulative frequency of top deflection range for strain gauge no 4 is shown. The data for 4 years of service 1997 through 2000, a graphically fitted lognormal distribution for cumulative frequency of top deflection range and limits from Kolmogorov-Smirnov test (α=0.05) are plotted.

Because of the truncation of the data, top deflection range100 mm, the fitted curve differs greatly from measure data at the lower end. A log-normal representation has been chosen for simplicity.

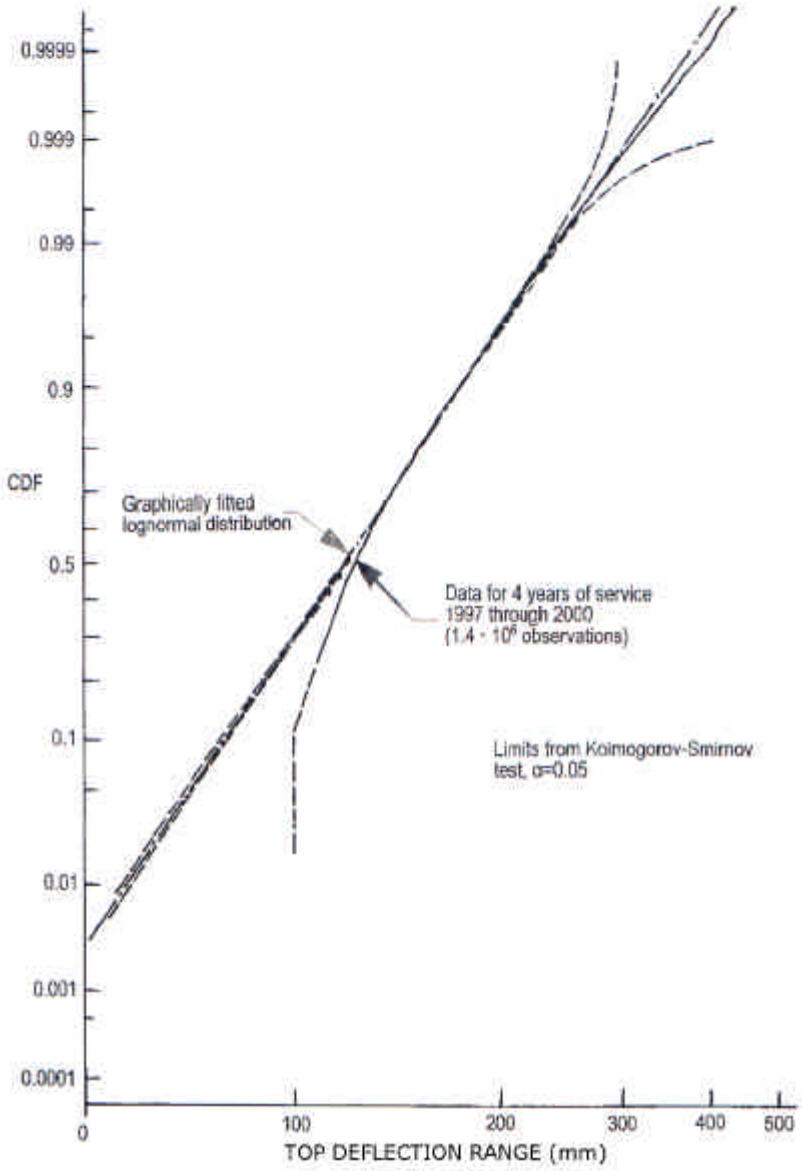

Figure 3.5 β Cumulative frequency of top deflection range for strain gauge no 4.

3.5.8 Frequency of wind velocity

The frequency distribution of wind velocity for the recording period 1997 through 2000 is plotted for 10 s, 1 min and 10 min mean values in Figure 3.5 *g* , 3.5 *d* and 3.5 *e* . The frequency distributions have a maximum at approximately 5 m/s. A Weibull distribution is fitted to each frequency distribution. Because top deflection ranges below 100 mm were truncated (Section 3.2.7) the fitted distribution consider the truncation effect.

The Weibull frequency distribution is described as

$$f(v,a,b) = \frac{a}{b^{\,b}} \cdot v^{a-1} \cdot e^{\left(-\frac{v}{b}\right)^a} \quad \text{.....(3.41)}$$

where v = Wind velocity in m/s
a = A Weibull distribution parameter
b = A Weibull distribution parameter

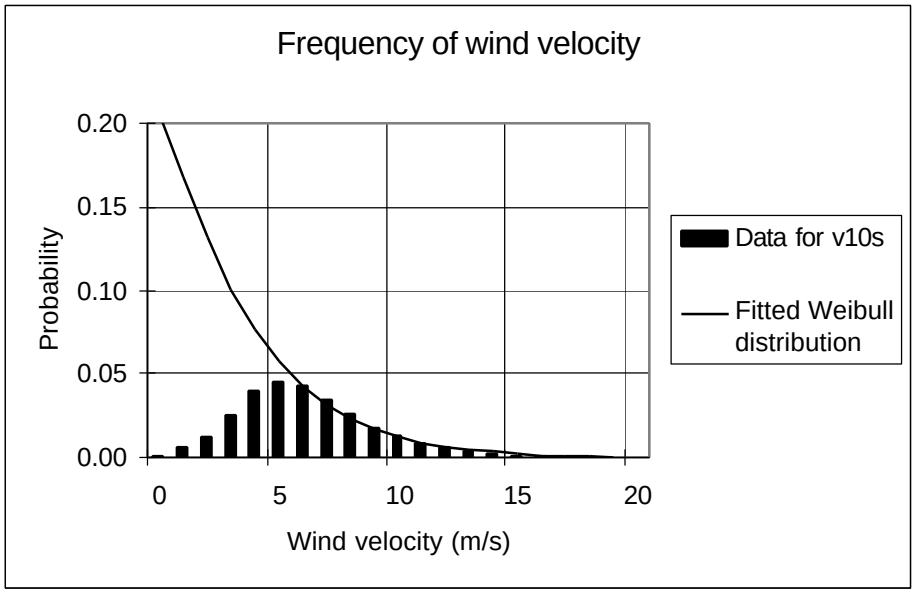

Figure 3.5 *g* Probability density function for wind velocity, 10-second wind velocity mean value. A fitted Weibull frequency distribution (α =1.1 and β=3.7) is included.

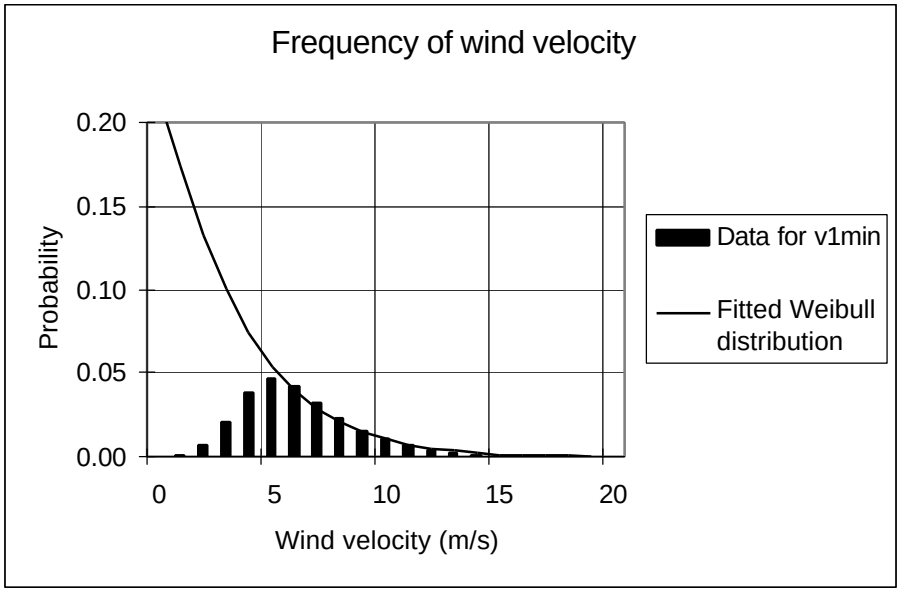

Figure 3.5 *d* Probability density function for wind velocity, 1-minute wind velocity mean value. A fitted Weibull frequency distribution (α =1.1 and β=3.5) is included

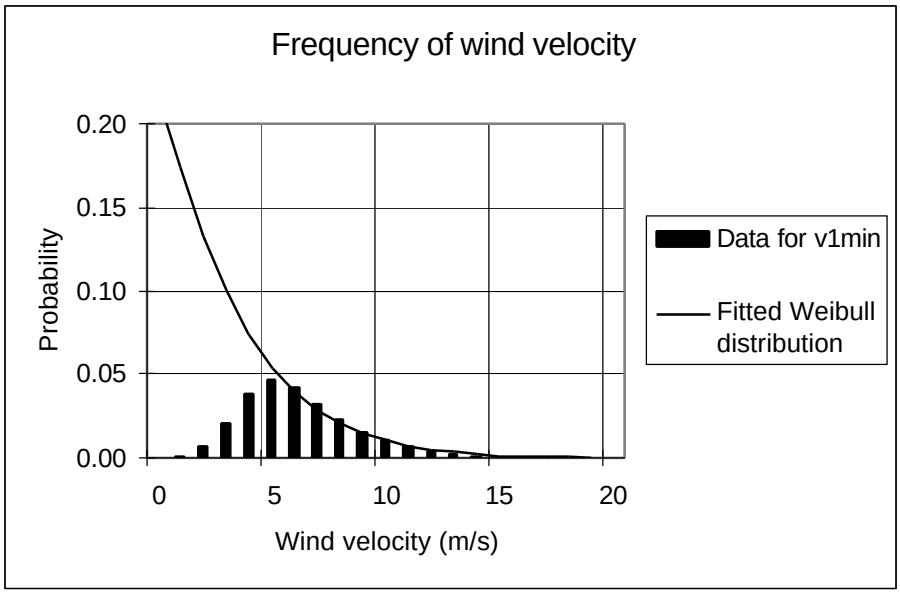

Figure 3.5 *e* Probability density function for wind velocity, 10-minute wind velocity mean value. A fitted Weibull frequency distribution (α =1.1 and β=3.3) is included

3.5.9 Iso-wind velocity plots

Iso-wind velocity plots for the recording period 1997 through 2000 are found in Figure 3.5 x, 3.5 h and 3.5 q.

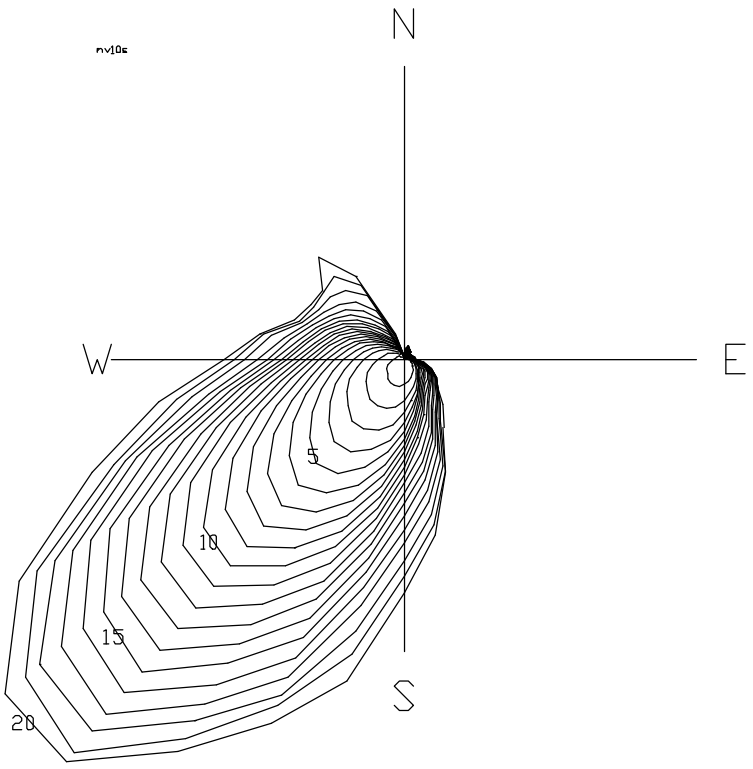

Figure 3.5 x Iso-wind velocity plot of 10 s wind velocity mean values. Unit m/s.

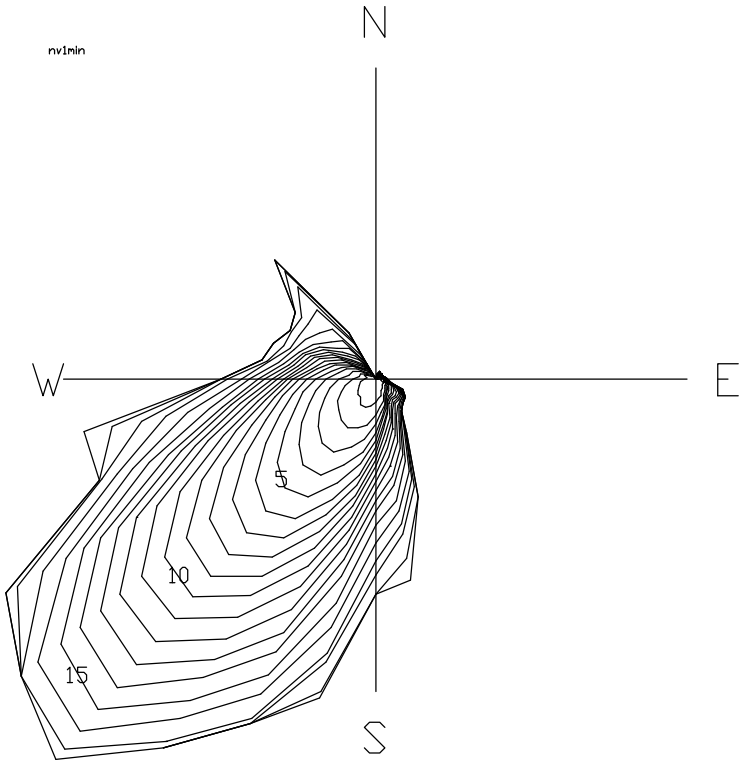

Figure 3.5 *h* Iso-wind velocity plot of 1 min wind velocity mean values. Unit m/s

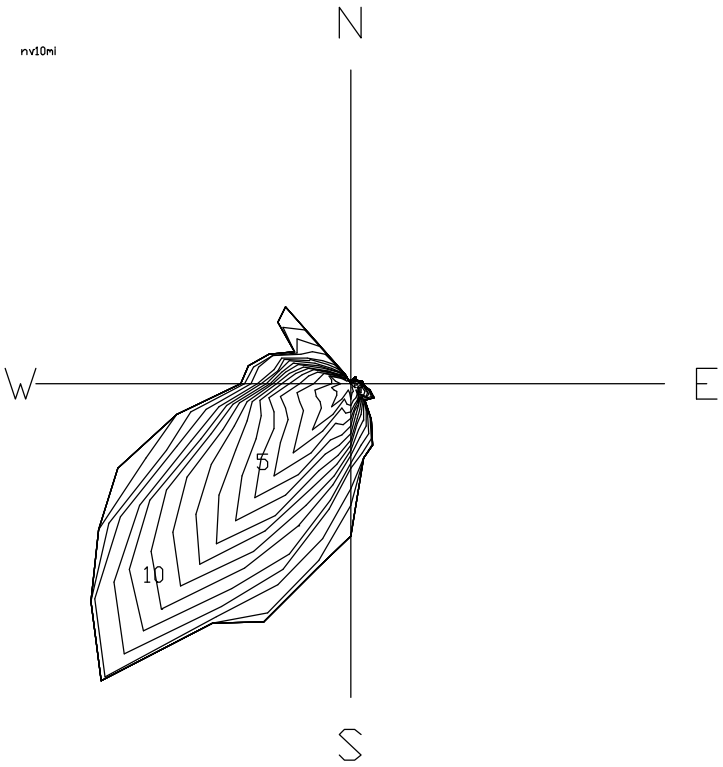

Figure 3.5 *q* Iso-wind velocity plot of 10 min wind velocity mean values. Unit m/s.

Iso-wind velocity plots similar to those in Figure 3.5 *x* , 3.5 *h* and 3.5 *q* , but where wind in opposite directions are added, are found in Figure 3.5 *i* , 3.5 *k* and 3.5 *l* .

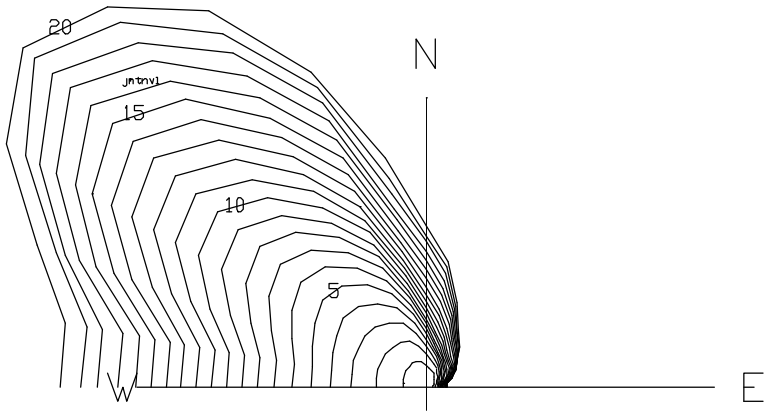

Figure 3.5 *i* Iso-wind plot of 10 s wind velocity mean values where values in 180 degrees opposite directions have been added. Unit m/s.

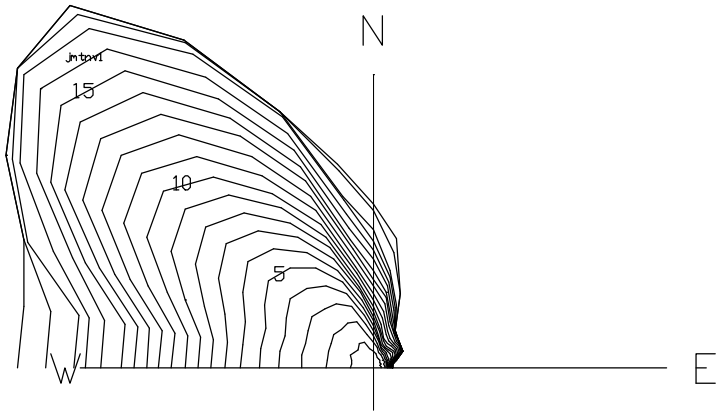

Figure 3.5 *k* Iso-wind plot of 1 min wind velocity mean values where values in 180 degrees opposite directions have been added. Unit m/s.

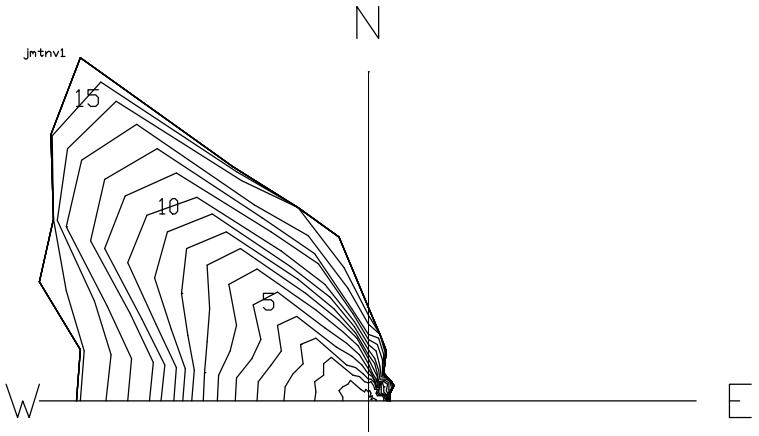

Figure 3.5 *l* Iso-wind plot of 10 min wind velocity mean values where values in 180 degrees opposite directions have been added. Unit m/s.

It was expected that Figure 3.5 *i* , Figure 3.5 *k* and Figure 3.5 *l* have shown iso-wind plots as half circles. This is not the fact because wind from south west is dominating for the recorded and truncated wind recordings (Section 3.2.7). The orientation of the Sandvik II plant buildings cover the bottom half height of the chimney. Therefore the wind direction could be partly influenced from the surrounding buildings.

3.6 Recordings of top deflection from deducted strain gauge measurements

From the recorded data, calculations were made, the data sorted and load spectra plotted. In Appendix E fatigue damage and cumulative fatigue damage are plotted for each month, per year and for the measure period 1997 through 2000. In this section a typical selection of load spectra (frequency distribution in the diagrams) and accumulated load spectra (spectrum in the diagrams) diagrams are shown.

For definition of directions see Figure 3.2 a.

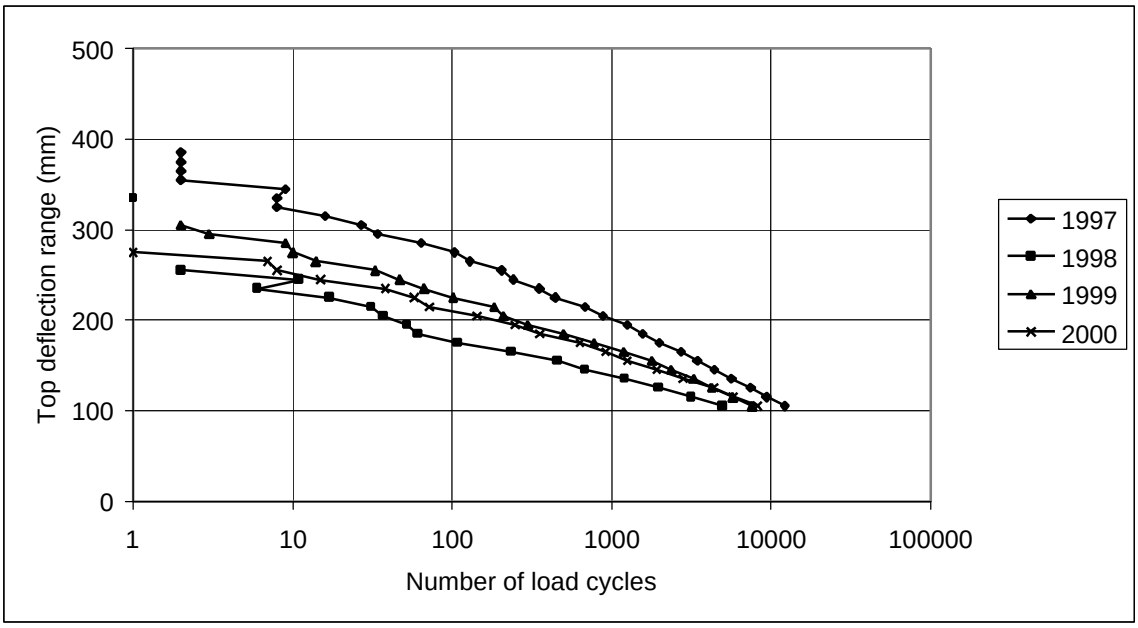

Figure 3.6 a Frequency distribution of top deflection range in direction 170 degrees for the month of September years 1997 through 2000.

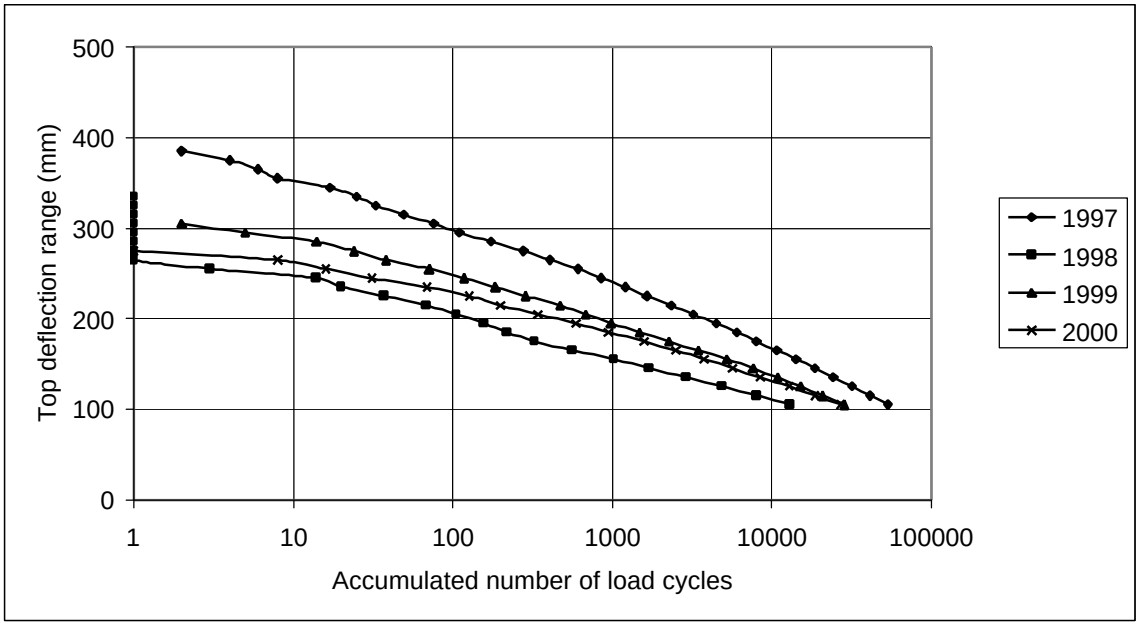

Figure 3.6 b Spectrum for top deflection range in direction 170 degrees for the month of September years 1997 through 2000.

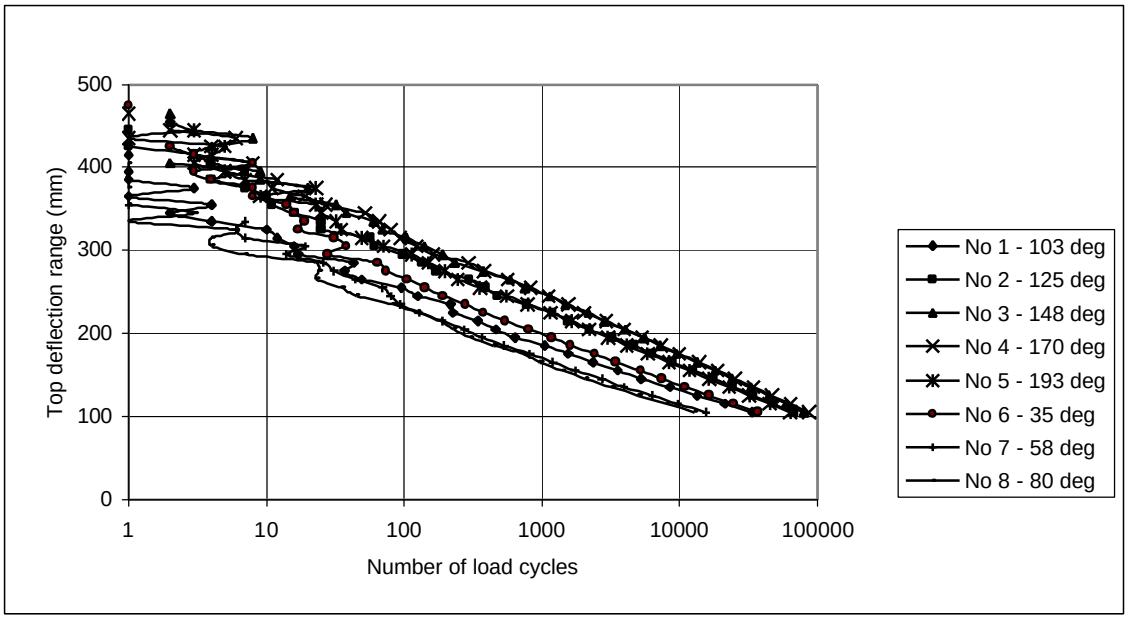

Figure 3.6 c Frequency distribution of top deflection range for the year of 1997 in the different directions.

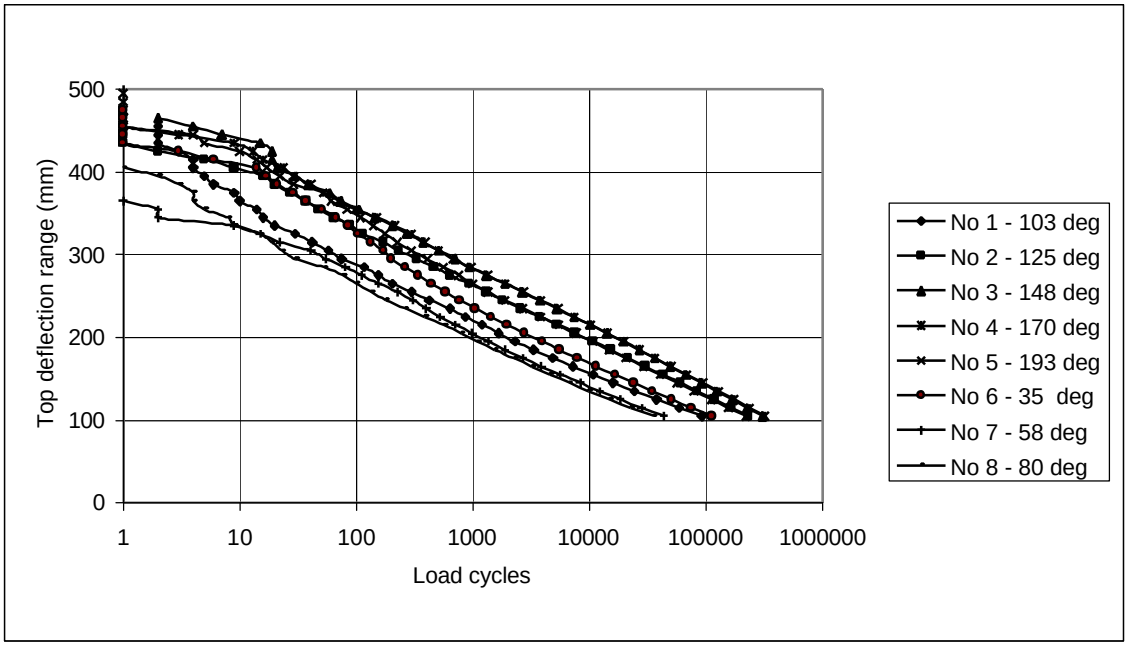

Figure 3.6 d Spectrum for top deflection range for the year of 1997 in the different directions.

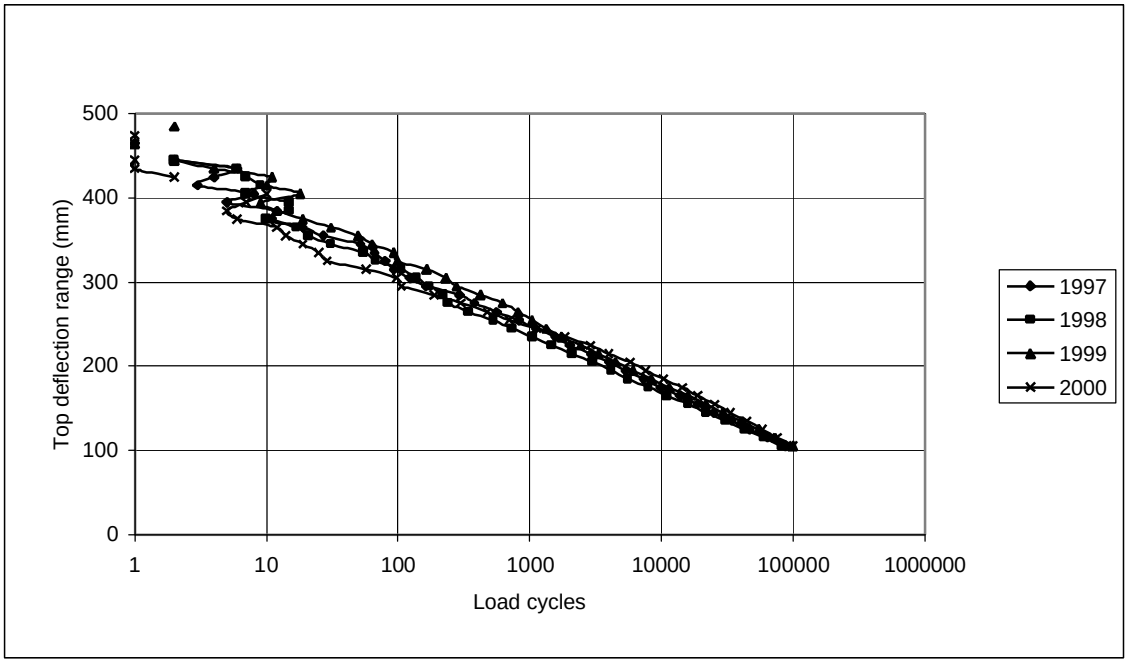

Figure 3.6 e Frequency distribution of top deflection range in direction 170 degrees for years 1997 through 2000.

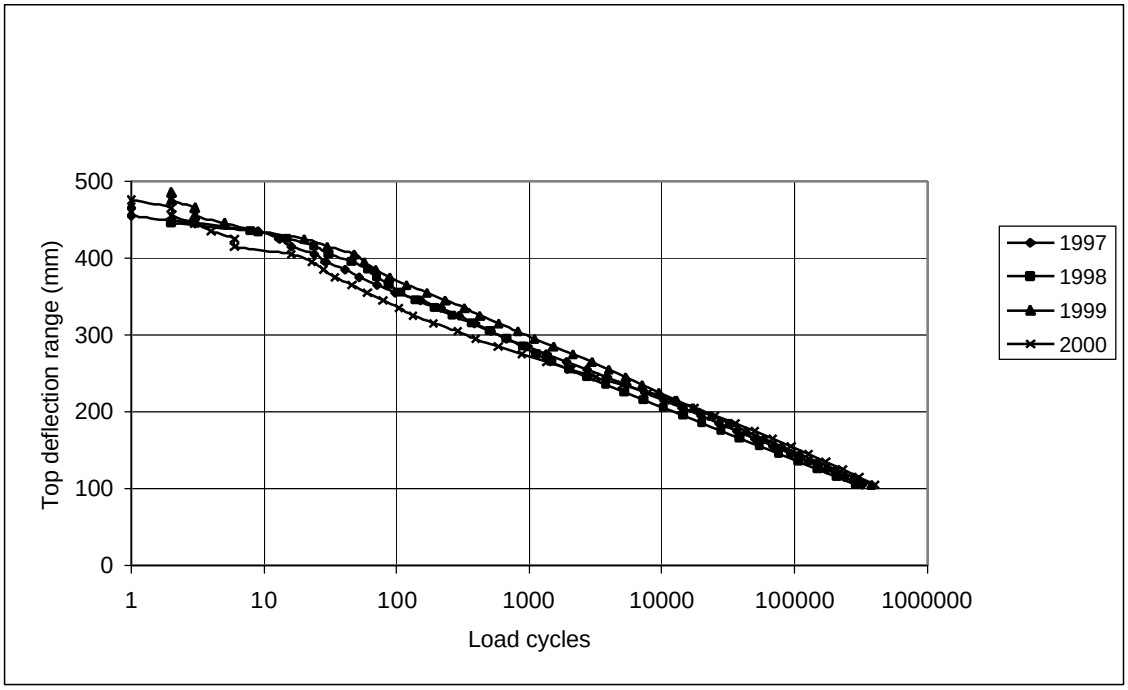

Figure 3.6 f Spectrum for top deflection range in direction 170 degrees years 1997 through 2000.

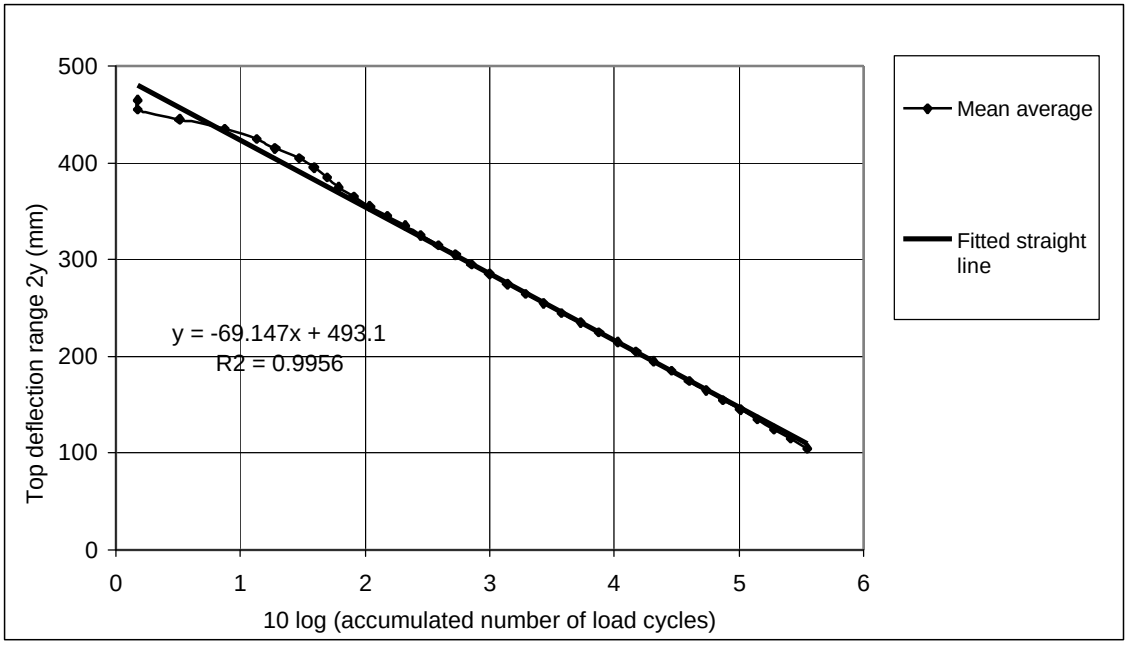

Figure 3.6 g Spectrum for top deflection range as mean per year in direction 170 degrees years 1997 through 2000. The thick line is a straight line fitted (least square method) to the results.

The straight line fitted to the data in Figure 3.6 g may be written

$$y = -35 \cdot^{10} \log(n_t) + 247 \quad \text{.....(3.43)}$$

where n_t = Accumulated number of load cycles
y = Top deflection amplitude in mm

By using Equation 4.6 the bending stress s_b in MPa per year at the chimney base is obtained as

$$s_b = y \cdot 0.087 = -3.01 \cdot^{10} \log(n_t) + 21.5 \quad \text{.....(3.44)}$$

Bending moment at the chimney base per year in Nm is found from Equation 3.5

$$M_b = s_b \cdot 10^6 \cdot \frac{2 \cdot I}{d} = s_b \cdot 73000 = \left[-0.220 \cdot^{10} \log(n_t) + 1.57 \right] \cdot 10^6 \quad \text{.....(3.45)}$$

Equation 2.10 gives the distributed load q N/m per year in Pa to

$$q = \frac{2 \cdot M_b}{H^2} = \frac{2 \cdot M_b}{90^2} = -54.2 \cdot^{10} \log(n_t) + 387 \quad \text{.....(3.46)}$$

If we assume that the distributed load will correspond to a wind pressure p in Pa per year of loads uniformly distributed over the chimney

$$p = \frac{q}{d} = -23.6 \cdot^{10} \log(n_t) + 168 \quad \text{.....(3.47)}$$

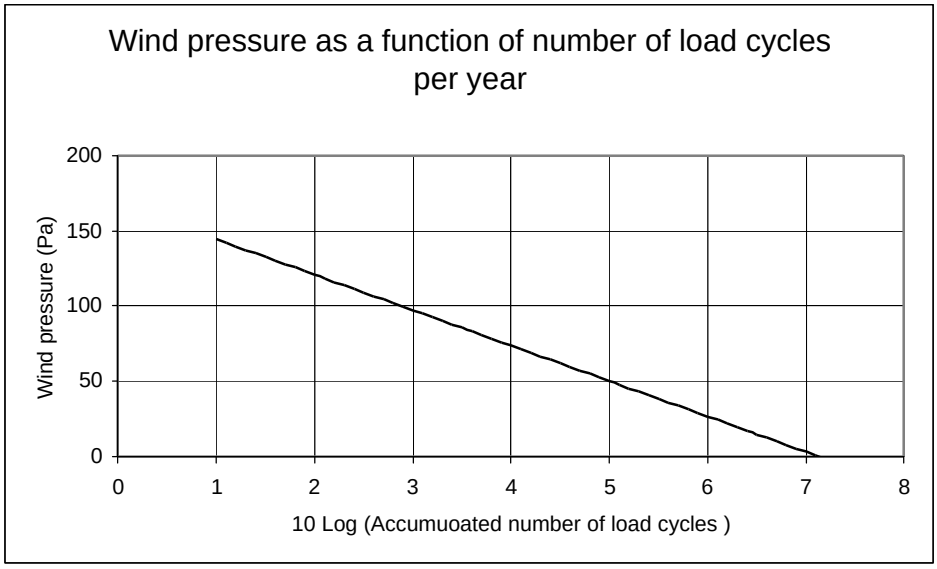

Figure 3.6 h Wind pressure, mainly caused by vortex shedding, as a function of number of load cycles per year.

In Section 6.3 and 6.4 comparisons between recorded spectrum and code spectra are made.

3.7 First and second mode oscillations

3.7.1 Screen plots

During the first half-year of measurements a lot of screen plots of the virtual instrument were made mainly to document the second mode oscillating behaviour. Below three typical plots are shown. More plots are found in Appendix D.

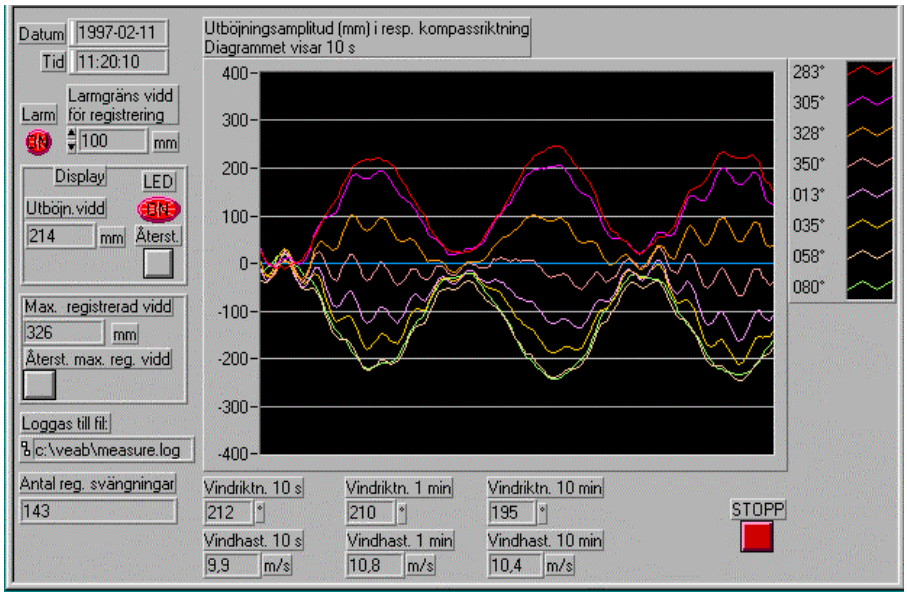

Figure 3.7 a Chimney oscillating in first mode and starting in second mode of natural frequency.

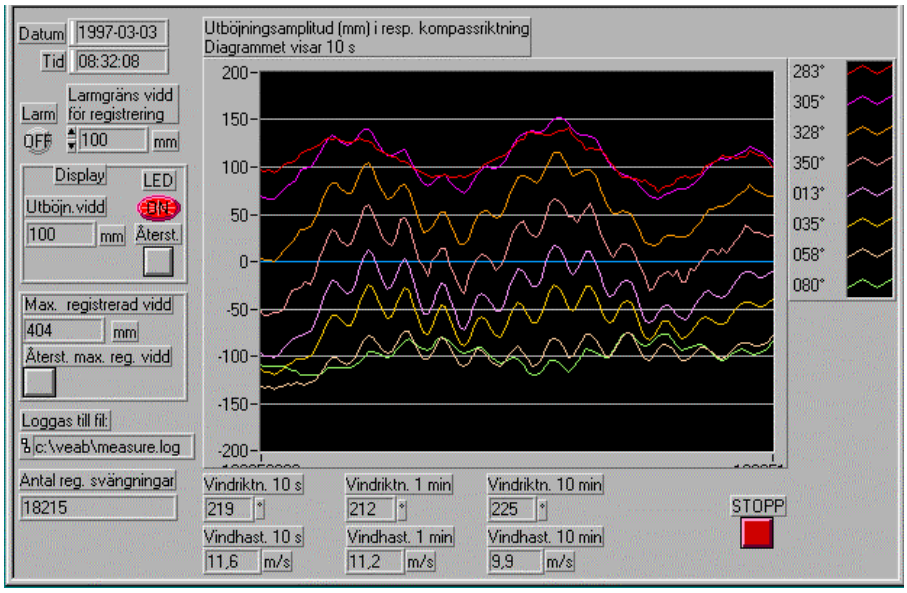

Figure 3.7 b Chimney oscillating in first and second modes of natural frequency.

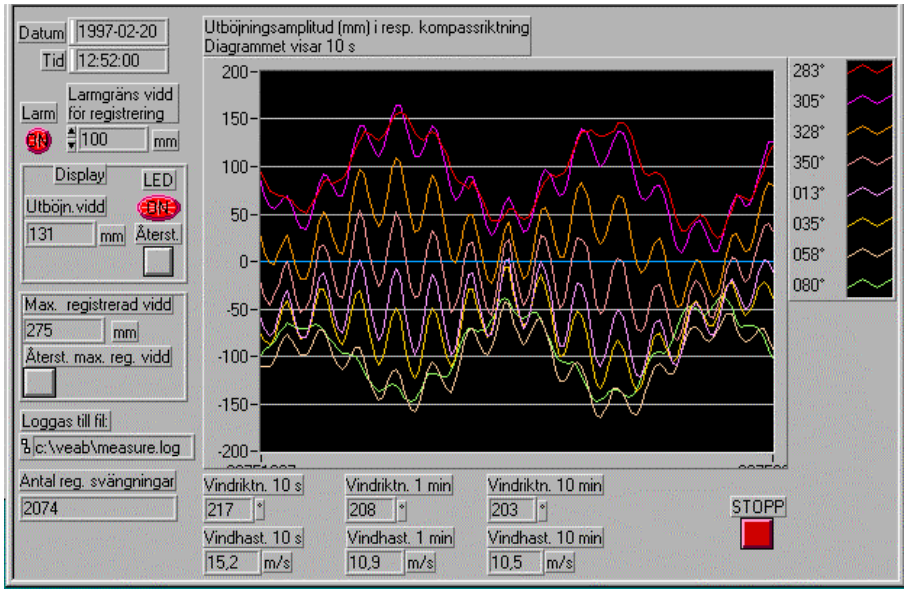

Figure 3.7 c Chimney oscillating in first and second modes of natural frequency.

By graphical determination in Figure 3.7 a to 3.7 c the natural frequency of the second mode is calculated to 1.45 Hz (approximately 5 times the first mode). This value may be compared to the calculated natural frequency of the second mode, 1.44 Hz.

From Figure 3.7 c maximum width for the second mode is found to be approximately 90 mm. This is representative of the complete data recorded.

The second mode was only observed at rare occasions as when the wind velocity calculated as a 10 min mean value exceeded approximately 10 m/s. The second mode frequency causes approximately 5 times more load cycles per time unit but the total amount of time is low.

3.7.2 Logged files

From logged recorded data, about two million loggings, natural frequency for the first mode has been calculated. In the log files there was no information about the second mode as described in Section 3.2.1.

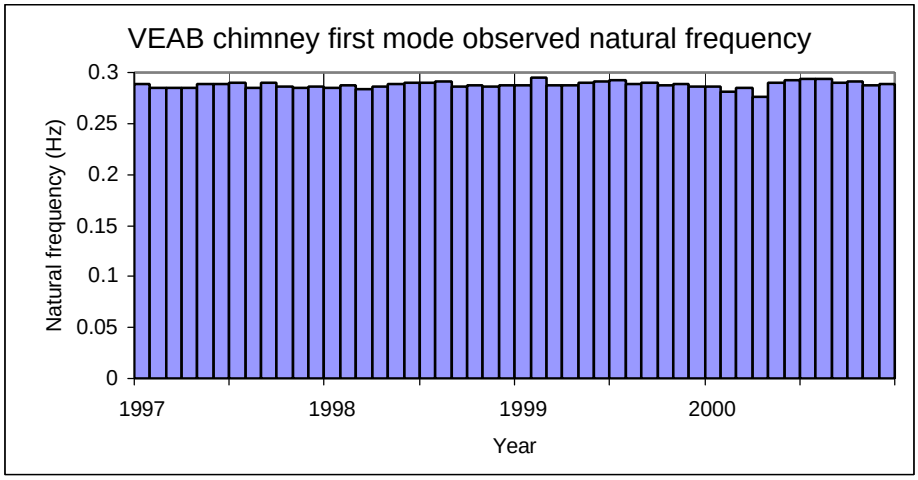

Figure 3.7 d Natural frequency as monthly mean values for the first mode during the observation period of 1997 through 2000.

Mean value for the observation period 1997 through 2000 is 0.288 Hz. See also Section 2.4.1.

3.7.3 First mode evaluation

From Section 3.4 and Appendix I it is found that first mode vortex shedding oscillations occur in the wind velocity interval of approximately $v_{10\text{min }45\text{m }1} = 4$ m/s to $v_{10\text{min }45\text{m }2} = 13$ m/s as observed from the wind transmitter at 45 m height. The larger values may be a combination between first and second order natural frequencies.

Wind velocities at the top of the chimney (90 m level) may to be corrected as (Section 3.2.3.2)

$$v_{10\text{min}90\text{m }1} = n_{\text{corr}} \cdot v_{10\text{min}45\text{m }1} = 1.10 \cdot 4 = 4.4 \text{ m/s to}$$
$$v_{10\text{min}90\text{m }2} = n_{\text{corr}} \cdot v_{10\text{min}45\text{m }2} = 1.10 \cdot 13 = 14.3 \text{ m/s}$$

It means that first mode natural frequency occurs at 4.4 to 14.3 m/s for 90 m level. According to Section 2.4.1 theory give first and second mode natural frequencies at 0.282 Hz respectively 1.44 Hz. Sections 3.7.1 and 3.7.2 gives 0.288 and 1.45 Hz respectively, which will be used in the following.

Temperatures at the time when the plots were created are:

Figure 3.7 a:	1997-02-11	T=3.5 °C
Figure 3.7 b:	1997-03-03	T=6.1 °C
Figure 3.7 c:	1997-02-20	T=3.5 °C

For the following calculations at a temperature of T=5 °C is assumed. The kinematic viscosity of the air is $13.7 \cdot 10^{-6}$ m^2/s at T=5 °C according to Section 3.8. The Reynold number is defined in Equation 1.1 and the Strouhal number in Equation 1.2.

The chimney diameter is 2.3 m, except for the damper house at the top where the diameter is 2.8 m. Reynold and Strouhal numbers corresponding to the wind velocity interval of 4.4 to 14.3 m/s will be

For d=2.3 m

$$R_{e1} = \frac{2.3 \cdot 4.4}{13.7 \cdot 10^{-6}} = 0.739 \cdot 10^6 \qquad St_1 = \frac{2.3 \cdot 0.288}{4.4} = 0.151 \text{ to}$$

$$R_{e2} = \frac{2.3 \cdot 14.3}{13.7 \cdot 10^{-6}} = 2.401 \cdot 10^6 \qquad St_2 = \frac{2.3 \cdot 0.288}{14.3} = 0.046$$

For d=2.8 m

$$R_{e1} = \frac{2.8 \cdot 4.4}{13.7 \cdot 10^{-6}} = 0.899 \cdot 10^6 \qquad St_1 = \frac{2.8 \cdot 0.288}{4.4} = 0.183 \text{ to}$$

$$R_{e2} = \frac{2.8 \cdot 14.3}{13.7 \cdot 10^{-6}} = 2.923 \cdot 10^6 \qquad St_2 = \frac{2.8 \cdot 0.288}{14.3} = 0.056$$

The above values for Strouhal numbers as a function of Reynold numbers are plotted in Figure 3.7 e into a diagram with literature data.

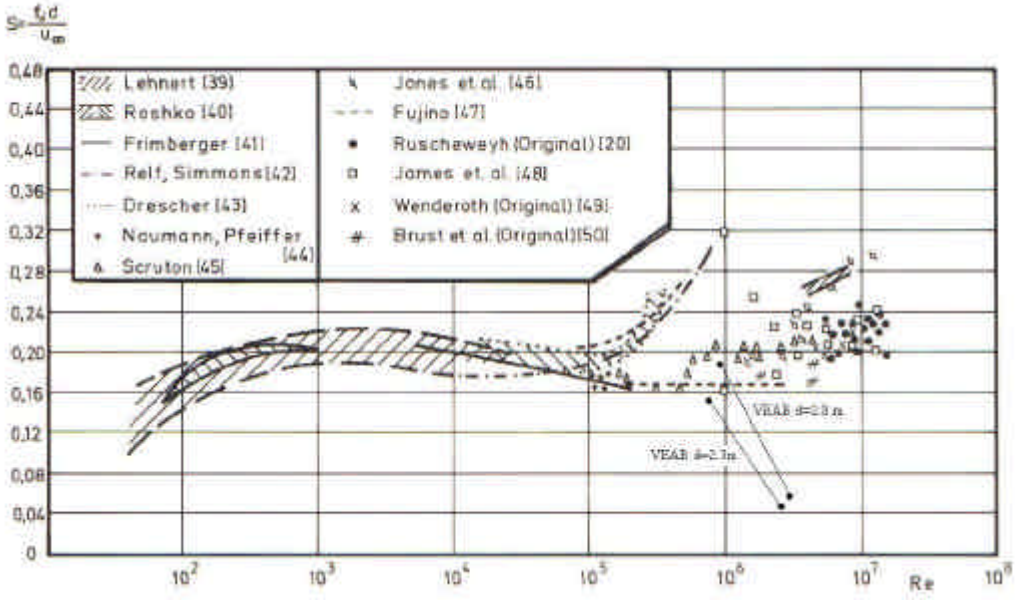

Figure 3.7 e Diagram taken from [6] where values for VEAB steel chimney during vortex shedding in the first mode have been added.

Fatigue caused by oscillation in the first mode of natural frequency is studied in Section 4.2 and 4.3.1.

3.7.4 Second mode evaluation

From the recordings, exemplified by Figure 3.7 a through 3.7 c, wind velocity mean value for 10 minutes is v_{10min}=10.5 m/s as measured at the wind transmitter at 45 m level. At 90 m height the corresponding wind velocity is (correction factor according to Section 3.2.3.2)

$$v_{10min90m} = n_{corr} \cdot v_{10min45m} = 1.10 \cdot 10.5 = 11.5 \text{ m/s}$$

It means that second mode mean wind velocity occurs at 11.5 m/s. According to Section 2.4.1 second mode critical wind velocity is 16.6 m/s.

At d=2.3 m $\quad R_e = \dfrac{2.3 \cdot 11.5}{15 \cdot 10^{-6}} = 1.76 \cdot 10^6 \quad S_t = \dfrac{2.3 \cdot 1.45}{11.5} = 0.29$

At d=2.8 m $\quad R_e = \dfrac{2.8 \cdot 11.5}{15 \cdot 10^{-6}} = 2.15 \cdot 10^6 \quad S_t = \dfrac{2.8 \cdot 1.45}{11.5} = 0.35$

The above values for Strouhal numbers as a function of Reynold numbers are plotted in Figure 3.7 f.

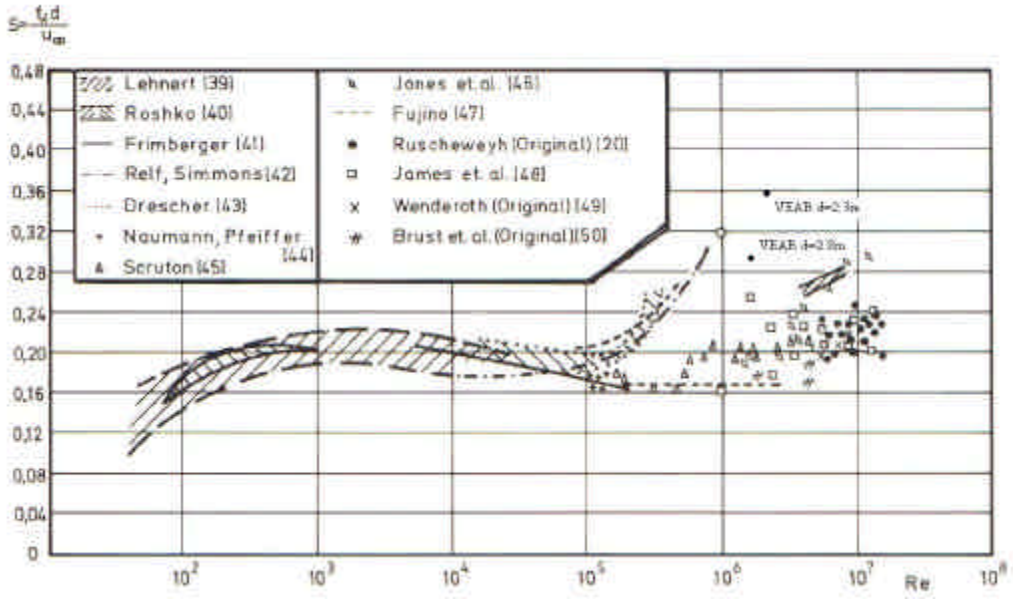

Figure 3.7.f Diagram taken from [6] where values for VEAB steel chimney during vortex shedding in the second mode have been added.

Fatigue caused by oscillations in the second mode is studied in Section 4.3.2.

3.7.5 Discussion

Strouhal number could be as big as 0.3, but forces exited are small. Therefore it is recommended that a Strouhal number of 0.2 should be used for engineering design calculations [1], [3], [5], [9]. For the first mode recorded results sometimes gives as small Strouhal number as 0.06. The effect explaining this is lock-in, where the vortex shedding starts at a lower wind velocities and continue to oscillate during increasing wind velocity. This is possible if the design has big slenderness ratio. Some codes, i. e. the Swedish BSV 97 manual [3] have limited the use of the code model to a maximum slenderness (height through diameter) of approximately 30. The results of this investigation support such a limit unless design loads are increased for slender structures, such as noted in some papers [1], [15]. The main problem with creating a code calculation model valid also for slender structures (slenderness much greater than 30) is the limited amount of recorded measure data. Sections 3.5.7 and 3.6 contain suggested load spectra and that this is more complex. Furthermore, chimneys with oscillations occurring in the second mode are more rare.

Second mode oscillations are seldom observed in structural steel chimneys [26]. For most steel chimneys only the first mode of oscillation is of practical importance for vortex shedding induced oscillations. The large slenderness of the VEAB chimney explains the relatively common and large second mode oscillations.

Because of the slender VEAB steel chimney (height through diameter = 39) correspondence between Strouhal number and Reynold number do not follow the predictions of Figure 3.7 e and 3.7 f [6]. For slender chimneys several codes give unconservative design loads for vortex shedding.

A damper applied at the top of the chimney is less efficient for second order than first order mode.

3.8 Temperatures and temperature dependent properties

3.8.1 Mean temperatures

VEAB Sandvik II plant records and stores in a database a lot of data about the plants behaviour and its environment. From the database the daily mean temperatures are collected and presented below. Appendix G contains a more complete description of the temperatures during the observation period. Those temperatures are used in Section 3.5 for calculating wind pressure. Some examples and a total summary are presented below.

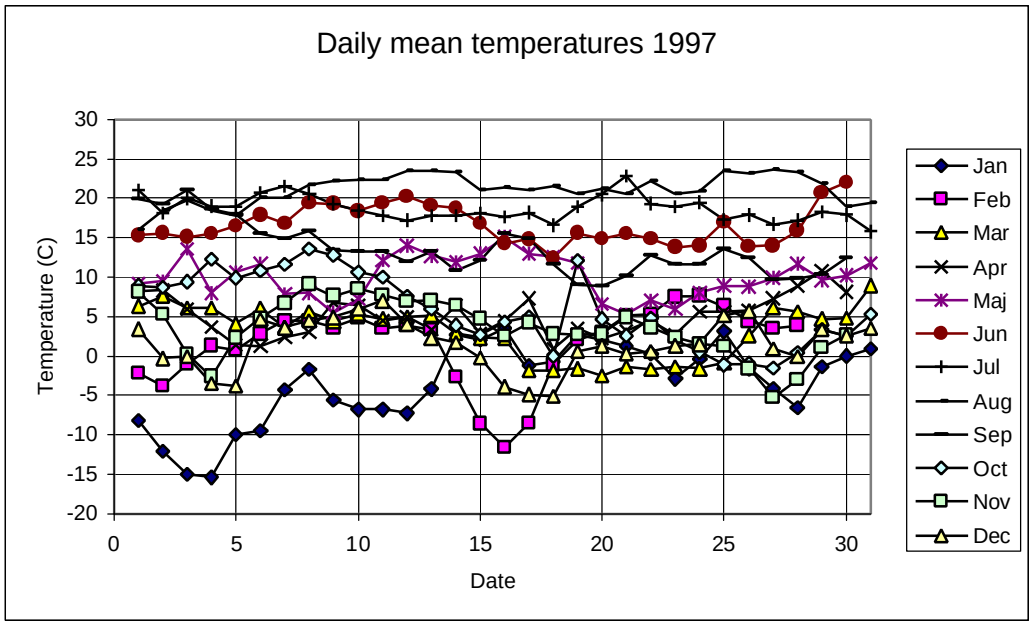

Figure 3.8 a Daily mean temperatures at VEAB Sandvik II plant for the year of 1997.

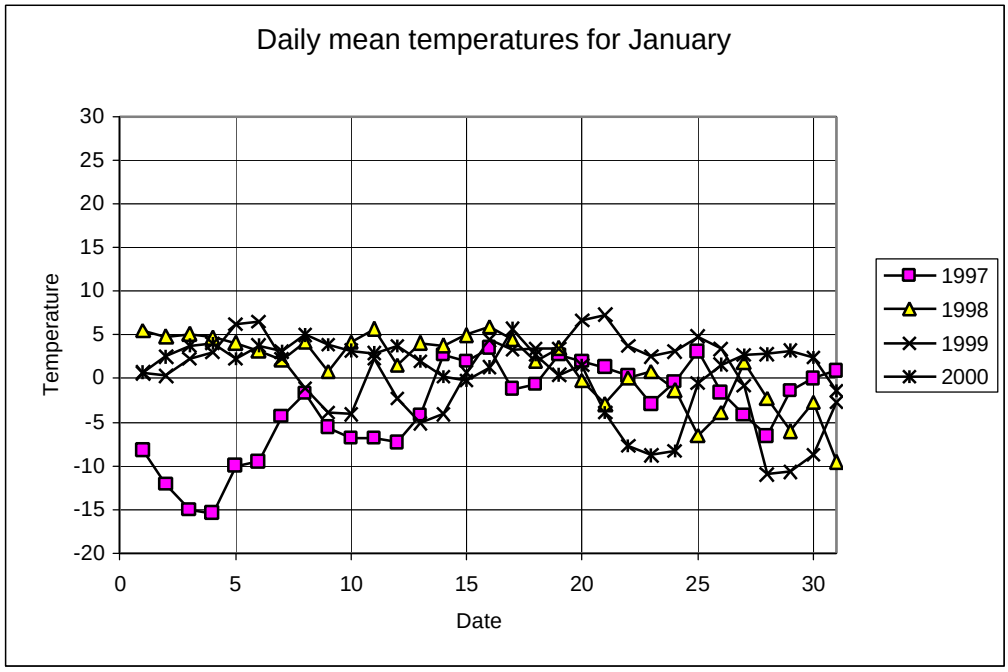

Figure 3.8 b Daily mean temperatures at VEAB Sandvik II plant for the month of January.

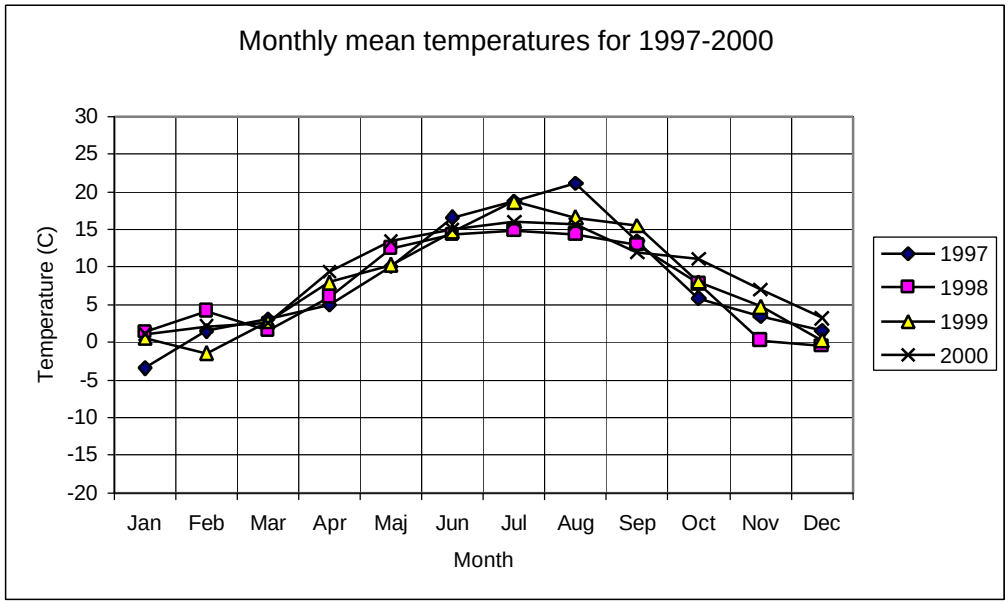

Figure 3.8 c Monthly mean temperatures at VEAB Sandvik II plant 1997 through 2000.

The VEAB Sandvik II plant was erected during the years 1995 and 1996. Therefore no recorded temperatures before 1996 are available. But for vortex shedding oscillations, which occurred during the interesting days between Christmas and New Year 1995 the temperature, was very low, about -20 °C.

3.8.2 Density and kinematic viscosity

Both density and viscosity of air vary with temperature. Unless otherwise is mentioned, all calculations in this report follow the temperature data in this section. Thus both density and viscosity follow the actual conditions. Influence of meterological pressure and humidity are neglected because that no such information were recorded. Their influences are also limited compared to the temperature.

According to [16] air densities follow the temperature as

$$r = r_0 \cdot \frac{T_0}{T} \quad \text{.....(3.48)}$$

where $r_0 = 1.29$ kg/m^3 at 0 °C and meterological air pressure 1 013 mbar

$T_0 = 273$ K

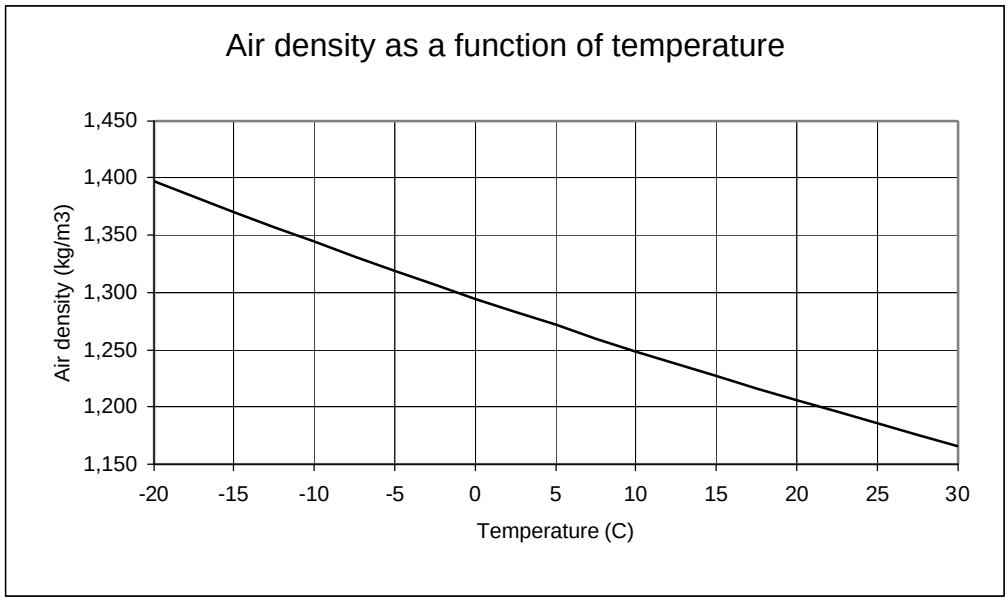

Figure 3.8 d Air density as a function of temperature at sea level when influence of meterological air pressure and air humidity is neglected.

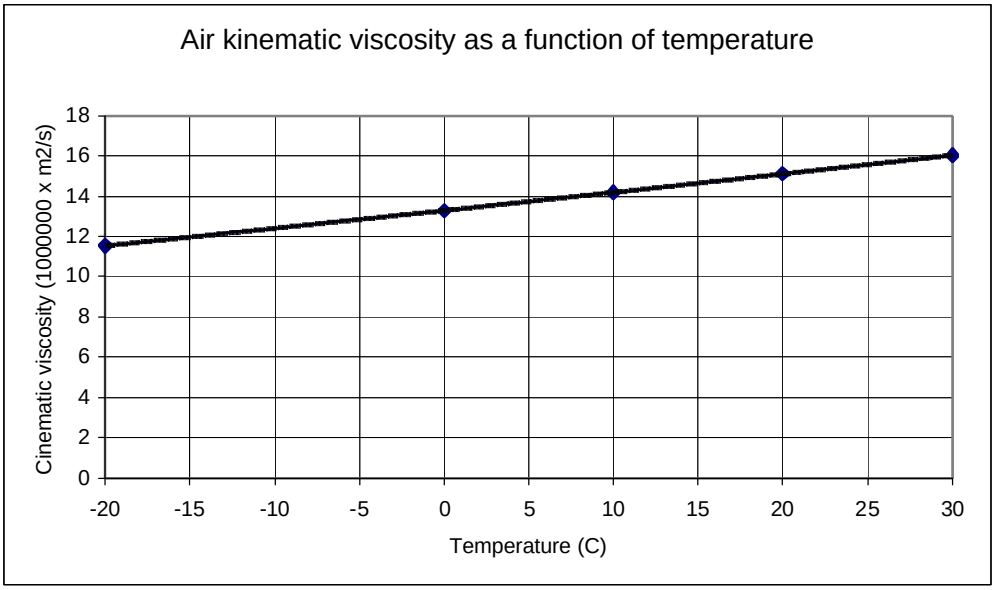

Figure 3.8 e Air kinematic viscosity as a function of temperature.

3.8.3 Discussion

Several codes and handbooks as for instance [3] suggest that the air density should be selected to 1.25 $\mathrm{kg/m^3}$ and that cinematic viscosity should be selected to $15 \cdot 10^{-6}$ $\mathrm{m^2/s}$ when calculating vortex shedding oscillating forces.

The air density 1.25 $\mathrm{kg/m^3}$ corresponds to an air temperature of 10 °C. At for instance a day with a temperature of -20 °C the density is instead 1.40 $\mathrm{kg/m^3}$. Calculated dynamic wind pressure will then be 12 percent greater than that determined for the nominal air density 1.25 $\mathrm{kg/m^3}$.

The viscosity $15 \cdot 10^{-6}$ $\mathrm{m^2/s}$ corresponds to an air temperature of 19 °C. At for instance a day with a temperature of –20 °C the cinematic viscosity is $11.5 \cdot 10^{-6}$ $\mathrm{m^2/s}$. Calculated Reynold number *Re* will be 30 % greater on the –20 °C day than on the 19 °C day. Extremely low turbulence levels due to stable stratification of the atmosphere (laminar air flow) during cold winter days characterise the airflow.

From Section 2.1 it is noted that the VEAB chimney is situated at a height of 164 m above sea level. The influence of air density depending of the height above sea level is being limited to some percent [3].

In evaluating the recorded data, the actual daily mean temperatures were considered when calculating the dynamic pressures and Reynold numbers. But the influence of level above sea level has been neglected.

4. Fatigue action

4.1 Fatigue model considered

For fatigue evaluation of the chimney the *Swedish Manual for Steel Structures BSK 99* [4] is followed.

The term stress range s_{rd} refers to the difference between maximum and minimum stress at a defined point, stresses being calculated according to elastic theory as normal stresses without consideration of local stress variations due to for instance the detailed geometry of the weld.

For normal stress, the design criterion with respect to fatigue is

$$s_{rd} \le f_{rd} \text{ [4]} \quad \text{.....(4.1)}$$

where $f_{rd} = f_{rk} / (1.1 \cdot g_n)$ is the design value of the fatigue strength.

The characteristic fatigue strength, f_{rk} is to be calculated with due regard to the stress concentration effects characterised by the class of detail C in accordance with [4], the number of stress cycles n_t during the service life of the structure, and the shape of the stress spectrum in accordance with [4].

The class of detail C is a measure of the characteristic fatigue strength for $2 \cdot 10^6$ stress cycles at a constant stress range.

Classes of detail for parent material and welded connections are given in [4]. The values given assume Workmanship GA or GB in accordance with [4].

For a spectrum with a constant stress range the characteristic value of the fatigue strength is

$$f_{rk} = C \cdot \left[\frac{2 \cdot 10^6}{n_t} \right]^{1/3}, \qquad n_t \le 5 \cdot 10^6 \text{ [4]} \quad \text{.....(4.2)}$$

$$f_{rk} = 0.885 \cdot C \cdot \left[\frac{2 \cdot 10^6}{n_t} \right]^{1/5}, \qquad 5 \cdot 10^6 \le n_t \le 10^8 \text{ [4]} \quad \text{.....(4.3)}$$

For structures not appreciably affected by corrosion, for instance where the corrosion protection is well maintained, it is assumed that the fatigue limit for a spectrum with constant stress range is assumed to be reached at 10^8 stress cycles.

The relationship between the characteristic value of the fatigue strength and the number of stress cycles is set out in [4].

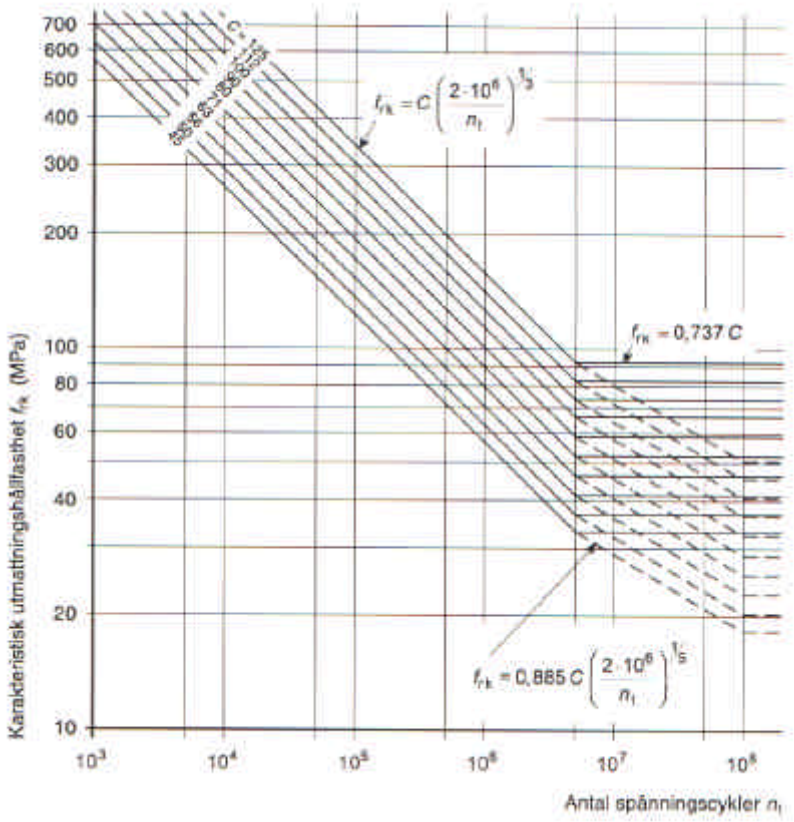

Figure 4.1 a Characteristic fatigue strength f_{rk} [4]. The full lines are applied for a stress spectrum with a constant stress range ($k = 1$). For a variable stress range, reference is to be made to [4].

For a stress spectrum with a variable stress range, the Palmgren-Miner cumulative damage hypothesis is to be applied [4] on the basis of the characteristic fatigue strength. The design value for each stress range is to be determined by multiplying the calculated nominal stress range for the design load effect by a factor $1.1 \cdot g_n$, where g_n depends on the safety.

In assembling the stress spectra, the 100 stress cycles that have the largest design values of the stress range, and stress cycles for which the design values of the stress range are smaller than values corresponding to the fatigue limit $n_t = 10^8$, may be ignored.

The design criterion in conjunction with a variable stress range is as follows

$$\Sigma\left(\frac{n_i}{n_{ti}}\right) \leq 1.0 \quad \text{.....(4.4)}$$

where

n_i = Number of stress cycles at a certain range s_i
n_{ti} = Number of stress cycles at a constant stress range which corresponds to the stress range s_{ri} .

Design is to be carried out in accordance with Equation 4.1, where s_{rd} is the largest nominal stress range in the stress spectrum being considered. Assembly of the stress spectrum may be carried out in accordance with the same principles, in accordance with the forgoing, apply in using the Palmgren-Miner hypothesis.

[4] states that the design value of the fatigue strength shall be determined as follows

$$f_{rd} = \frac{f_{rk}}{1.1 \cdot g_n} \quad \text{.....(4.5)}$$

Where g_n depends on the safety class according to [4].

For first mode oscillations, the relationship between top deflection in mm and characteristic chimney base bending stress for a distributed load, was calculated by the manufacturer of the chimney to

$$s_{rk\ Base} = y \cdot \frac{11.6\ \text{MPa}}{133.6\ \text{mm}} = y \cdot 0.087 \quad \text{.....(4.6)}$$

where *y* is in mm and $s_{k\ Base}$ in MPa.

For second mode oscillations it is found from Section 2.4.2 and 3.7.1 that the relationship between fictitious top deflection (superimposed oscillations on the first mode) and characteristic chimney base bending stress for a distributed load are the same as for the first mode of natural frequency. But plate thickness decreases from base to top of the chimney according to Section 2.1.2. A separate evaluation for the influence of second mode oscillations at worst location was made.

$$s_{rk\ mode\ 2} = y \cdot \frac{11.6}{133.6} \cdot \frac{90}{2 \cdot 133.6} = y \cdot 0.0292 \quad \text{.....(4.7)}$$

For fatigue design calculations [17] states that

$$s_{rd} = s_{rk} \quad \text{.....(4.8)}$$

At chimney base gusset plates the class of detail should have been *C* = 45 MPa according to Section 3.1. But because of defective manufacturing it was not achieved. Actual class of details were estimated to *C* = 30 MPa according to Section 3.1. It is below the lowest accepted level in [4] *C*=45 MPa.

4.2 Estimated cumulative damage for period with mal-functioning damper

From Section 4.1 we find that the damper was mal-functioning during the first nine months of service.

Elapsed time in hours during nine months is $9 \cdot \text{months} \cdot 30 \cdot \text{days} \cdot 24 \cdot \text{hours} = 6480 \cdot \text{hours}$.

By using the observations in Section 4.1 the following estimated distribution of top amplitude deflections versus time for the first nine months in service were made:

Table 4.2 a Estimated top deflection distribution for the first nine months in service

Amplitude *y* +/- (mm)	1 500	1 150	700	500	300	150	100	Total
Time *t* (h)	5	15	25	80	100	150	300	675
Relative time (percent of elapsed time)	0.08	0.23	0.39	1.23	1.54	2.31	4.63	10.42

The manufacturer calculated the stiffness/top amplitude deflection relationship to (Equation 4.6)

$$\frac{s}{y} = 0.087 \text{ N/mm}^3$$

The calculations in Section 3.3.2.2 give

Distributed load	w_{eq}	=	135	N/m
Reaction bending moment at chimney base	M_b	=	546 750	Nm
Top amplitude deflection	y	=	87.71	mm
Area moment of inertia at h=0 m	I	=	0.084	m^4
Diameter	d	=	2.3	m

Equation 3.5 and Figure 3.3 k give

$$s = \frac{M_b}{\frac{2 \cdot I}{d}} = \frac{546750}{\frac{2 \cdot 0.084}{2.3}} = 7.5 \text{ MPa}$$

$$\frac{s}{y} = \frac{7.5}{87.71} = 0.085 \text{ N/mm}^3$$

The manufacturers calculation of ratio of bending stress through top deflection and the corresponding calculation in this report gives similar result. In the following the manufacturers result $\frac{s}{y} = 0.087$ N/mm^3 was used.

The mean value for the natural frequency for the period 1997 through 2000 f=0.288 Hz (Section 2.4.1 and 2.7.2) was used.

From Section 4.1

$$f_{\mathrm{rk}}(n = 5 \cdot 10^6) = 30 \cdot \left(\frac{2}{5}\right)^{\frac{1}{3}} = 22.1 \text{ MPa}$$

$$f_{\mathrm{rk}}(n = 1 \cdot 10^8) = 0.885 \cdot 30 \cdot \left(\frac{2 \cdot 10^6}{10^8}\right)^{\frac{1}{5}} = 12.1 \text{ MPa}$$

$$f_{\mathrm{rd}}(n = 5 \cdot 10^6) = \frac{22.1}{1.1 \cdot 1.1} = 18.3 \text{ MPa}$$

$$f_{\mathrm{rd}}(n = 1 \cdot 10^8) = \frac{12.1}{1.1 \cdot 1.1} = 10.0 \text{ MPa}$$

$$n_{\mathrm{ti}} = \left(\frac{C}{s_{\mathrm{rd}}}\right)^3 \cdot 2 \cdot 10^6 \qquad s_{\mathrm{rd}} \geq 18.3 \text{ MPa}$$

$$n_{\mathrm{ti}} = \left(\frac{0.885 \cdot C}{s_{\mathrm{rd}}}\right)^5 \cdot 2 \cdot 10^6 \qquad 10.0 \leq s_{\mathrm{rd}} \leq 18.3 \text{ MPa}$$

The cumulative fatigue damage values have been calculated in Table 4.2 b.

Table 4.2 b Cumulative fatigue damage according to Table 4.2 a for an estimated load spectrum for the first nine months of service and $g_{\mathrm{n}} = 1.1$.

y (mm)	t (h)	s_{rki} (MPa)	s_{rdi} (MPa)	n	n_{ti}	n/n_{ti}
1500	5	261	315.8	5184	1715	3.02
1150	15	200.1	242.1	15552	3806	4.09
700	25	121.8	147.4	25920	16862	1.54
500	80	87.0	105.3	82944	46250	1.79
300	100	52.2	63.2	103680	213916	0.48
150	150	26.1	31.6	155520	1711325	0.09
100	300	17.4	21.1	311084	6308707	0.05
						11.1

It means that the cumulative damage fatigue according to the Palmgren-Miner Hypothesis will be about 11 at a resistance factor $g_n = 1.1$ corresponding to a probability of damage of approximately 10^{-4}.

If the probability of failure is set to 0.5 the resistance factor will be approximately $1.1 \cdot 0.75 = 0.825$ [18].

$$f_{rd}(n = 5 \cdot 10^6) = \frac{22.1}{1.1 \cdot 0.75} = 26.8 \text{ MPa}$$
$$f_{rd}(n = 1 \cdot 10^8) = \frac{10.0}{1.1 \cdot 0.75} = 12.1 \text{ MPa}$$

The cumulative fatigue damage will then be as calculated in Table 4.2 c.

Table 4.2 c Cumulative fatigue damage for an estimated load spectrum for the first nine months of service and $g_n = 0.825$, which corresponds to a probability of damage of approximately 0.5.

y (mm)	t (h)	s_{rki} (MPa)	s_{rdi} (MPa)	n	n_{ti}	n/n_{ti}
1500	5	261	215.3	5184	5411	0.96
1150	15	200.1	165.1	15552	11999	1.30
700	25	121.8	100.5	25920	53198	0.49
500	80	87.0	71.8	82944	145888	0.57
300	100	52.2	43.1	103680	674469	0.15
150	150	26.1	21.5	155520	5743284	0.03
100	300	17.4	14.4	311084	42612809	0.00
						3.50

The large number of cracks is in correspondence with the above-calculated cumulative damage fatigues.

4.3 Cumulative damage for period with functioning damper

4.3.1 First mode of natural frequency

4.3.1.1 Foundation level

The strain gauges were primarily aimed to study the influence of first mode of natural frequency to the fatigue strength (Section 3.2.1).

The recording period is the years 1997 through 2000. To reduce the amount of data to be stored, values were truncated if maximum range was less than 100 mm according to Section 3.2.7.

For strain gauge 1 and 3 there are a number of unrealistic values from January until April 2000. They are truncated because of errors at the strain gauges, see Section 3.2.8.

Cumulative fatigue damage has been calculated for the recording period 1997 through 2000. Because of the difference between design assumptions and true values for class of detail both *C*=45 and *C*=30 are assumed. *C*=45 is the design assumption and *C*=30 the accurate class of detail. *C*=45 corresponds to a class of detail similar to a class of weld of WC according to [4]. It means that *C*=30 corresponds to a class of weld below WC. In the cumulative damage calculations nothing else than geometric stress concentrations from the weld alone was included. For the original design of the gusset plates at foundation level (Figure 2.2 c and 2.2 d) and 30 m level (Figure 2.2 e) it is reasonable to add an additional geometric stress concentration. Because of the changed design after two years of service (Figure 2.2 g and Figure 2.2 i) no additional stress concentrations are added to the class of detail *C*.

Table 4.3.a Damage fatigue for 1997 at class of detail *C*=30 respective *C*=45

C	Gauge no 1	Gauge no 2	Gauge no 3	Gauge no 4	Gauge no 5	Gauge no 6	Gauge no 7	Gauge no 8
30	0.0016736	0.00625349	0.0099898	0.01003540	0.00578685	0.00235369	0.00080252	0.00067543
45	0.00013162	0.00057027	0.00102408	0.00099927	0.00052442	0.00019323	0.00006214	0.00005592

Table 4.3.b Damage fatigue for 1998 at class of detail *C*=30 respective *C*=45

C	Gauge no 1	Gauge no 2	Gauge no 3	Gauge no 4	Gauge no 5	Gauge no 6	Gauge no 7	Gauge no 8
30	0.00109454	0.00580580	0.01042424	0.01130228	0.00630474	0.00181172	0.00025356	0.00021740
45	0.00007902	0.00061170	0.00126551	0.00133086	0.00063884	0.00011620	0.00001215	0.00001095

Table 4.3.c Damage fatigue for 1999 at class of detail *C*=30 respective *C*=45

C	Gauge no 1	Gauge no 2	Gauge no 3	Gauge no 4	Gauge no 5	Gauge no 6	Gauge no 7	Gauge no 8
30	0.00171796	0.00612419	0.01083196	0.01212821	0.00726709	0.00267103	0.00077496	0.00070521
45	0.00013927	0.00056558	0.00115432	0.00128465	0.00070408	0.00023725	0.00006437	0.00005421

Table 4.3.d Damage fatigue for 2000 at class of detail *C*=30 respective *C*=45

C	Gauge no 1	Gauge no 2	Gauge no 3	Gauge no 4	Gauge no 5	Gauge no 6	Gauge no 7	Gauge no 8
30	0.00102202	0.00559000	0.00897362	0.01298475	0.00749771	0.00227207	0.00054623	0.00033561
45	0.00017150	0.00040299	0.00084157	0.00117389	0.00056996	0.00012609	0.00004032	0.00001880

Table 4.3.e Damage fatigue for the entire measure period 1997 through 2000 at class of detail *C*=30 respective *C*=45

C	Gauge no 1	Gauge no 2	Gauge no 3	Gauge no 4	Gauge no 5	Gauge no 6	Gauge no 7	Gauge no 8
30	0.00566482	0.02405545	0.04046838	0.04659365	0.02689582	0.00911692	0.00238477	0.00197968
45	0.00053598	0.00218143	0.00430908	0.00479834	0.00243850	0.00067287	0.00017906	0.00014352

From Table 4.3 e it is found that greatest fatigue damage during the recording period (four years) was at bridge no 4 where utilization was 0.047 at *C*=30 and 0.0048 at *C*=45. If the measurement period is representative for the complete service life of 30 years the fatigue damage for the service life will be

For *C*=30 $0.04659365 \cdot \frac{30 \text{ Years}}{4 \text{ Years}} = 0.35$

For *C*=45 $0.00479834 \cdot \frac{30 \text{ Years}}{4 \text{ Years}} = 0.036$

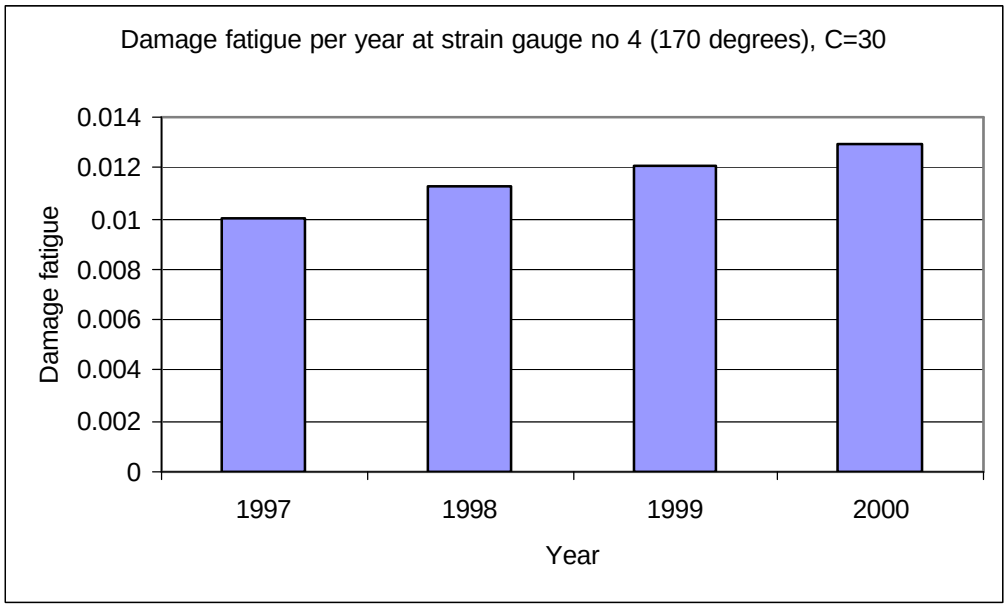

Figure 4.3 a Fatigue damage per year for recordings at strain gauge no 4 (170 degrees) and class of detail *C*=30.

In Figure 4.3 a the fatigue damage shows an increasing magnitude during the years. There are only four years of recordings. Therefore the statistical material is limited. It is not possible to determine if the increase is an actual trend accidental.

4.3.1.2 Other heights than base level

According to Section 2.4.3 the bending moment and the area moment of inertia (Equations 2.10 and 2.11) are described as

$$M(x) = \frac{q}{2} \cdot (H^2 - x^2)$$

$$I(x) = \frac{p}{64} \cdot \left[D^4 - (D - 2 \cdot t)^4 \right] \text{ at each height x}$$

By using Equation 3.5 bending stress is described as

$$s_b(x) = \frac{M(x)}{\frac{2 \cdot I(x)}{d}} \quad \text{.....(4.9)}$$

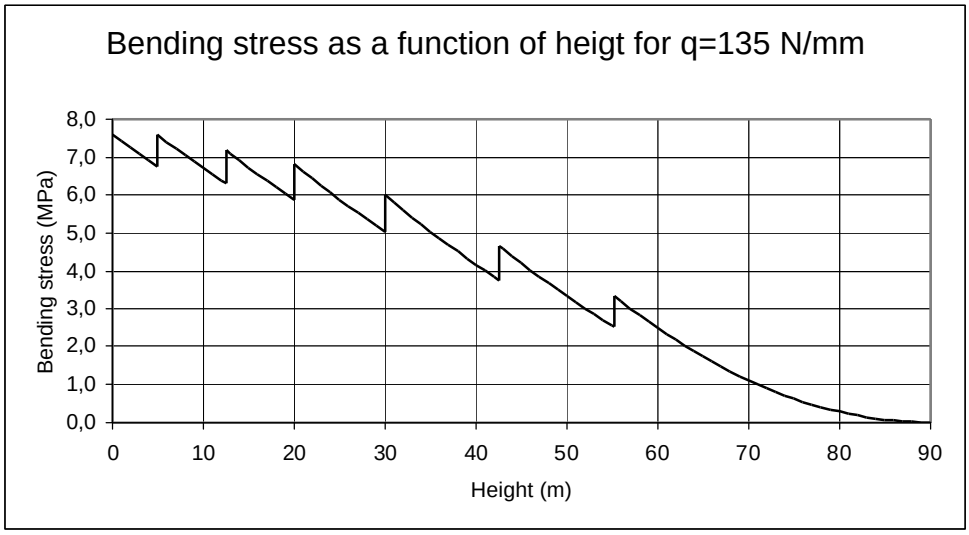

Figure 4.3 b Bending stress as a function of the height for a distributed load of 135 N/m.

From diagram 4.3 b it is obvious that, for a given stress concentration effect, the base level will govern the design.

4.3.2 Influence of second mode of natural frequency

Natural frequency at second mode was 1.44 Hz (Section 2.4.1). By comparing Equations 2.10 and 2.11 and considering Figure 4.3 b it was obvious that first mode oscillations govern the design when the stress concentration effect is similar. Second mode oscillations are below the

endurance limit. Therefore no superposition of first and second mode oscillations has been made.

5 Crack propagation

5.1 Method of analysis

To get an estimation of the safety against fracture of the VEAB chimney, at the point of time when the damper was malfunctioning and before the cracks were repaired, a simplified crack propagation analysis was made. The complete calculation is shown in Appendix L.

In this simplified estimation study the linear method was used as presented in [18].

The observed cracks at the erection splice at the 30 m level were found to be most critical.

The studied crack was of type 1 according to Figure 3.1 a. The shell plate thickness was 10 mm. Typical crack length was 10 mm and a crack depth of 3 mm into the shell plate according to Appendix J.

The pitch is approximately 180 mm between the gusset plates. Several welds at the gusset plates were damaged by cracks. Therefore acceptable crack width was expected to be << 180 mm.

A lock-in factor of two is assumed for this analysis. It is based on results from Sections 3.4 and 3.5.

5.2 Results

From a simple finite element analysis (FEA) calculation the geometric stress concentration was found to be 2 (Appendix K).

For the case with a functioning damper allowable crack length for a non-propagating surface crack was calculated to 0.3 mm. For the case with a malfunctioning damper the corresponding crack length was calculated to 0.2 mm.

The cracks were found to propagate critical if the damper is functioning after
1 200 000 +114 000 = 1 300 000 cycles, or 48 + 4.6 = 53 days of continuous vortex shedding oscillation.

The cracks were found to propagate critical if the damper is malfunctioning after
225 000 + 21 400 = 250 000 cycles, or 9 + 1 = 10 days of continuous vortex shedding oscillating.

The corresponding number of load cycles during vortex shedding according to Section 3.5.7 is $13.1 \cdot 10^6$ according to the observations and $21 \cdot 10^6$ according to [3]. The load spectrum is discussed in chapter 3.6.

Considering the assumed load spectrum it is obvious that the chimney before it was repaired had a high probability for collapse.

6 Discussion

6.1 The reliability of buildings with mechanical movable devices

The reliability of typical ordinary buildings is only depending on its support structure transferring loads from the entire part of the building to the supports. A chimney or any other construction equipped with a mechanical damper relies both on the support structure and on the function of the damper.

Therefore the first question to discuss is whether reliability of building structures should be depending on a devise or not. If the device is properly designed and functions as expected there are no problems. But if the device is mal-functioning in any way it could be hazardous for the reliability of the building.

For mechanical pendulum tuned dampers at steel chimneys we have noted the following risks:

- There will be condensation in the damper house. An estimating calculation shows that there is risk of condensation in the damper house at some weather conditions, but the amount of condensed water is small. Thus the friction between friction mass and damper house bottom will be other than assumed in the design calculations and the damper properties could be changed.

- There may be corrosion in the damper house caused by condensation in the damper house. The friction mass could corrode and get caught to the damper house bottom and the damper will be locked. There may require excessive accelerations to loosen the friction mass from the damper house bottom.

- The friction mass will freeze to the damper house bottom caused by the condensation water and the damper will be locked. There will be required large accelerations to loosen the friction mass from the damper house bottom.

- The chimneys are aimed to operate for a period of many years. For the VEAB chimney the design lifetime was decided to 30 years, which is common practice for chimneys in Sweden. Because of the long lifetime there could be worries about dangerous wear eventually in combination with corrosion.

- Error in handling or careless handling during erection and service could make the damper inoperable by mistake.

- Design errors as wrongly calculated natural frequencies, error in selection of pendulum masses, error in selection of friction devices may result in a mistuned damper with limited damping. [19] and Section 3.3.2.4 deals with the problem of mistuned dampers on steel chimneys. There could be a lot of reasons for why calculated natural frequency differ from the real one, such as errors in calculating the natural frequency, simplified calculation model which miss some effects or different mass distribution than assumed.

- The mechanical pendulum tuned damper requires a regular maintenance program. For the VEAB chimney it was decided to once a year. If the maintenance is neglected the reliability of the chimney is impaired. As for the aircraft and nuclear industry the inspection interval has to be smaller than the time required for a crack to grow critical with a mal-functioning damper. According to Section 5, 10 days of continuous vortex shedding oscillations could create critical crack and collapse. For the VEAB chimney there were only one yearly inspection planned and acceptable inspection interval therefore were to long.

- Ice on the chimney during the winter periods add mass and changes the natural frequency resulting in a mistuned damper.

- Reynold number is changed if the chimney is charged with rainwater as discussed in [20]. Then the shape factor during vortex shedding oscillations could be increased with hazardous consequences for the chimney.

By paying attention to the risks above the economic incitement have to be big for using mechanical pendulum tuned dampers. According to our experiences that is not the fact especially if the inspection and maintenance costs are included in the cost estimate. A chimney with any form of not movable device to reduce oscillations caused by vortex shedding is only requiring a limited amount of inspection and is therefore as economic as the pendulum device.

To rely on movable devices in buildings is a form of risk management. Which risk is acceptable for a building? Our recommendation is that chimneys as other important buildings should not be depending on movable devices unless a careful risk management analysis have been made.

By using two differently tuned mechanical dampers some of the above mentioned disadvantages could be avoided.

Vortex shedding oscillations are also a little surprising, in fact that no appreciate oscillations could appear for decenniums and suddenly a winter period when critical meteorological conditions occur the chimney start to oscillate hazardous for a period as discussed in [1]. Therefore it is easy to be lulled into security about the reliability after some years of satisfactory operating experience. Oscillations recorded during the current four-year program on the VEAB chimney never approached those observed in December 1996.

6.2 Comparable chimney data

Some investigations similar to that presented in this report have been published after this investigation was started. Those other investigations involving measurements over time are limited to a much shorter time period than for this investigation. The investigation presented in this report cover a measurement period twice or more that of other investigations [1], [2], [15], [19], [21] and [22].

In [1] Table 6.2 a data as Scruton number and calculated and observed top amplitude deflection for a number of steel chimneys are shown. To the table has been added the VEAB chimney, a chimney at Varberg [21] with great oscillations from vortex shedding, a chimney at Magdeburg [15] and with four chimneys presented in [22].

In Table 6.2 a the chimneys from [1] are named number 1 to 9, the chimneys in [22] with long term recordings number 10 to 14, the VEAB chimney number 15, the Varberg chimney [21] number 16 and.

The following notifications are made in Table 7.1:

h	=	Height
d	=	Diameter
$?$	=	Slenderness ratio h/d
t_{topp}	=	Top shell thickness
f	=	Natural frequency
d	=	Logarithmic decrement
Sc	=	Scruton number
v_{cr}	=	Critical wind velocity
Re	=	Reynold number
c_{lat}	=	The basic value of the aerodynamic exiting force
$l_{effcorr}$	=	Effective correlation length
$K_?$	=	Eurocode 1 calculation variable
K_w	=	Eurocode 1 calculation variable
y_{max}	=	Calculated top amplitude deflection according to Eurocode 1
y_{obs}	=	Observed top amplitude deflection
$y_{measured}$	=	Measured top amplitude deflection

M	=	Measured
O	=	Observed
*	=	The difference in Scruton numbers is due to differences in structural damping and mode shape
**	=	The bigger diameter concern outer diameter of the damper.
***	=	Estimated top mass

15a	=	The VEAB chimney with a mal-functioning damper.
15b	=	The VEAB chimney with a functioning damper.

Table 6.2 a Data for a number of chimneys

	1	2	3	4	5	6	7	8	9	10	11	12	13	14	15a	15b	16
	Nykøbing	Skjern	Brovst	Thyrborøn	Odense	Herning	Chimney (A)	Chimney (B)	Distil column	Magdeburg	Aachen	Köln	Pirna	Rechling-hausen	Växjö, VEAB	Växjö VEAB	Varberg
h (m)	50	45	54	64	75	56	26	30	80	48.7	28	35	60	38	90	90	35
d (m)	2.2	1.1	2.2	2.8	2.4	1.8	1.25	0.816	3.96	1.62	0.914	0.813	2	10.16	2.3/2.8**	2.3/2.8**	0.728
?	22.7	40.9	24.5	22.9	31.3	31.1	20.8	36.8	20.2	30.1	30.6	43.1	30	37.4	39.1	39.1	48.1
t_{ap} (mm)	6	5	8	8	5	6	5	5		6					6	6	4
f (hz)	0.92 (M)	0.63 (M)	0.61 (M)	0.58/0.60	0.37 (EC1)	0.49 (EC1)	1.88 (calc.)	1.06 (M)	0.53 (M)	0.723	1.72	0.61	0.77	0.68	0.29 (M)	0.29 (M)	0.51 (M)
d	0.014 (M)	0.034 (M)	0.059 (M)	0.014/0.03	0.03 (EC1)	0.025) (EC1)	0.03 (M9	0.02 (M)	0.02 (M)	0.012/0.07	0.015	0.015	0.125	0.03	0.04	0.07	0.03
Sc	4.27	11.3	15.9	3.03/4.42*	4.08	4.77	6.1	6.5	10.4	4.27	2.6	7.3	17.2	10.7	8***	14 ***	14
v_{cr} (m/s)	10.1	3.5	6.7	8.1/8.4	4.4	4.4	11.8	4.3	10.5	5.9	7.9	2.5	7.7	3.5	3.3	3.3	1.9
Re x 10^5	14.8	2.5	9.8	15.1/15.7	7.08	5.26	9.8	2.4	27.7	6.3	4.8	1.3	10.3	2.3	6.7	6.7	0.9
c_{lat}	0.2	0.7	0.2	0.2/0.2	0.2	0.2	0.2	0.7	0.2	0.2	0.2	0.2	0.2	0.2	0.2	0.2	0.7
$l_{effcorr}$	6	6	6	6.35/6	6	6	6	6.7	6	6	6	6	6	6	6	6	6
K_y	0.13	0.13	0.13	0.13/0.13	0.13	0.13	0.13	0.13	0.13	0.13	0.13	0.13	0.13	0.13	0.13	0.13	0.13
K_w	0.06	0.379	0.569	0.6/0.599	0.472	0.474	0.6	0.454	0.6	0.487	0.480	0.363	0.488	0.408	0.393	0.393	0.330
y_{max} (mm)	201	84	51	361/247	181	116	80	130	149	120	110	26	37	25	104	60	39
y_{obs} (mm)	-	-	-	>1000	>1000	>500 (O)	250 (O)	300 (O)	690 (O)	-					1500 (0)	-	-
$y_{measured}$ (mm)	35	28	26	98	-	-	-	-	-	200					-	240	85
Observation period											2 years	2 years	2 years	2 years	One winter	4 years	2 months

As [1] notifies Table 6.2 a show that Eurocode 1 often underestimates the top amplitude deflections during vortex shedding oscillations. BSV 97 [3] has limits for slenderness and top deflection as noted in Section 2.4.2.

It is worth noticing that non-professional persons often overestimate visual observations of chimney top deflections. That is a reasonable fact, but that is not the same as saying that visual observations of chimney top deflection always are overestimated. The professional is aware of necessary references needed for the estimation.

6.3 Codes

6.3.1 General

Rules for designing slender structures under wind loading as chimneys are found in various codes. Most countries have their own national codes but organisations such as CEN and Comite International Des Cheminées Industrielles (CICIND) have developed common codes as the Eurocode and the CICIND code.

There are great deviations between the national codes as well as the common codes. Most codes deals with static wind loads in a similar way. However action from vortex shedding is treated in different ways. Some codes limit the allowable slenderness ratio (height/diameter), for applicability of the code design model. Limit restrictions for the top deflection at vortex shedding are also used.

There is a discussion going on about the requirement of revision the codes. See for instance [1] and [15].

For static design the 50-year maximum wind load (gust included) considering global and local buckling and plasticity are applied combined with dead load and other loads.

For dynamic loads fatigue has to be considered. The spectra of fatigue effects will be made up of response from gust wind, vortex shedding and ring oscillations (ovalling).

As a complement to the codes, handbooks have to be used for evaluation of buckling modes, welds and details. In most cases also a finite element (FEA) computer program is necessary for calculating natural frequencies with an acceptable accuracy.

Selection of the applicable code is in most cases depending on in which country the chimney will be erected. Some codes for designing steel chimneys are found in [3], [4], [5], [9], [17] and [23].

6.3.2 Comparison between some codes and behaviour of the VEAB chimney

6.3.2.1 BSV 97 - Snö och vindlast [3]

Calculations according to BSV 97 [3] are made in Section 2.4.2. In Section 3.3.2.2 the corresponding top deflection is calculated and in Section 3.5.7 the number of stress cycles. It is important to notice that BSV 97 is used outside of its limitations according to Section 2.4.2. Therefore the results may be unconcervative. For the VEAB chimney with a locked damper the top deflection will be a multiplication with the relationship between the logarithmic decrements for the unlocked and locked dampers (0.07/0.04).

6.3.2.2 EC1 - Eurocode 1 [23]

In Section 6.2 calculations according to Eurocode 1 are performed except for the number of stress cycles. The number of stress cycles will be

$$N = 6.3 \cdot 10^7 \cdot T \cdot f \cdot e_0 \cdot \left(\frac{v_{cr}}{U_0} \right)^2 \cdot e^{-\left(\frac{v_{cr}}{U_0} \right)^2} \quad \text{.....(6.1)}$$

where T = Lifetime in years
f = Natural frequency
e_0 = Bandwidth factor

$$U_0 = \frac{1}{5} \cdot U_{\mathrm{m,Li}} \quad \text{.....(6.2)}$$

$$U_m = v_{ref} \cdot b \cdot \ln\left(\frac{z}{z_0} \right) \quad \text{.....(6.3)}$$

For the VEAB chimney we achieve

$$U_{\mathrm{m,Li}} = 24 \cdot 0.19 \cdot \ln\left(\frac{90 - 6 \cdot 2.3 \cdot \frac{1}{2}}{0.05} \right) = 33.8 \ \frac{\mathrm{m}}{\mathrm{s}} \quad \text{at centre of the correlation length}$$

$$U_0 = \frac{1}{5} \cdot 33.8 = 6.76 \ \frac{\mathrm{m}}{\mathrm{s}}$$

$$N = 6.3 \cdot 10^7 \cdot 1 \cdot 0.282 \cdot 0.3 \cdot \left(\frac{3.24}{6.76} \right)^2 \cdot e^{-\left(\frac{3.24}{6.76} \right)^2} = 0.97 \cdot 10^6 \ \text{cycles for one year}$$

6.3.2.3 DIN 4133 [9]

In Section 6.2 calculations according to Eurocode 1 are performed except for the number of stress cycles. The Eurocode 1 gives results as DIN 4133 except for the number of stress cycles. The number of stress cycles for a 50-year period will be

$$N = 10^9 \cdot f \cdot \left(\frac{v_{cr}}{v_0}\right)^2 \cdot e^{-\left(\frac{v_{cr}}{v_0}\right)^2} \quad \text{.....(6.4)}$$

where v_0 = Reference wind velocity for vortex shedding number of stress cycles (5 m/s)

$$N = 10^9 \cdot 0.282 \cdot \left(\frac{3.24}{5}\right)^2 \cdot e^{-\left(\frac{3.24}{5}\right)^2} \cdot \frac{1}{50} = 1.55 \cdot 10^6 \text{ cycles per year}$$

6.3.2.4 CICIND [1]

The CICIND model code is based on the spectral model using a large number of full-scale observations to estimate relevant observations [1]. To the Figure 7.15 in [1] the VEAB chimney is implemented.

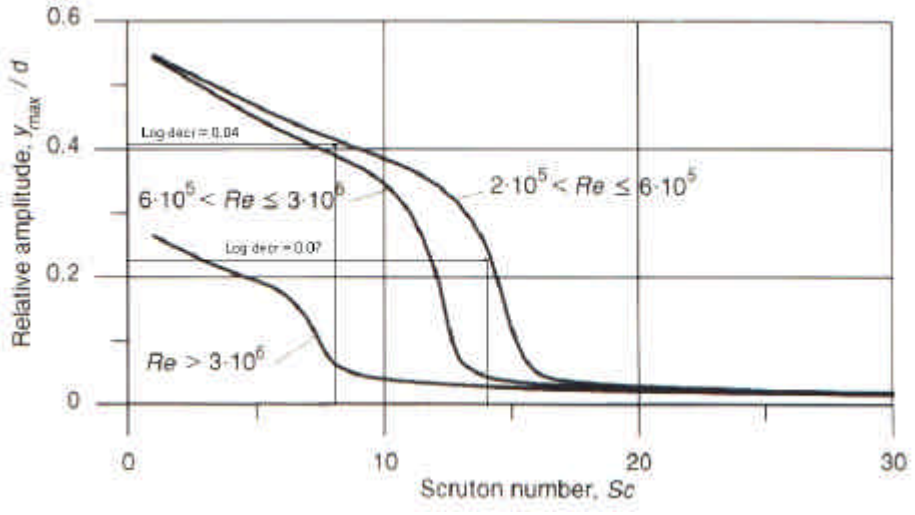

Figure 6.3 a Relative amplitude as a function of Scruton number according to the CICIND model code [1].

For the functioning damper the top deflection is found to be $0.23 \cdot 2300 = 530$ mm and for the mal-functioning damper $0.41 \cdot 2300 = 940$ mm.

6.3.2.5 ISO 4354:1997(E) – Wind actions on structures [24]

Provided that $?_{str} > r_{aer} = \frac{r_{air} \cdot D^2}{m_i} \cdot C_2$ the top deflection during vortex shedding is calculated as

$$y_0 = \frac{C_3 \cdot \left(r_{air} \cdot \frac{D^2}{m} \right)}{\sqrt{\frac{h}{D}} \sqrt{V_{str} - \left(r_{air} \cdot \frac{D^2}{m} \right) \cdot C_2}} \cdot D \quad \text{.....(6.5)}$$

where
C_3 = A constant (2)
r_{air} = Density of air (1.2 kg/m^2)
D = Diameter of chimney (2.3 m)
m = Mass per length of top third of the chimney ($\approx$700 kg/m)
h = Height of chimney (90 m)
V_{str} = Structural damping ratio
C_2 = A constant = 1.2

From Section 3.3.1.4 V_{str} is found to be 0.0111 for the functioning damper and 0.0065 for the mal-functioning damper.

For the functioning damper $?_{str} - \frac{r_{air} \cdot D^2}{m_i} \cdot C_2 \approx 0$

For the mal-functioning damper $?_{str} - \frac{r_{air} \cdot D^2}{m_i} \cdot C_2 \approx -0.0044$

The motion will be unstable and large amplitudes up to the value of D may result [24]. Special treatment is then required either by referral to experts, special codes (e. g. on steel stacks) or special investigations [24].

6.3.2.6 Measurements

From Equation 3.43 the top deflection for the recording period was found to follow

$$y = -35 \cdot^{10} \log(n_t) + 247 \quad \text{mm}$$

6.3.2.7 Observations

From Table 4.2 a the top deflection for the first nine months of mal-functioning damper is found. For the comparison with the codes the load spectrum is extrapolated to one year of mal-functioning damper.

Table 6.3 a Assumed top deflection amplitude distribution for the first nine months in service.

Top deflection y +/- (mm)	1 500	1 150	700	500	300	150	100	Total
Relative time (percent)	0.08	0.23	0.39	1.23	1.54	2.31	4.63	10.42
Number of cycles	7 266	20 889	35 421	111 713	139 868	209 803	420 514	946 000
Accumulated number of cycles	7 266	28 155	63 576	175 289	315 157	524 960	946 000	-

6.3.2.8 Comparison between the codes, measurements and observations

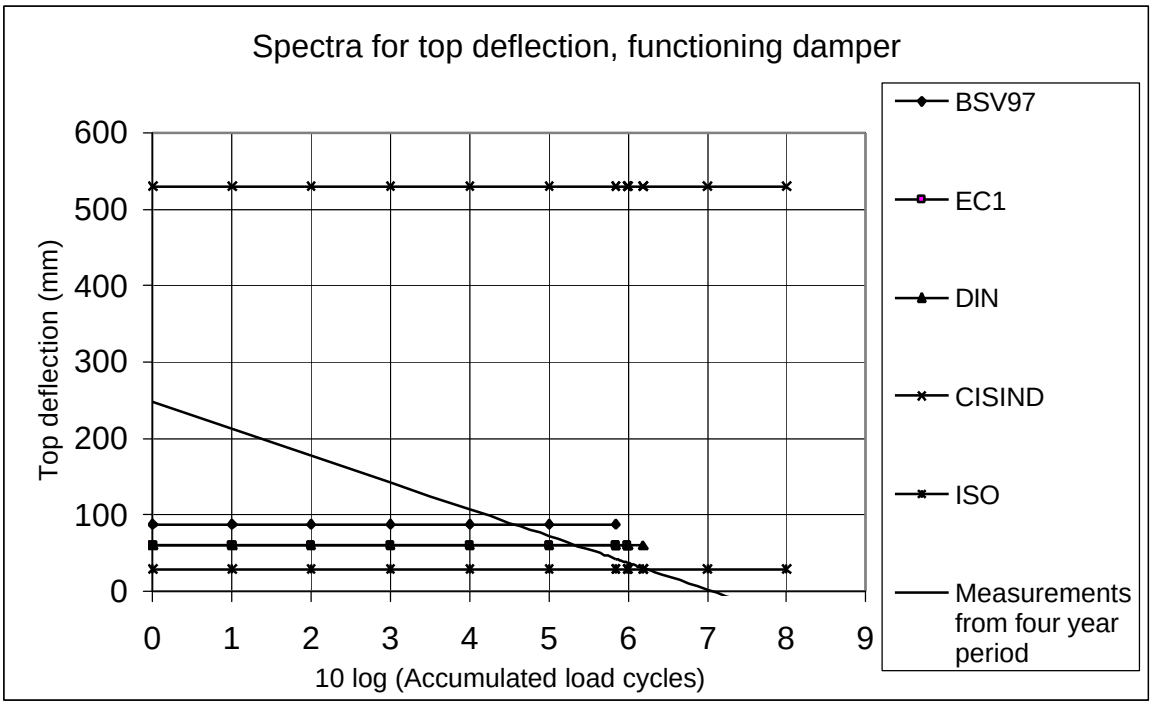

Figure 6.3 b Spectra for top deflection per year and a functioning damper. Codes discussed in previous sections as well as results from the recording period are plotted.

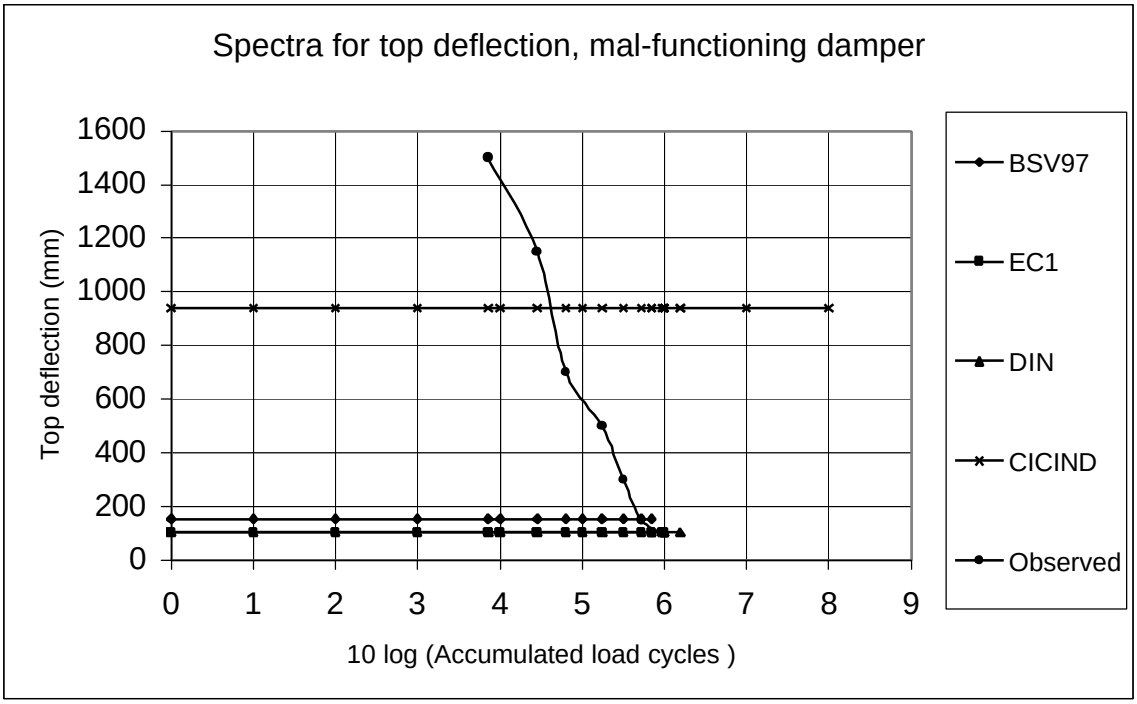

Figure 6.3 c Spectra for deflection per year and a mal-functioning damper. Codes discussed in previous sections as well as results from the recording period are plotted.

For the functioning damper, Figure 6.3 b shows that only the CICIND code is safe to use calculating top deflection. For the mal-functioning damper Figure 6.3 c, no code is safe calculating top deflection. The influence on fatigue damage using the Palmgren-Miner hypothesis is more complicated and could give other results.

Both BSV 97 and ISO 4354 have limitations for their use and do not cover the VEAB chimney properties. Especially the limitations in ISO 4354 points out that the VEAB chimney operates in or in the neighbourhood to an unstable vortex shedding section. The geometric properties of the VEAB chimney had been different from the actual geometric properties if one of the BSV 97, CICIND or ISO codes had been followed strictly.

There is a need for revision of the model to estimate the response caused by vortex shedding of very slender chimney structures ($h/d \gtrsim 30$).

6.4 Comparison of spectra from literature data and the VEAB chimney

The long-term observations at the VEAB chimney have been in operation during four years. It is two times longer than previously reported literature data. Detailed data about observation time and structural data are found in Table 6.2 a.

In Figure 6.4 recorded spectra for Aachen, Colonge, Pirna, Recklinghausen [22] and the VEAB chimney are drawn.

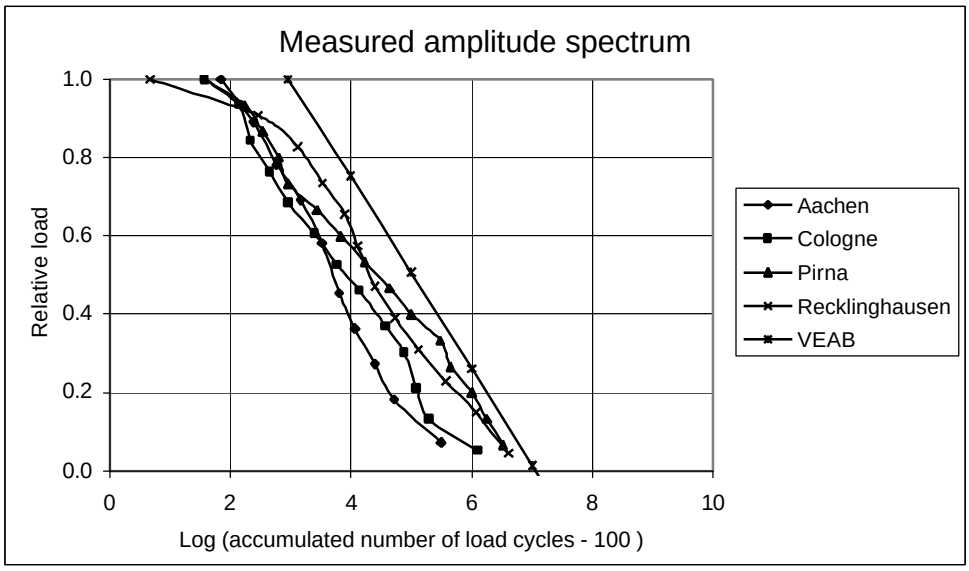

Figure 6.4 a Measured amplitude spectra for the chimneys [22] and the VEAB chimney.

In Figure 6.4 b a typified load spectrum calculated with the least square method for the VEAB chimney is drawn.

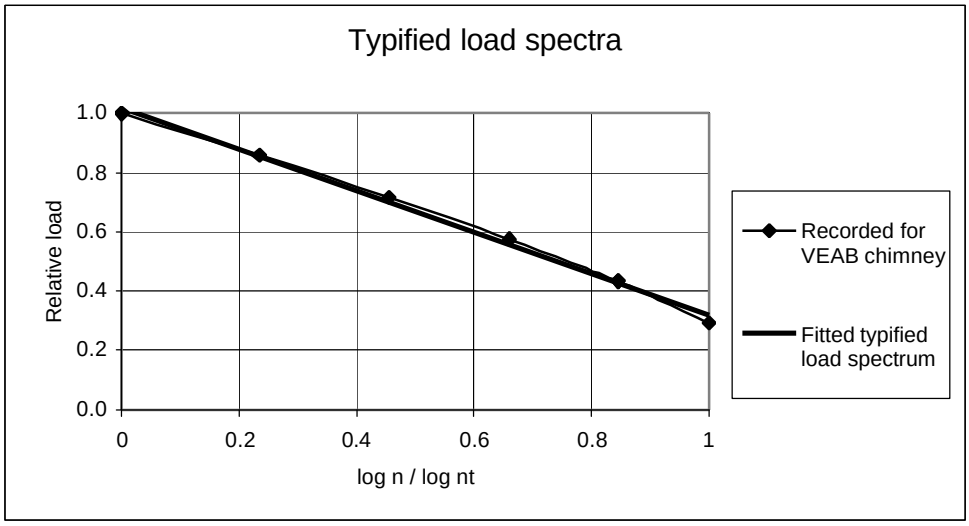

Figure 6.4 e Typified amplitude spectrum for the VEAB chimney. κ=0.32.

6.5 Second mode

In this report reviews briefly the influence of second mode oscillations on the VEAB chimney. Based on a limited number of observations the first mode is found designing for fatigue strength. From Section 3.6 and 3.7.1 it is shown that the second mode occurs at rare occasions and that the number of load cycles are low.

6.6 The future

Initially the recordings of the VEAB chimney were planned to continue until December 2003 followed by an evaluation of the recorded results as shown in Table 3.2 c.

Table 6.6 c Actions to be taken for the VEAB chimney

Result of evaluation	Action
1. Acceptable probability for collapse	a. The VEAB chimney is OK. Finish the recordings.
2. Unclear	b. Continue the recordings.
	c. Add additional damping to the chimney. An assumption is that the accumulated fatigue damage is acceptable.
3. Unacceptable probability for collapse	c. Add additional damping to the chimney. An assumption is that the accumulated fatigue damage is acceptable.
	d. Replace the chimney with a new and modified one.

Unfortunately the strain gauges were damaged in the spring of 2001, probably by mistake, when applying corrosion protection on the inside of the chimney. It was expensive to repair the recording system. For economic reasons it was decided that additional damping had to be installed to provide an acceptable safety with respect to fatigue. Two dampers connected the boiler house at roof level (45 m) to the chimney erection splice at 55.2 m level. That is action 3 c in Table 3.2 c.

7 Summary

7.1 In English

The long-term observations at the VEAB chimney have been in operation during four years. It is two times longer than previously available data in the literature for other chimneys.

The report contains data on the behaviour of a major chimney with a mass damper. The measured damping was less than expected, probably because the limited space in the damper house not did allow necessary pendulum movements, and too low pendulum mass.

The VEAB chimney was found to oscillate in both first and second mode of natural frequency. Second mode oscillations are rare for normal chimneys. The damping of second order oscillations is much greater than for first order. The evaluation of the measurements showed that the influence of second order oscillations could be neglected.

A comparison with some other chimneys reported in the literature shows that the VEAB chimney is unique in height and slenderness.

Typified linear load effect spectra describe the chimney behaviour well.

A full scale damping measurement was performed and evaluated for the VEAB chimney with and without functioning damper.

A comparison with a number of code regulations has been performed.

A refinement of a theoretical calculation model for the behaviour of tuned mass dampers was performed.

Actual meterological data were considered in evaluation the action for the VEAB chimney.

Geometric properties of the VEAB chimney had been selected to other dimensions if one of the BSV 97, CICIND or ISO codes had been followed strictly. The diameter had been selected to a greater size.

There is a need for revising the calculation model for vortex shedding of very slender chimneys, that is for chimneys with slender ratio height through diameter above approximately 30.

7.2 In Swedish

Mätsystemet för långtidsövervakning av VEAB stålskorsten har varit i drift under fyra år. Det är två gånger längre än tidigare i litteraturen beskrivna mätningar för skorstenar.

Rapporten innehåller uppgifter om beteende för en skorsten försedd med massdämpare. Den uppmätta dämpningen var mindre än väntat, antagligen på grund av att begränsat utrymme i dämparhuset inte tillät nödvändig pendelrörelse samt att pendelmassan var för låg.

VEAB stålskorsten observerades svänga i både första och andra modens egenfrekvens. Svängningar i andra moden är ovanliga för stålskorstenar. Dämpningen är mycket större för andra modens svängningar än för första modens. Utvärderingen av mätdata visade att andra modens inflytande kunde försummas.

En jämförelse med ett antal andra skorstenar beskrivna i litteraturen visade att VEAB skorstenen är unik i höjd och slankhet.

Skorstenens uppförande beskrivs väl av ett lastspektrum.

En mätning av dämpning genomfördes i full skala för VEAB stålskorsten med både fungerande och låst dämpare.

En jämförelse med ett antal normer är gjord.

Verkliga meteorologiska data beaktades vid utvärderingen.

En förbättrat förslag på beräkningsmodell för pendelförsedda massdämpare är utarbetat.

Aktuella meteorologiska data har beaktats vid alla utvärderingar.

Dom geometriska storheterna för VEAB stålskorsten hade valts annorlunda om någon av normerna BSV 97, CICIND or ISO hade följts konsekvent. Skorstenens diameter hade då valts större.

Det är behov av en översyn av beräkningsmodellen för att uppskatta responsen från virvelavlösning för mycket slanka stålskorstenar. Med mycket slanka stålskorstenar avses ett slankhetstalet (höjd genom diameter) över ungefär 30.

8. References

[1] Claës Dyrbye, Svein O Hansen: *Wind loads on structures*, John Wiley & Sons, 1997.

[2] Hans Ruscheweyh, Thomas Galemann: *Full-scale measurements of wind induced oscillations of chimneys*, Journal of Wind Engineering and Industrial Aerodynamics 65 (1996) 55-62.

[3] BSV 97, *Snö- och vindlast (Snow and wind loading)*, 2nd Edition, Boverket 1997 (in Swedish).

[4] BSK 94: *Boverkets handbok om stålkonstruktioner*, Boverket 1994 (in Swedish) later replaced by BSK 99: *Boverkets handbok om stålkonstruktioner*, Boverket 1999 (in Swedish).

[5] Eurocode 3: *Design of steel structures. Part 3-2: Towers, masts and chimneys - Chimneys*, ENV 1993-3-2, 1997.

[6] Hans Ruscheweyh: *Dynamische Windwirkung an Bauwerken. Band 2: Praktische Anwendungen*, Bauverlag GmbH, Wiesbaden und Berlin, 1982.

[7] Chr. Petersen: *Windinduzierte Schwingungen und ihre Verhütung durch Dämpfer*, Der Stahlbau 11/1982, 336-341.

[8] Costantin Verwiebe: *Überschlägliche Berechnung der Querschwingungsbeanspruchung von Schornsteinen aus Stahl nach Din 4133*, Stahlbau 68 (1999), Heft 10, 846-851.

[9] DIN 4133, *Schornsteine aus Stahl*, November 1991.

[10] Cyrril M. Harris: *Shock and Vibration handbook*, third edition 1988, Mc Graw-Hill Inc.

[11] Christian Petersen: *Baupraxis und Aeroelastik, Probleme – Lösungen - Schadenfälle*.

[12] Bengt Sundström: *Handbok och formelsamling i Hållfasthetslära*, Kungliga Tekniska Högskolan 1999 (in Swedish)

[13] F. M. Sauer, C. F. Garland: *Performance of the Viscously Damped Vibration Absorber Applied to Systems Having Frequency-Squared Excitation*, Berkeley, Calif., 109-117.

[14] Costantin Verwiebe: *Winderregte Schwingungen und Massnahmen zur Dämpfungserhöhung im Stahlschorsteinenbau*, Schorsteinbau – Symposium 23. Januar 1997, Bad Hersfeld.

[15] Constantin Verwiebe & Waldemar Burger: *Unerwartet starke wirbelerregte Querschwingungen eines 49 m hohen Stahlschornsteins*, Stahlbau *67*, Heft 11, 1998, p 876-878.

16] Dubbel*: Taschenbuch für den Maschinenbau*, 14. Auflage, Springer Verlag Berlin Heidelberg New York 1981.

[17] BKR 99: *Boverkets konstruktionsregler*, Boverket 1999 (in Swedish).

[18] Urban Bergström, et al: *Plåthandboken*, SSAB Tunnplåt AB, 1993, Utgåva 5.

[19] Max Beaumont, Dennis E. Walshe: *Investigation into wind induced oscillation on three 76 high self supporting steel chimneys*, 4th Chimney Symposium, 127-135.

[20] Costantin Verwiebe: *Neue Erkenntnisse über die Erregungmechanismen Regen-Wind-induzierter Schwingungen*, Stahlbau 65 (1996), Heft 12.

[21] Göran Alpsten: *Dynamisk vindlast av virvelavlösning (Dynamic wind loading from vortex shedding)*, Document 9835a, Stålbyggnadskontroll AB, May 1998 (in Swedish).

[22] H. Ruscheweyh, W. Langer, C. Verwiebe: *Long-term full-scale measurements of wind induced vibrations of steel stacks*, Journal of Wind Engineering and Industrial Aerodynamics 74-76 (1998) 777-783.

[23] Eurocode 1: *Basis of design and actions on structures, Part 2-4: Wind actions*, ENV 1991-2-4, 1994.

[24] ISO 4354:1997(24): *Wind actions on structures*, International Organisation of Standardisation, 1997.

[25] Kamal Handa: *Kompendium i Byggnadsaerodynamik*, Chalmers Tekniska Högskola, Göteborg, 1993 (in Swedish).

[26] Göran Alpsten: *Svängningsproblem vid en 35 m stålskorsten utan spriralfenor dimensionerad enligt SBN 1975 (Vibration problems for a 35 m steel chimney without helical strakes designed according to SBN 1975), Internal report 8464-1, Stålbyggnadskontroll AB, Feb. 1985 (in Swedish*).

[27] Pär Tranvik: *VEAB Steel Chimney – Computer programs for data reduction*, *Internal report S 02 003* , Alstom Power Sweden AB, 2002.